

AD-A034 505

M AND S COMPUTING INC HUNTSVILLE ALA

PAR AURORAL STUDY. VOLUME V. RADAR AURORAL MAGNETIC ASPECT SENS--ETC(U)

OCT 76 M J MITCHELL, J L BROWN

F/G 17/9

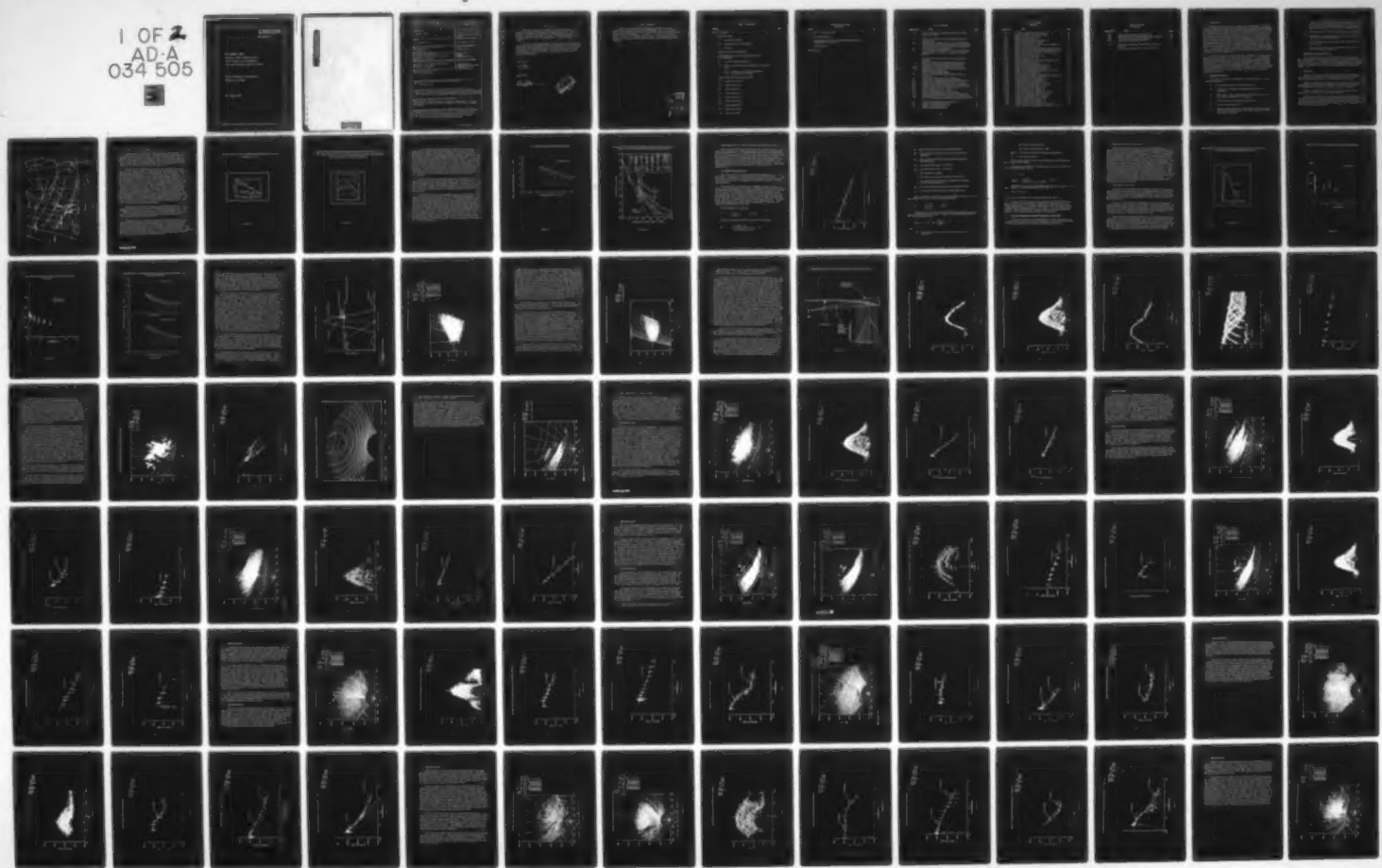
DASG60-74-C-0026

NL

UNCLASSIFIED

76-0052

1 OF 2  
ADA-A  
034 505



U.S. DEPARTMENT OF COMMERCE  
National Technical Information Service

AD-A034 505

PAR AURORAL STUDY  
VOLUME V. RADAR AURORAL MAGNETIC  
ASPECT SENSITIVITY MEASUREMENTS  
FROM THE PERIMETER ACQUISITION RADAR

M AND S COMPUTING, INCORPORATED  
HUNTSVILLE, ALABAMA

19 OCTOBER 1976

ADA034505

REPRODUCED BY  
NATIONAL TECHNICAL  
INFORMATION SERVICE  
U. S. DEPARTMENT OF COMMERCE  
SPRINGFIELD, VA. 22161

UNCLASSIFIED

SECURITY CLASSIFICATION OF THIS PAGE (When Data Entered)

REPORT DOCUMENTATION PAGE		READ INSTRUCTIONS BEFORE COMPLETING FORM
REPORT NUMBER Volume V	2. GOVT ACCESSION NO.	3. RECIPIENT'S CATALOG NUMBER
TITLE (and Subtitle) PAR Auroral Study		5. TYPE OF REPORT & PERIOD COVERED Interim-One of six volumes
7. AUTHOR(s) M. J. Mitchell et al		6. PERFORMING ORG. REPORT NUMBER 76-0052 8. CONTRACT OR GRANT NUMBER(s) Army DASC60-74-C-0026
9. PERFORMING ORGANIZATION NAME AND ADDRESS M&S Computing Inc. P. O. Box 5183 Huntsville, Ala. 35805		10. PROGRAM ELEMENT, PROJECT, TASK AREA & WORK UNIT NUMBERS Not Applicable
11. CONTROLLING OFFICE NAME AND ADDRESS U. S. Army Ballistic Missile Def Sys Cmd BMDSC-WE, P. O. Box 1500 Huntsville, Ala. 35807		12. REPORT DATE 19 Oct 76 13. NUMBER OF PAGES 110
14. MONITORING AGENCY NAME & ADDRESS (if different from Controlling Office) U. S. Army Ballistic Missile Def Sys Cmd BMDSC-WE, P. O. Box 1500 Huntsville, Ala. 35807		15. SECURITY CLASS. (of this report) UNCLASSIFIED 15a. DECLASSIFICATION/DOWNGRADING SCHEDULE Not Applicable
16. DISTRIBUTION STATEMENT (of this Report) Unlimited Distribution		
17. DISTRIBUTION STATEMENT (of the abstract entered in Block 20, if different from Report) Unlimited Distribution		
18. SUPPLEMENTARY NOTES This is one of six volumes of reports that present the aurora borcalis data collected by a multi-megawatt phased array radar. The radar has excellent sensitivity and range resolution affording very precise aurora detail.		
19. KEY WORDS (Continue on reverse side if necessary and identify by block number) Aurora Borcalis, phased array radar, radar/aurora efforts, back scattering characteristics, radar reflectivity, geomagnetic field effects, ionospheric scintillation.		
20. ABSTRACT (Continue on reverse side if necessary and identify by block number) This report describes the measurements of the relationship of the apparent radar auroral reflectivity to the magnetic aspect angle. Also discussed is an evaluation of the effects of auroral clutter on the sidelobe blanker and measurement of effects of active auroral noise generation on the radar noise level.		

## PREFACE

This report describes the results of the auroral magnetic aspect sensitivity studies being performed by M&S Computing, Inc., under Contract No. DASG60-74-C-0026 for the Ballistic Missile Defense Systems Command in Huntsville, Alabama. PAR Auroral Study, Volume V, dated October 19, 1976, constitutes M&S Computing's Report No. 76-0052.

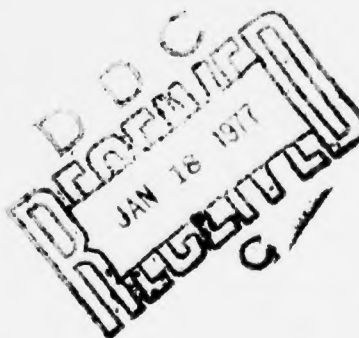
The purpose of this investigation was to determine the relationship between the radar reflectivity of the aurora borealis and the angle between the magnetic field lines and the radar propagation path. The mass of high resolution data collected during the 1 1/2 years of PAR auroral studies has provided the means to study this relationship and achieve results previously unattainable.

Prepared by:

M. J. Mitchell  
J L. Brown

Approved by:

W. E. Salter  
W. E. Salter



## ACKNOWLEDGEMENT

The results described herein required the efforts of many individuals. We wish to thank the entire team from BMDSCOM, IBM, Bell Telephone Laboratories, and the Western Electric Company for their support and contributions. Special credit is extended to P. L. Alley, L. R. Bowers, M. Cochran, T. L. Dunn, F. L. Guza, L. Jacobs, and J. M. Roe, all of whom developed the analysis tools, performed the data processing, and participated in the data analysis.

DISTRIBUTION FOR	
STIS	White Section <input type="checkbox"/>
DOC	Buff Section <input type="checkbox"/>
UNANNOUNCED <input type="checkbox"/>	
JUSTIFICATION	
BY	
DISTRIBUTION/AVAILABILITY CODES	
DISP	AVAIL. AND OR SPECIAL
A	

## TABLE OF CONTENTS

<u>Section</u>	<u>Page</u>
LIST OF FIGURES	
1. INTRODUCTION	1
1.1 Features of the PAR	1
1.2 Applications of this PAR Study	2
1.3 Overview	2
2. ASPECT STUDY BACKGROUND	5
3. DETERMINATION OF THE MAGNETIC ASPECT RELATIONSHIP	11
3.1 The Reflectivity Scatter Plot	11
3.2 Special Techniques Employed to Enhance the Aspect Data	14
3.2.1 Pulse-to-Pulse Echo Decorrelation	15
3.2.2 The Effects of Resolution	15
4. DATA CASES USED IN THE ANALYSIS	39
4.1 Test Case 270/1058	39
4.2 Test Case 70/666	44
4.3 Test Case 78/12	44
4.4 Test Case 86/576	53
4.5 Test Case 86/632	53
4.6 Test Case 86/5557	63
4.7 Test Case 86/5571	63
4.8 Test Case 86/5622	73
4.9 Test Case 92/681	79

TABLE OF CONTENTS  
(Continued)

<u>Section</u>	<u>Page</u>
4.10 Test Case 92/723	87
5. ANALYSIS RESULTS	93
6. PERTURBATION OF THE GEOMAGNETIC FIELD BY IONOSPHERIC CURRENTS	97
7. CONCLUSIONS	101
REFERENCES	103

## LIST OF FIGURES

<u>Figure No.</u>	<u>Title</u>	<u>Page</u>
1-1	105 km Geomagnetic Off-Perpendicular and L-Shell Contours for PAR	3
2-1	Two Curves of Radar Auroral Scattered Power Versus Frequency [4]	6
2-2	Aspect Angle in Degrees Versus Average Amplitude of 139, 398, 850, and 1210 MHz for 497 Elevation Sweeps, Using the Maximum Echo Amplitude for Each Sweep [4]	7
2-3	Volume Reflection Coefficient [5]	9
2-4	Auroral Clutter Reflectivities ( $\rho$ ) Versus Geomagnetic Aspect Angle ( $\alpha$ ) for Various Conditions of Observation [7]	10
3-1	Scatter Plot with Manual Curve-Fit Showing Aspect Response	12
3-2	Observed Amplitude Distribution Compared with a Theoretical Calculated Rayleigh Distribution [5]	16
3-3a/b	Scatter Plots Showing Effects of Superscanning	17
3-4a/b	Differences in Apparent Aspect Response with Two Different Pulse Lengths [6]	19
3-5	Near-Boresight Antenna Pattern	21
3-6	Profile Reflectivity Map Showing Effects of Beam Broadening	22
3-7	Profile View Showing Auroral Reflectivity	24
3-8	Mislocation of Scattering Center from Beam Divergence	26
3-9	Altitude Versus Reflectivity Profile for One Pulse	27
3-10	Altitude Versus Reflectivity Profile for an Entire Scan	28
3-11	Aspect Response for all Altitudes at One Pointing Angle	29
3-12	Aspect Response Curve for All Altitudes	30
3-13	Aspect Response for 105 - 106 km	31
3-14	Top-Down Reflectivity Map Showing Voids	33
3-15	Aspect Response Showing Discrete Reflectivity Sheet	34
3-16	Top-Down Overlay with Pointing Angles at Intersections	35
3-17	Top-Down Reflectivity Map with L-Shell Contour at 105 km	37
4-1	Top-Down Reflectivity Map of Scan 1058	40
4-2	Scatter Plot Showing Arc Center	41
4-3	Scatter Plot from Region "B"	42
4-4	Scatter Plot from Region "A"	43

**LIST OF FIGURES**  
**(Continued)**

<u>Figure No.</u>	<u>Title</u>	<u>Page</u>
4-5	Top-Down Reflectivity Map of Scan 667	45
4-6	Altitude Profile for All Aspect Angles	46
4-7	Scatter Plot from Region "A"	47
4-8	Scatter Plot from Region "B"	48
4-9	Top-Down Reflectivity Map of Scan 12	49
4-10	Scatter Plot Showing Arc Center	50
4-11	Aspect Scatter Plots of Scans 12-22 from Region "A"	51
4-12	Scatter Plot from Region "B"	52
4-13	Top-Down Reflectivity Map Showing Aspect Contours	54
4-14	Map of Scan 576 Showing L-Shell Contours at 105 km	55
4-15	Scatter Plot Showing Altitude Versus Reflectivity	56
4-16	Scatter Plot from Region "A"	57
4-17	Aspect Response from Region "B"	58
4-18	Top-Down Map of Scan 633	59
4-19	Altitude Reflectivity Profile Showing Center of Arc	60
4-20	Scatter Plot from Region "A"	61
4-21	Aspect Scatter Plot from Region "B"	62
4-22	Top-Down Reflectivity Map of Scan 5558	64
4-23	Scatter Plot Showing Altitude Profile	65
4-24	Scatter Plot Showing Aspect Response Along "A"	66
4-25	Scatter Plot from Region "B"	67
4-26	Scatter Plot from Regions "B" and "C"	68
4-27	Top-Down Map of Auroral Reflectivity for Scan 5571	69
4-28	Aspect Response Along Region "A"	70
4-29	Aspect Scatter Plot Along Region "B"	71
4-30	Aspect Response from Region "C"	72
4-31	Top-Down Reflectivity Map of Scan 5626	74
4-32	Altitude Profile Showing Arc Center	75
4-33	Aspect Response from Region "A"	76
4-34	Aspect Response from Region "B"	77
4-35	Aspect Response from Regions "B" and "C"	78
4-36	Top-Down Reflectivity Map of Scan 681	80
4-37	Top-Down Reflectivity Map of Scan 690	81
4-38	Altitude Profile Showing Arc Center	82
4-39	Aspect Response from Region "A"	83
4-40	Aspect Response Along Region "B"	84
4-41	Aspect Response from Regions "B" and "C"	85
4-42	Composite Aspect Response from Regions "B" and "D"	86

**LIST OF FIGURES**  
**(Continued)**

<u>Figure No.</u>	<u>Title</u>	<u>Page</u>
4-43	Top-Down Reflectivity Map of Scan 727	88
4-44	Distribution of Echo Reflectivities After Averaging	89
4-45	Aspect Response from Along Region "A"	90
4-46	Aspect Response Along "B" and "C"	91
6-1	Quiescent Geomagnetic Aspect Contours at 105 km for PAR	99
6-2	Perturbed Aspect Contours at 105 km for PAR	100

## 1. INTRODUCTION

The purpose of this report is to describe the measurements of the relationship of the apparent radar auroral reflectivity to the magnetic aspect angle, the angle between the propagation path and the magnetic field lines in the vicinity of the apparent source of the reflection. This research has been performed as part of the PAR Auroral Study which began in early 1975. Data collection was performed on several occasions in the fall of 1975 and in the spring of 1976. Over 200 reels of magnetic tape were recorded altogether, representing about 40 hours of auroral observation. On four of these data gathering periods, continuous observation and recording was performed throughout the night. The recorded data consisted of auroral backscatter measurements as well as simultaneous satellite tracking data. In addition to the normal data collecting activities, a number of special tests were performed to evaluate the effects of auroral clutter on the sidelobe blanker and to measure the effects of active auroral noise generation on the radar noise level.

A number of special computer programs, including a versatile graphics package, were developed for use as tools in this analysis. A more detailed description of these tools, and of the PAR auroral study containing numerous auroral maps and special plots, has already been published in three volumes [References 1, 2, and 3] which preceded this document. The development of this report depends heavily on background information supplied in those volumes, which are identified in the List of References. Copies of these documents may be obtained from the Army Ballistic Missile Defense Systems Command in Huntsville, Alabama.

### 1.1 Features of the PAR

The PAR is particularly well-suited for auroral backscatter studies. Among its features are:

- An operating frequency in the 450 MHz band.
- Phased array steering, providing rapid wide-angle scan capabilities.
- Exceptionally high-peak and average transmit powers, allowing a range coverage well over 2000 km.
- Excellent sensitivity and noise performance.
- Narrow receive beam,  $1.5^\circ$ .
- Excellent range resolution of better than 1.5 km accompanied by very high transmit pulse energy which is attained by pulse compression techniques.

- Optimum face orientation to minimize distortion and steering loss in direction of maximum auroral backscatter. Figure 1-1 shows the location of the PAR along with its geomagnetic off-perpendicular and L-shell contours at an altitude of 105 km.
- High performance data processing and recording capabilities.
- Capability to perform simultaneous measurements of auroral backscatter and satellite tracking.
- Sidelobe suppression capabilities to minimize unwanted sidelobe returns.
- Either right or left circular polarization which can be selected for both transmit and receive.

### 1.2 Applications of This PAR Study

With these capabilities, auroral data from the PAR provides its users with a clear picture of its interaction with the aurora and the effect of the aurora on its performance. It can provide valuable engineering data to the designers of future radar systems. In addition, it is hoped that this study can provide the scientific community with certain valuable geophysical data concerning the aurora.

### 1.3 Overview

Section 2 of this report introduces the subject of aspect sensitivity, what it is, and why it is of interest. This section also provides a short historical background describing the results of some earlier aspect studies.

Section 3 describes the techniques used to determine the magnetic aspect relationships, including the data selection process, the data reduction task, and the identification and handling of a number of analytical problems.

Section 4 presents the test cases, their supporting data, and the resultant scatter plots which show the aspect response curves.

Section 5 describes the results of the analysis and summarizes the data from the test cases. Some interesting observations have been made; the reader is cautioned, however, that some of these observations may be illusory. This situation is discussed in further detail in Section 6, which provides possible explanations for the observations.

105 KM GEOMAGNETIC OFF-PERPENDICULAR AND L-SHELL CONTOURS FOR PAR

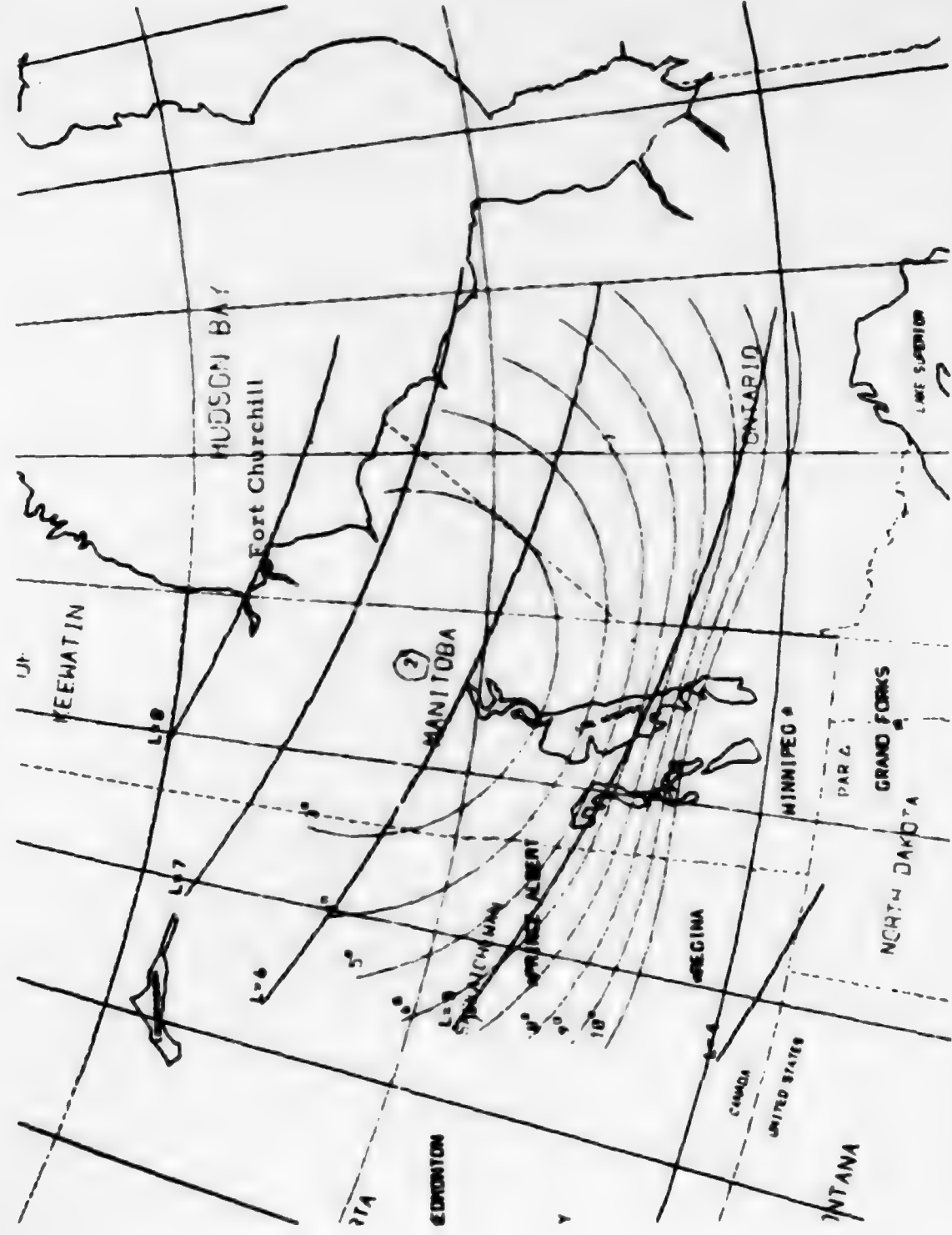


Figure 1-1

## 2. ASPECT STUDY BACKGROUND

The phenomena of radio wave reflections from auroral ionization has been observed since the early 1930's. These reflections have been measured throughout the UHF range of 30 MHz to 3000 MHz, but most of the measurements have been made in the 50-500 MHz region. At frequencies lower than these, the radar equipment becomes large, cumbersome, and very expensive. At higher frequencies, the reflectivity of the auroral irregularities is reduced, resulting in very weak echoes, as shown in Figure 2-1.

One particularly significant fact about auroral backscatter is that the intensity of the observed returns depends upon the angle between the radar beam and the magnetic field lines at the reflecting point. This phenomena, called geomagnetic aspect dependence, has long been of interest to scientists. A number of theories attempting to explain the geomagnetic aspect dependence have been developed over the years. Most of the earlier theories have now been abandoned in favor of those which relate the irregular plasma structure responsible for the observed aspect dependence to magnetohydrodynamic wave action. This wave action is thought to result from instabilities in the plasma which occupies the ionospheric E region. When aurora occurs, the plasma density is enhanced and also subject to dynamic interactions related to the geomagnetic disturbances and particle precipitation. The resulting wave action forms the field-aligned irregularities which, in turn, serve as reflectors of radar signals. The radar signals encounter cyclic changes in the index of refraction in the propagation path due to the intensification and rarification of the wave fronts. Basic electromagnetic theory predicts that energy will be reflected from these irregularities. The echoes detected at the radar consist of reflections from a great number of these closely spaced irregularities.

The precise processes which control the formation and dynamics of the magnetohydrodynamic wave action are not completely understood, but one popular explanation has been proposed, known as "Two-Stream Instability" [5]. It is not within the scope of this report to discuss in detail the various theories which attempt to explain the phenomena but primarily to provide data which may be used to support and advance those theories.

Scientists have, for a number of years, been trying to determine the geomagnetic aspect sensitivity relationship using radar measurements. Most of these studies were hampered by the equipment used, low power, broad beam-width, and poor range resolution. W. G. Chestnut, a prominent figure in auroral backscatter studies, made aspect measurements at numerous frequencies. An example of his results is shown in Figure 2-2. The solid line represents the measured aspect data, and the dashed line represents a prediction based on the measured data of what the aspect relation was expected to be.

TWO CURVES OF RADAR AURORAL SCATTERED POWER VERSUS  
FREQUENCY [4]

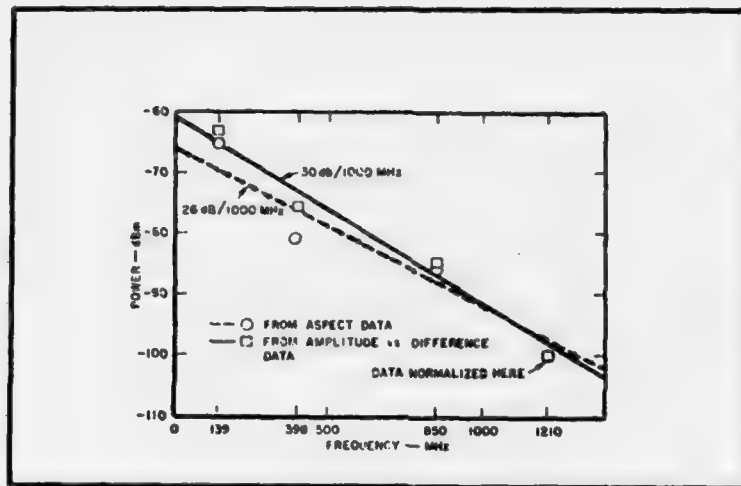


Figure 2-1

ASPECT ANGLE IN DEGREES VERSUS AVERAGE AMPLITUDE OF 139, 398,  
850, AND 1210 MHz FOR 497 ELEVATION SWEEPS, USING THE MAXIMUM  
ECHO AMPLITUDE FOR EACH SWEEP [4]

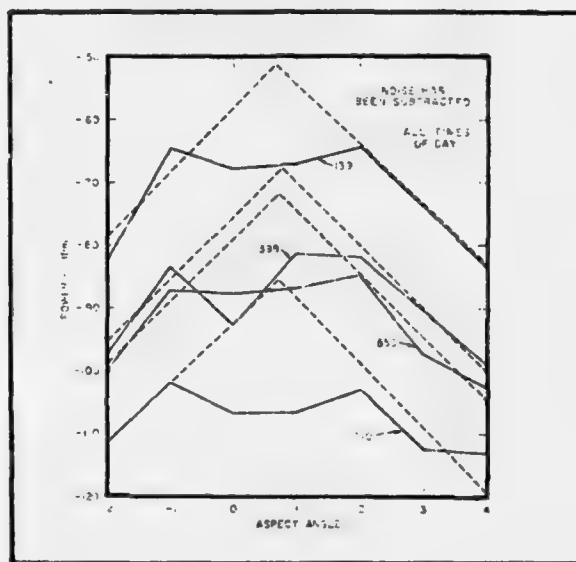


Figure 2-2

A more recent effort which employed considerably more advanced radar equipment was undertaken at the Prince Albert Radar Laboratory (PARL) in Saskatchewan, Canada. This study, a joint effort of Bell Telephone Laboratories, MIT Lincoln Laboratories, and Stanford Research Institute, is especially significant because of the similarities between the PARL and the PAR. The results of this study have been published in two documents, [4] and [7]. One significant factor of note in the PARL reports is the use of "reflectivity" to describe the volume backscatter properties of the aurora. The use of reflectivity, or effective radar cross-section per unit volume, normalizes the range and pulse-width dependence of the range resolution cell as well as most of the constant radar parameters. This technique is used almost exclusively for the processing of meteorological radar data providing those researchers with an improved level of standardization. For a discussion of the techniques employed in this similar field, see [8].

Auroral measurements, described in terms of reflectivity, allow the direct comparison of data from different radars, if these comparisons are made carefully in regard to the magnetic aspect dependence. Figure 2-3 is an example of some of the PARL aspect data using the same type of chirp waveform as that used by the PAR. Another set of aspect response curves is shown in Figure 2-4. These curves were published as part of an excellent study of radar auroral phenomena [7].

Unfortunately, the PARL was located in such a way that measurements could not be made closer than about  $4.5^{\circ}$  to normal magnetic incidence. Three significant observations were made, however. The first was that the "apparent" magnetic aspect sensitivity depends on the planetary geomagnetic disturbance index ( $K_p$ ). This index indicates changes in the ionospheric current system. The second observation was that the slope of the magnetic aspect sensitivity tends to become progressively flatter (less aspect-sensitive) at greater off-perpendicular angles. A third observation showed that the reflectivity depends on the effective radar pulse width. It has been reasoned that this last phenomena is merely a manifestation of the non-homogeneity of the auroral mass. It has been suggested [7] that with the longer pulses, the range resolution cells contain voids and weakly reflecting regions. Voids such as these in the range resolution cell decrease the average reflectivity. These observations are all supported by the PAR Auroral Study.

VOLUME REFLECTION COEFFICIENT [5]

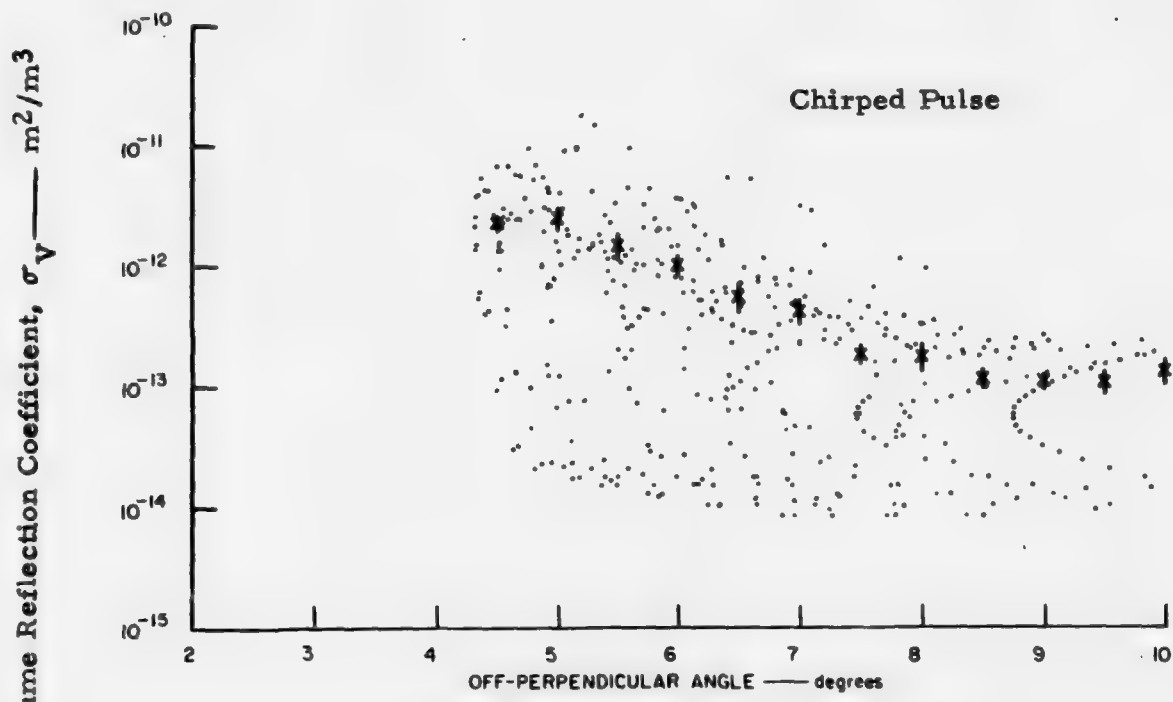


Figure 2-3

AURORAL CLUTTER REFLECTIVITIES ( $\rho$ ) VERSUS GEOMAGNETIC ASPECT ANGLE ( $\alpha$ ) FOR VARIOUS CONDITIONS OF OBSERVATION [7]

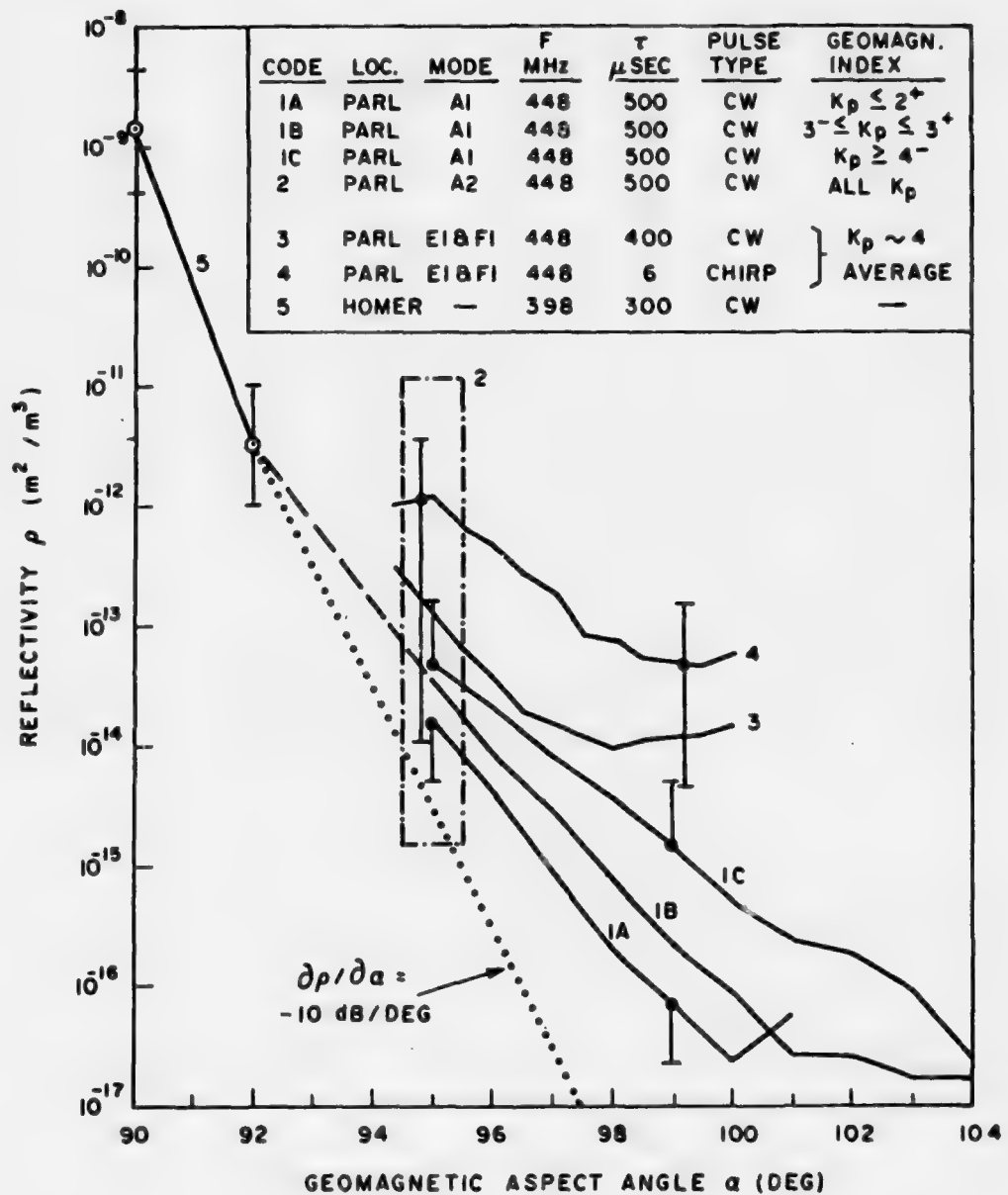


Figure 2-4

### 3. DETERMINATION OF THE MAGNETIC ASPECT RELATIONSHIP

The primary intent of this portion of the study was to determine the magnetic aspect relationship for different geomagnetic conditions for both discrete and diffuse auroral forms. The tapes from five nights of data collecting during the fall of 1975 and the spring of 1976 served as data cases. Specific data bases were selected with the aid of magnetometer data from Churchill, Canada, as well as the auroral maps and histograms which had been generated for general support of the various auroral study tasks. Measured echoes generally had signal-to-noise ratios in excess of 15 dB and as high as 101 dB. A noise threshold required detected returns to exceed about 10 dB signal-to-noise ratio, thus limiting errors.

#### 3.1 The Reflectivity Scatter Plot

The scatter plot was chosen as the media for outputting the processed aspect data. An example of a typical scatter plot is shown in Figure 3-1. These scatter plots are generated by calculating the reflectivity and off-perpendicular angles of each echo value. In this figure, a linear fit to the data has been performed manually.

Two important factors which must be defined are the calculation of reflectivity and the off-perpendicular angle. A detailed development of the equation associated with these parameters has been provided in a previous PAR auroral study report [2]. The definition of reflectivity is simply the effective radar cross-section per unit of illuminated volume. This is determined by dividing the apparent radar cross-section  $\sigma$  by the volume of the range resolution cell  $V(R, \rho)$ , where  $R$  is the apparent range of the echo and  $\rho$  is the total off-boresight angle. The PAR is a phased array radar, the beamwidth, gain, etc., depend on the off-boresight angle. These dynamic parameters must be taken into account in the processing of each echo.

The reflectivity ( $Z$ ) is given by:

$$Z = \frac{\sigma}{V(R, \rho)} \quad m^2/m^3$$

3.1

From [2], the effective radar cross-section  $\sigma$  is given by:

$$\sigma = \frac{(4\pi)^3 P_R R^4}{P_T G_T G_R \lambda^2 L_R L_p L_T \cos^3 \rho} \quad m^2$$

3.2

SCATTER PLOT WITH MANUAL CURVE-FIT SHOWING ASPECT RESPONSE

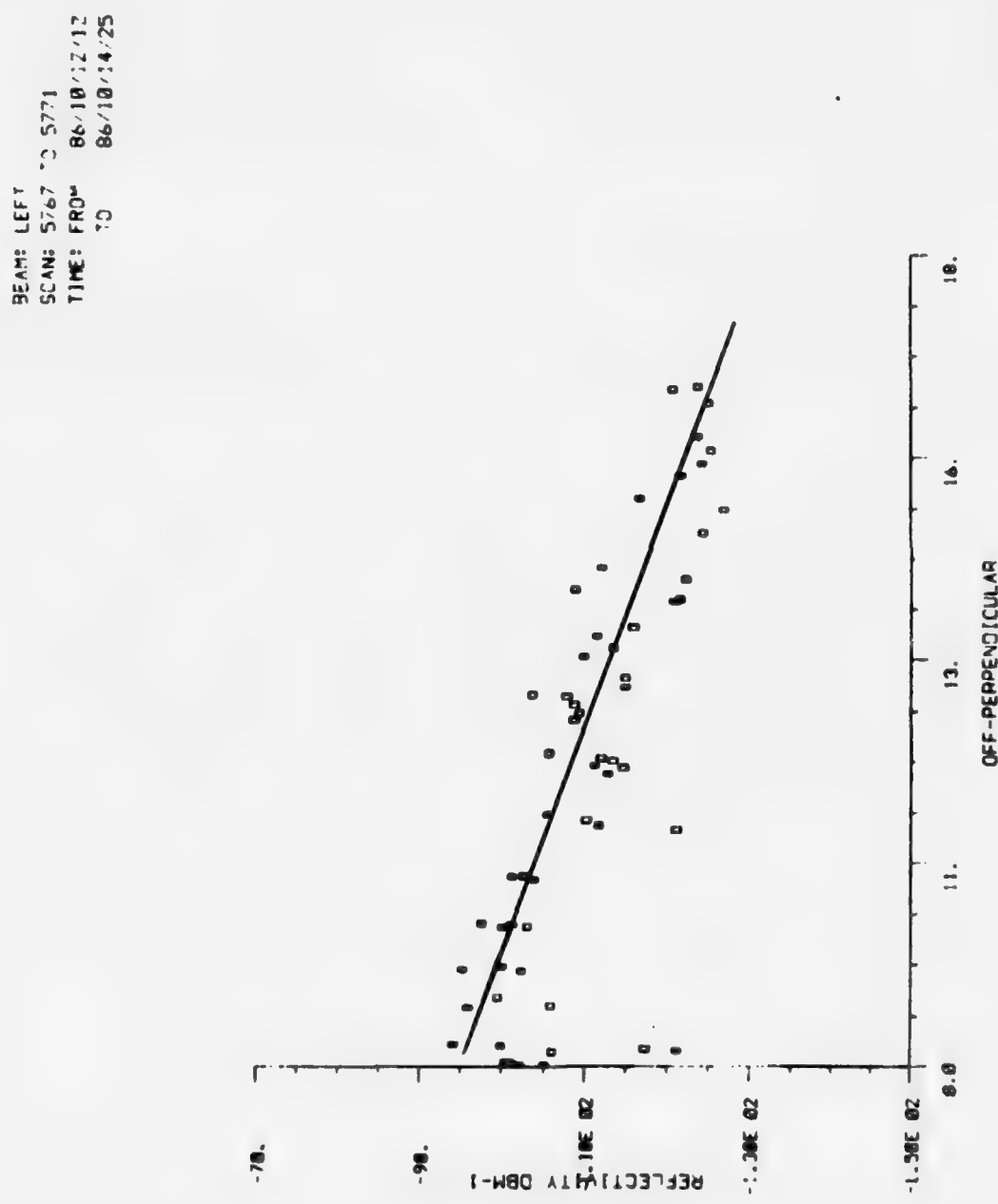


Figure 3-1

where:

$P_R$  = the echo power measured at the signal detector.

$P_T$  = the peak power measured at some convenient point in the system.

$L_T$  = the loss from the transmit power measurement point to the antenna face.

$G_T$  = the antenna power gain for transmit.

$G_R$  = the antenna power gain for receive.

$\lambda$  = the operating wavelength.

$R$  = the range to the center of the range resolution cell.

$\rho$  = the angle between the antenna boresight and the direction of the range resolution cell.

$L_R$  = the loss between the antenna face and the signal detector.

$L_p$  = the two-way attenuation along the propagation path.

After combining the constant terms and assuming a nominal, two-way propagation path loss ( $L_p$ ) of 0.4 dB, the equation becomes:

$$\sigma = \frac{P_R R^4}{Q \cos^3 \rho} \quad m^2/m^3 \quad 3.3$$

Calculation of the volume of the range resolution cell depends on whether the auroral arc fills the radar beam. If the arc only partially fills the beam, the cell volume is given by:

$$V_{\text{eff } p} = R \Delta H \frac{c r}{2} \frac{B \theta(0^\circ)}{\cos \theta} \quad m^3 \quad 3.4$$

where:

$\Delta H$  = the assumed thickness of the backscattering portion of the auroral arc.

c = the nominal velocity of light.

r = the compressed radar pulse width.

B<sub>θ</sub>(0°) = the azimuth beamwidth broadside to the antenna.

θ = the steered azimuth.

The cos θ term adjusts for the azimuth component of beam broadening as it is steered off-broadside.

Combining these equations and inserting the necessary parameters into the reflectivity equations yields:

$$Z = \frac{\sigma}{V}$$

$$Z_{\text{partial}} = \frac{P_r R^3}{1.18 \times 10^{16} \Delta H \cos \theta \cos^2 \rho} \text{ m}^2/\text{m}^3 \quad 3.5$$

Reflectivity is normally represented in logarithmic form with the reference being 1 M<sup>2</sup>/M<sup>3</sup>. The logarithmic form is given by:

$$Z \text{ dB} = 10 \log Z \quad 3.6$$

In this form, the quantity Z dB is called ZdB<sub>m</sub><sup>2</sup>/m<sup>3</sup> or ZdB<sub>m</sub>-1.

Generation of the scatter plot also requires the calculation of the off-perpendicular angle for each data point. This process requires a model of the earth's magnetic field. The model used in this study was developed using the "International Geomagnetic Reference Field 1965.0." [9]. The implementation employs a sixth-order spherical harmonic solution; the 48 terms used were updated to 1975 validity using the provided rate coefficients.

### 3.2 Special Techniques Employed to Enhance the Aspect Data

A number of problems and potential problems were encountered during the aspect study. These problems were minimized or eliminated using a number of techniques which will be described in the following paragraphs.

### 3.2.1 Pulse-to-Pulse Echo Decorrelation

It has been observed that the pulse-to-pulse echo intensity, from a given point in space, fluctuates very rapidly, becoming completely decorrelated in about 10 ms [6]. The observed distribution of echo intensities approximates the theoretical Rayleigh distribution shown in Figure 3-2. The use of data distributed in this fashion will produce a scatter plot with a significant dispersion, thus degrading the confidence interval of the curve fit. The quality of the aspect data has been improved through the point-by-point averaging of several, usually 6 to 10, volume scans. In this process, called "superscanning," a set of synthetic range bins are created for each pointing angle, then all the echo peaks from the corresponding range/bins of the different scans are averaged. This result is used as an estimate of the true mean echo intensity. It can be shown that a significant improvement is realized from this operation. Figure 3-3a shows the reflectivity of all the echo peaks from a single pulse plotted versus their off-perpendicular angles. Figure 3-3b shows the results when nine pulses from the same pointing angle, but from nine different scans, have been averaged. The improvement in dispersion is evident immediately. For this reason, averaging or superscanning is used in the processing of all aspect sensitivity data used in this study.

### 3.2.2 The Effects of Resolution

The primary factors which tend to degrade the results of aspect sensitivity analysis are the association of an echo sample with the wrong off-perpendicular angle, the allowing of other natural variations in auroral reflectivity to be attributed to changes in off-perpendicular angle, and the use of a geomagnetic field model which is not representative of the field which existed during the data collection.

The errors which result from limitations in radar resolution have a significant effect on the outcome of the analysis. The types of resolution which are of concern include not only the range, angle, and beamwidth resolution of the radar, but temporal resolution determined by the time required to perform the volume scans. The faster these volume scans can be performed, the less large-scale restructuring takes place during the scan.

Range resolution is determined primarily by the effective pulse width of the radar. Poor range resolution not only results in the association of echo peaks with the wrong off-perpendicular angles, but may result in an overall distortion in the shape of the aspect response characteristic. This phenomena has been reported by two sources [6] [7]. Figure 3-4a shows an aspect sensitivity plot at the PARL from a 400  $\mu$ s continuous wave pulse and Figure 3-4b shows the effect of using a chirped pulse with a compressed pulse width of 6  $\mu$ s.

OBSERVED AMPLITUDE DISTRIBUTION COMPARED WITH A THEORETICAL  
CALCULATED RAYLEIGH DISTRIBUTION [5]

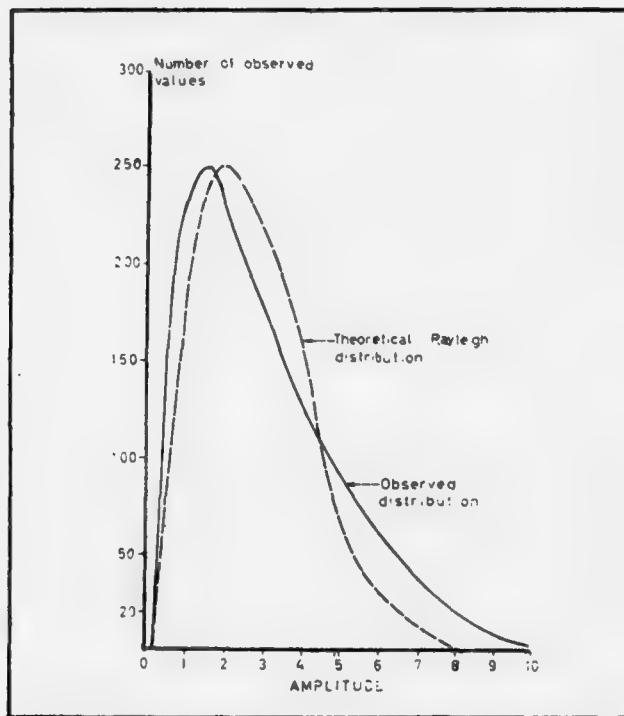


Figure 3-2

SCATTER PLOTS SHOWING EFFECTS OF SUPERSCANNING

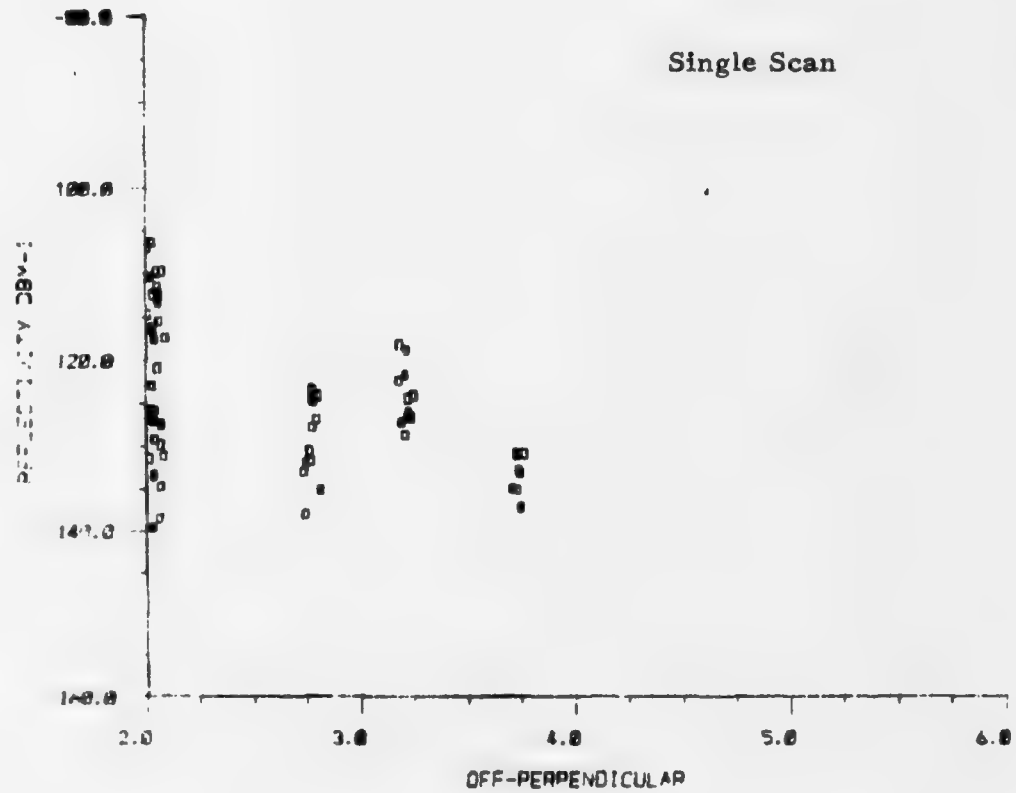


Figure 3-3a

SCATTER PLOTS SHOWING EFFECTS OF SUPERSCANNING  
(Continued)

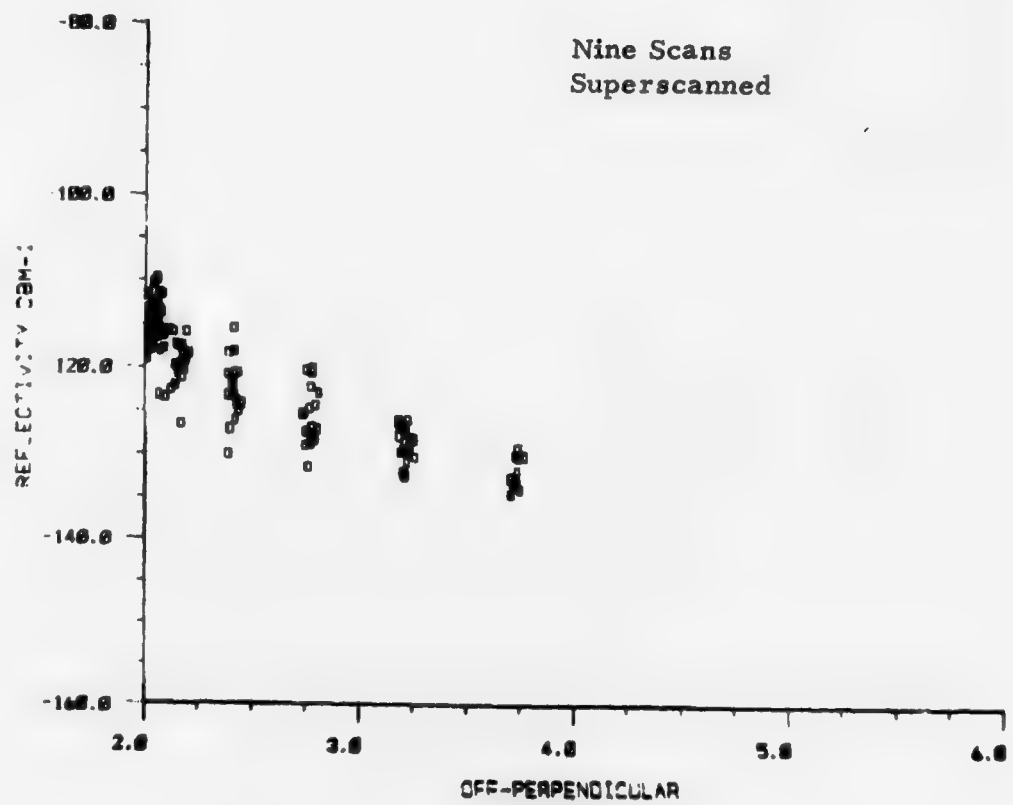


Figure 3-3b

DIFFERENCES IN APPARENT ASPECT RESPONSE WITH TWO DIFFERENT  
PULSE LENGTHS [6]

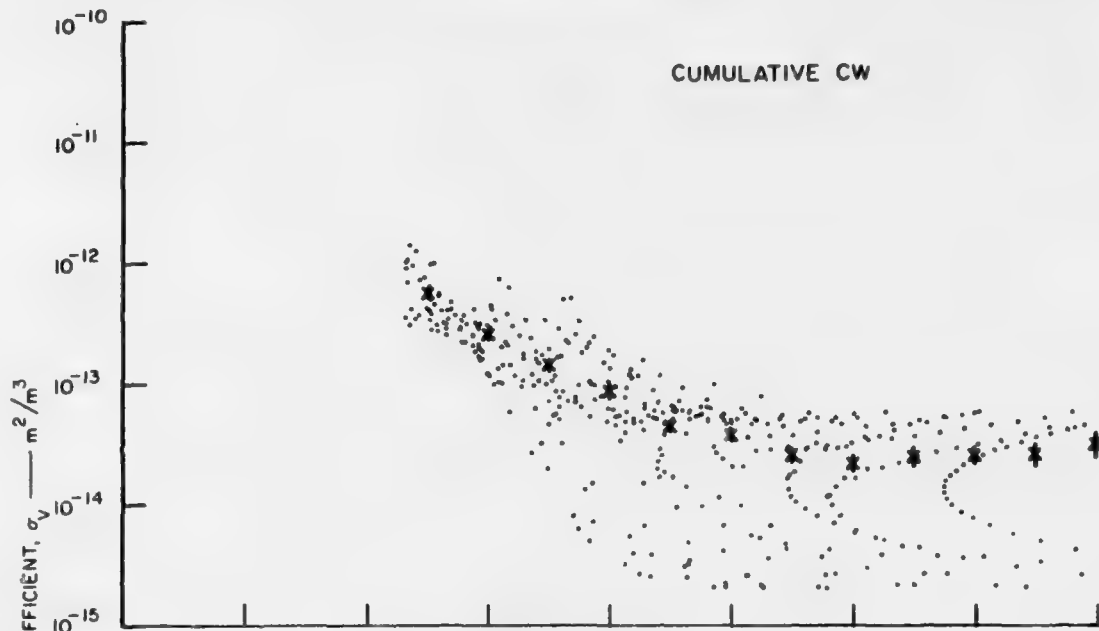


Figure 3-4a

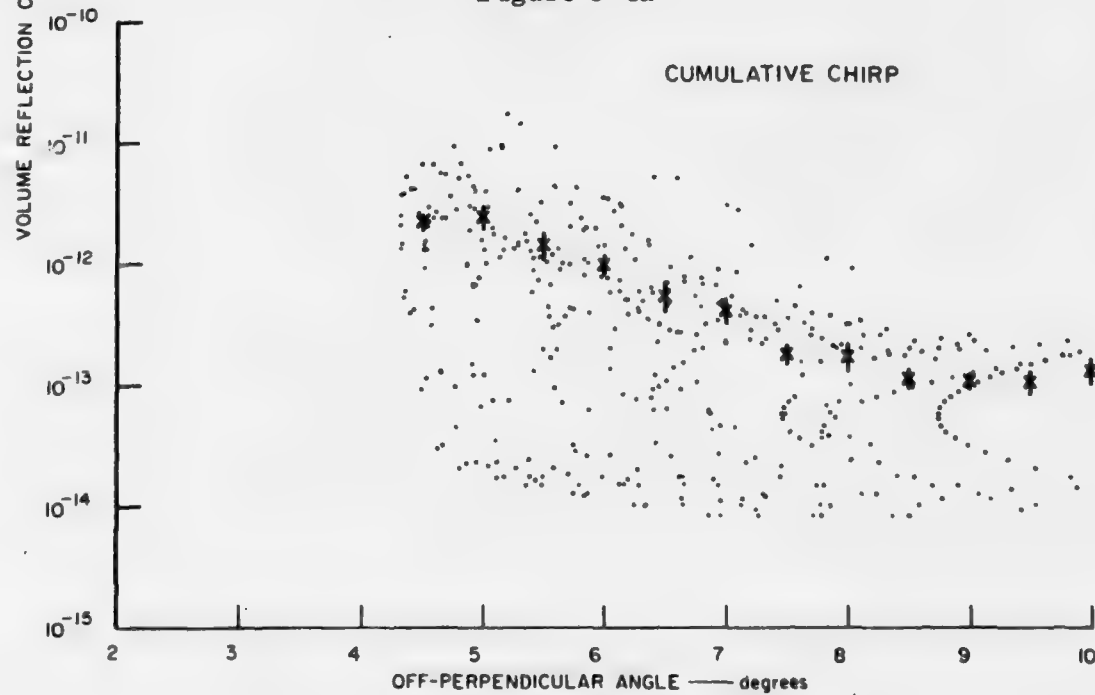


Figure 3-4b

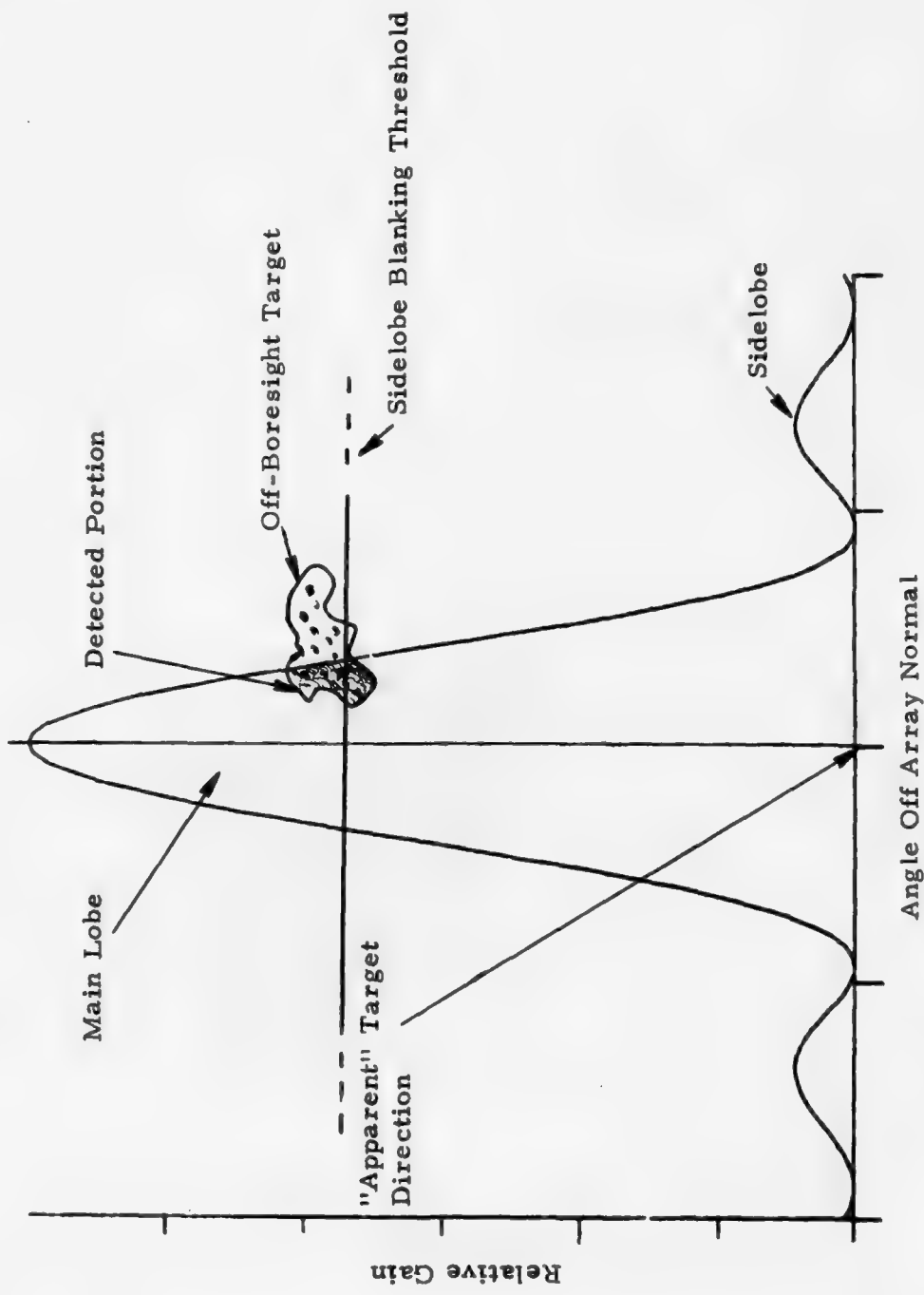
In this case, the slopes of the two aspect functions are similar, but the absolute reflectivity is about  $10\text{dBm}^2/\text{m}^3$  less for the CW pulse. This phenomena occurs because in each range resolution cell, the power measured in the echoes is a composite of the reflections from all regions within this cell; the total cell volume is then used to calculate the reflectivity. If there are inconsistencies in the scattering medium, then, for longer pulse widths, the measured echo may no longer be representative of the reflectivity of a finer-grained irregularity structure. Because of its increased resolution, the shorter pulse width produces a more accurate representation of the local reflectivity.

Angular resolution is determined by the accuracy involved in pointing the center of the radar beam. This error is usually small in comparison to the effects of beamwidth and divergence. The beamwidth resolution problem occurs because in the search mode, the radar associates the angular origin of all echoes with the center of the beam. The scatterers from which the measured energy was reflected are not necessarily located at the center of the beam. In fact, when the reflectivity of the scatterers is high, echoes which originated several degrees from the center of the beam can still be detected, as shown in Figure 3-5 which shows the region near the main lobe of a radar beam. This means that during the radar's volume scan the same scattering region may be detected several times. Detections with the strongest amplitude will occur when the beam is pointed directly at the scatterer, but weaker echoes will occur whenever the beam gets within a few degrees of the scattering region. This effect spreads and distorts the apparent aurora in a predictable fashion. For the PAR, the maximum off-beam-center angle at which the radar could record auroral returns is limited by the sidelobe blanking system or Q-channel. The Q-channel provides a high probability of rejecting most echoes which originate from over about  $1.7^\circ$  from beam center. It should be noted that a number of sidelobe returns will also be detected because of the statistical properties of the auroral echoes and because the Q-channel becomes less effective for weak echoes.

It is important to understand that the echo power measured at any instant by the receiver is a superposition of echo power from the same slant range but from all directions -- main beam as well as sidelobes. When there is large-scale blanketing aurora, significant power may be reflected from many angles. The Q-channel cannot eliminate these echoes when they return simultaneously with echo power in the main lobe. This unwanted power is thus added to and processed with the main beam echoes. An unavoidable error in the determination of auroral reflectivity has thus been identified.

The divergence of the conical beam makes this distortion a function of range, thus the spreading is more extreme at the greatest ranges. Figure 3-6, a profile plot of an auroral arc, illustrates this effect very clearly. The apparent thickness of the arc is a function of range and appears to be converging to its true value directly over the radar, as would be expected. Unfortunately, loss

NEAR-BORESIGHT ANTENNA PATTERN



**M&S COMPUTING**

Figure 3-5

PROFILE REFLECTIVITY MAP SHOWING EFFECTS OF BEAM BROADENING

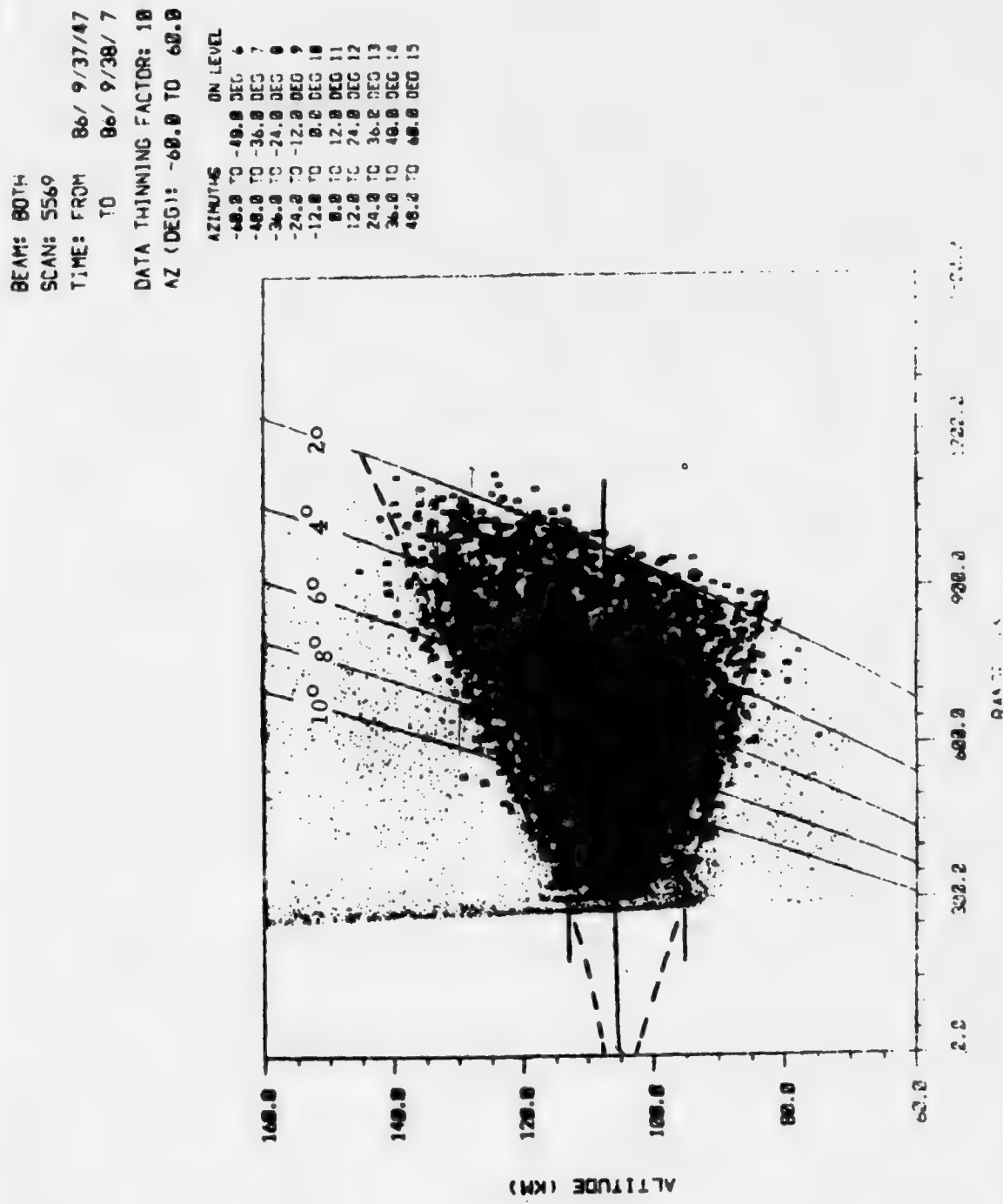


Figure 3-6

in signal strength due to the magnetic aspect response, as well as hardware limitations, precluded direct overhead observation. But with some analysis it can be shown that the arc is very thin. In a region of high reflectivity such as that shown in Figure 3-6, auroral echoes can be expected to originate out to the extreme of the  $1.7^\circ$  blanking limit. The weak echoes above and below the dense region result from sidelobe returns which are not blanked by the Q-channel. Thus, near the radar at the cutoff range, the beamwidth effect should increase the apparent thickness of the arc by about 18 km. The "apparent" thickness of the arc is shown in Figure 3-6 to be only about 20 km. It is apparent that if the reflecting region was much over a few km thick, the profile would be correspondingly thicker at the indicated range. From this simple analysis, the thickness of the reflecting region could be estimated to be from 2 to 5 km. This estimate is not far from the results of previous studies [7, 10] in which the arc was estimated to be 6 to 8 km thick in the first case and in the latter, 2.5 km thick. Unger determined the arc thickness by deconvoluting the measured data by using the known characteristics of the radar beam [7].

Using this same technique, it is possible to calculate the shape of the distorted arc as it appears to the radar. The boundary of this region has been plotted on the profile plot of Figure 3-6. It can be seen that the observed arc matches very closely the predicted shape.

It can be shown by this analysis of beamwidth effects that large errors can occur if one attempts to use the backscatter data from all altitudes to characterize the aspect response function. Figure 3-7, a profile view of the "apparent" arc, shows the off-perpendicular contours at  $0^\circ$  azimuth. It can be seen from this plot how the apparent location of the dispersed echoes changes their relationship to the magnetic field. This results in an improper determination of the aspect response function. Scattering centers can be mislocated by over 60 km resulting in errors of over  $2^\circ$  off-perpendicular. It is therefore important to eliminate any echoes which did not originate from near the center of the beam. This can be done easily because of one very important fact: when an echo originates near beamcenter, both the apparent and the actual location of the scatterer conicide. Furthermore, if the altitude of the arc is known and only echoes which originated near this altitude are selected, then essentially all off-axis echoes will have been eliminated. From Figures 3-6 and 3-7, the altitude of the arc can be closely estimated to be about 105 km.

Another means of estimating the altitude of the center of the arc is by use of a scatter plot to generate a profile of reflectivity versus altitude. Figure 3-8 has been prepared to illustrate the techniques to be described. The radar beam intersects the thin auroral arc at a low elevation, as shown. Because of

PROFILE VIEW SHOWING AURORAL REFLECTIVITY

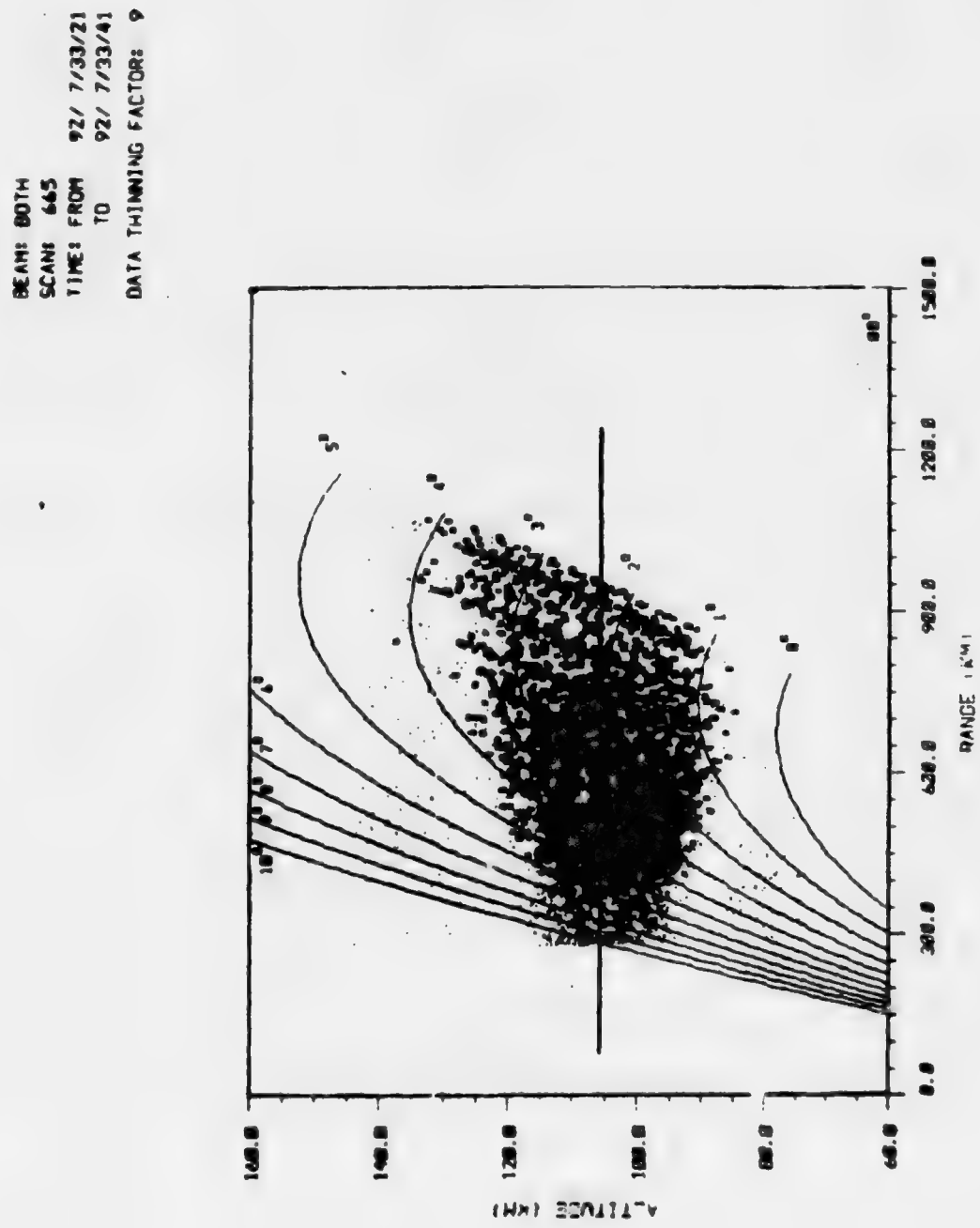


Figure 3-7

its high resolution, there are many range resolution cells which will return echoes to the radar. The radar, however, cannot properly locate the angle of the echoes from those cells which are not on beamcenter.

The radar provides an accurate measurement of range to the cell. However, the direction of the cell can only be assumed to lie along the central angle of the beam (the dashed line in Figure 3-8). The echo cells are thus mislocated in altitude except for the cell which was actually in the center of the beam. Furthermore, the gain of the antenna is lower for all but the center cell, so the relative response during a single pulse would be expected to resemble that shown in the lower portion of Figure 3-8. This plot peaks near the location of the center cell which is also the cell with minimum altitude error and thus truly represents the reflectivity of the arc. Thus, on a scatter plot showing reflectivity versus altitude, a peak should occur at the altitude where the center of the arc occurs. Figure 3-9 is a single pulse example showing this phenomena and that the arc is indeed centered near 105 km. Figure 3-10 is a similar plot of all the pulses in a scan. The shape of this curve demonstrates the distortion in the "apparent" reflectivity which occurs if echoes are used which did not originate near beamcenter. A plot of reflectivity versus off-perpendicular angle for a single pointing angle is shown in Figure 3-11. Data from all altitudes is included in this plot. In this plot, the off-perpendicular angle increases with slant range and thus with increasing altitude. From the plot, it can be seen that the reflectivity steadily increases with altitude until it peaks; it then falls above this height. It can be shown that this peak occurs near the center of the arc, in this case about 105 km. The shape of the curve approximates the shape of the peak of the radar beam, in that the image of the aurora is the convolution of the entire radar beam with the "actual" auroral scattering region. The curve trails off at a decreased slope beyond  $4^{\circ}$  off-perpendicular because of the superposition of sidelobe returns with those from the mainbeam.

Figure 3-12, which includes a large number of pointing angles, shows what happens if auroral backscatter data from all altitudes is used in the scatter plot. The curves from the individual pointing angles are still discernable as well as the low reflectivity independent sidelobe returns.

It is readily apparent from this plot that little confidence could be placed in any curve fit through this superposition of data. Figure 3-13 has been generated using the same data as Figure 3-12, except that data from 105 to 106 km only is included. It can be seen that these data points consist of the peak reflectivities from the individual pulses or from near the center of the reflecting arc. As a result of this analysis, all data for succeeding scatter plots was selected from within 1 km of the estimated center of the reflecting region. The peak of the altitude versus reflectivity plots is broad enough so that an error of even  $\pm 3.5$  km in the estimation of this peak would result in little error.

## MISLOCATION OF SCATTERING CENTER FROM BEAM DIVERGENCE

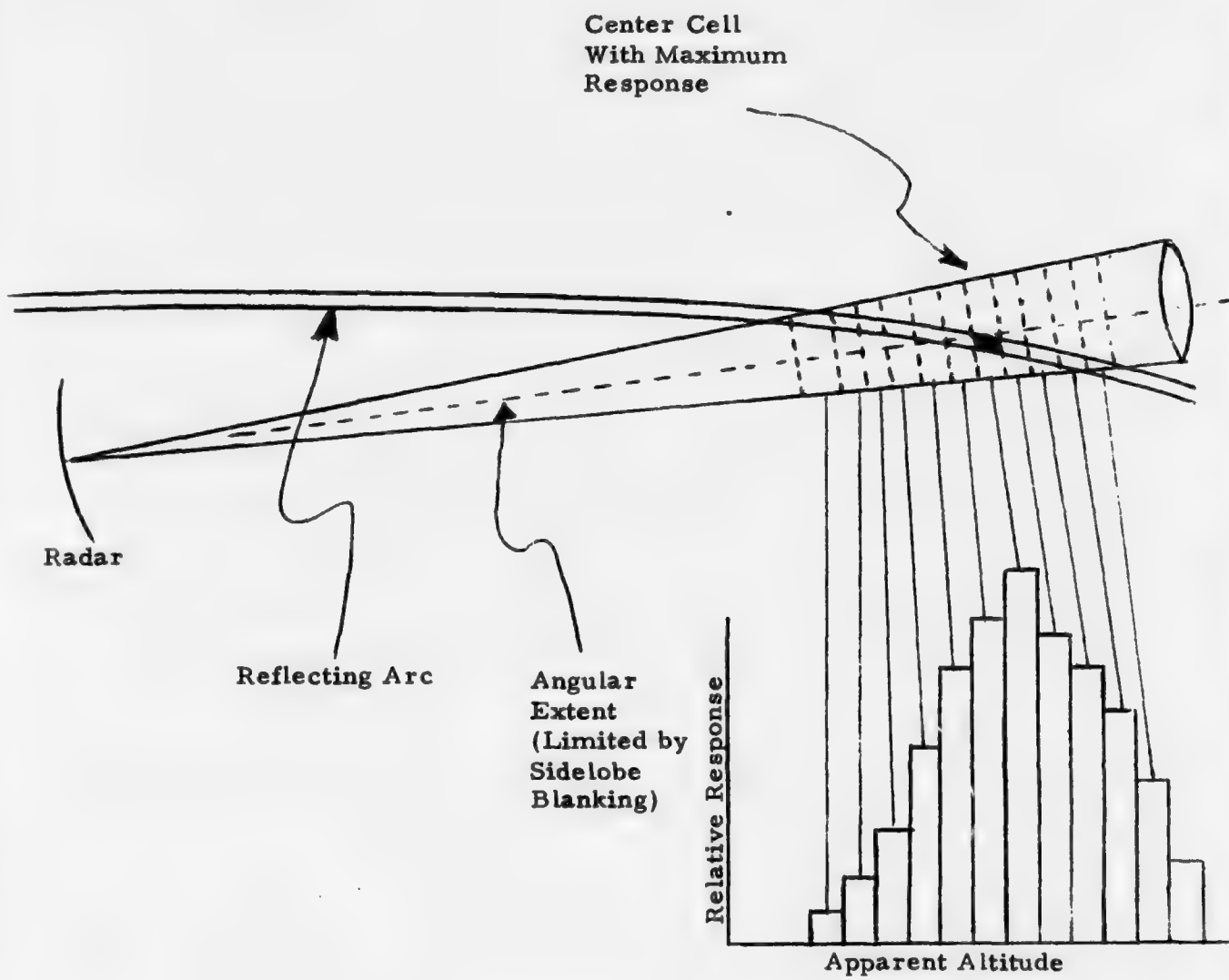


Figure 3-8

ALTITUDE VERSUS REFLECTIVITY PROFILE FOR ONE PULSE

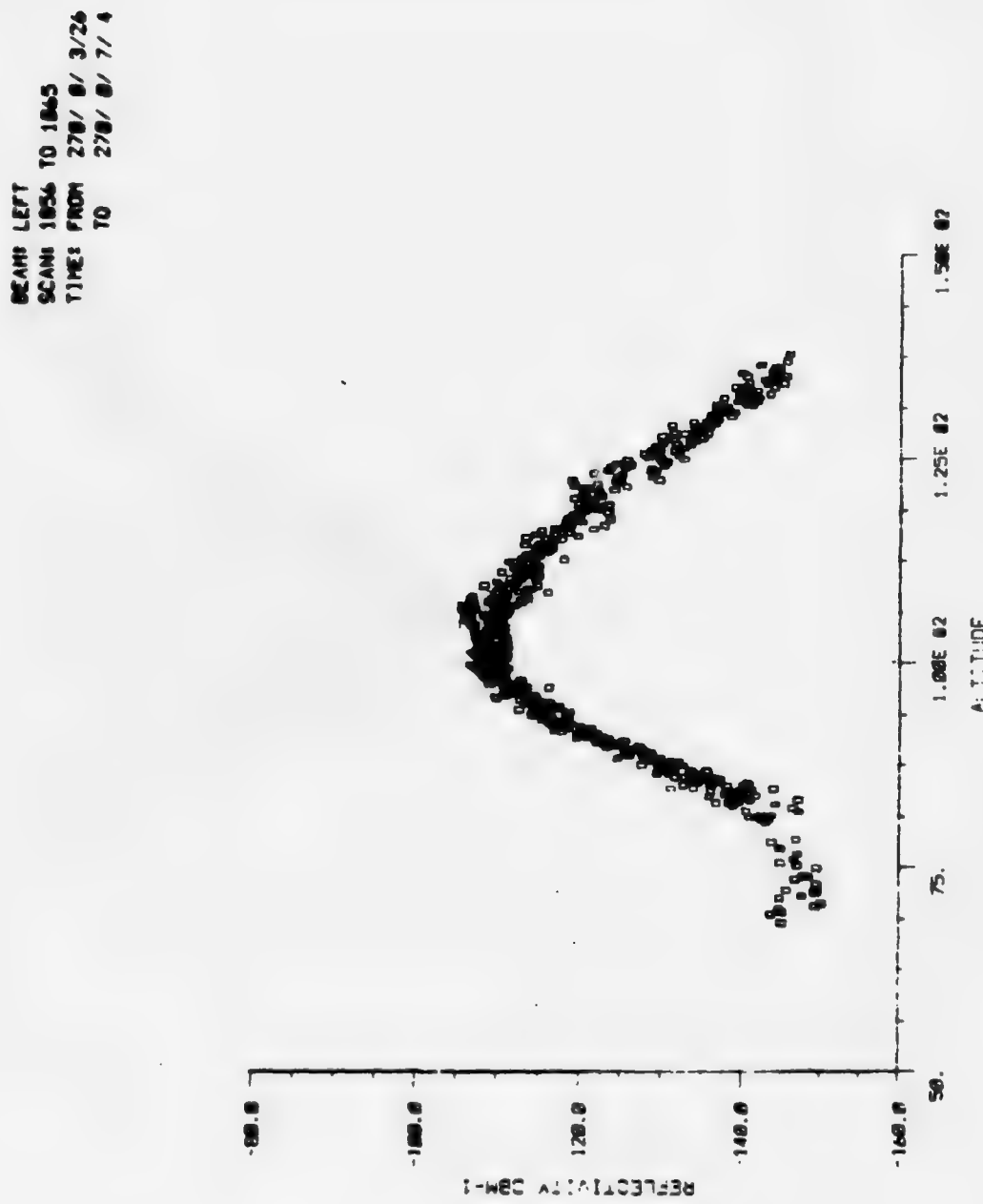


Figure 3-9

ALTITUDE VERSUS REFLECTIVITY PROFILE FOR AN ENTIRE SCAN

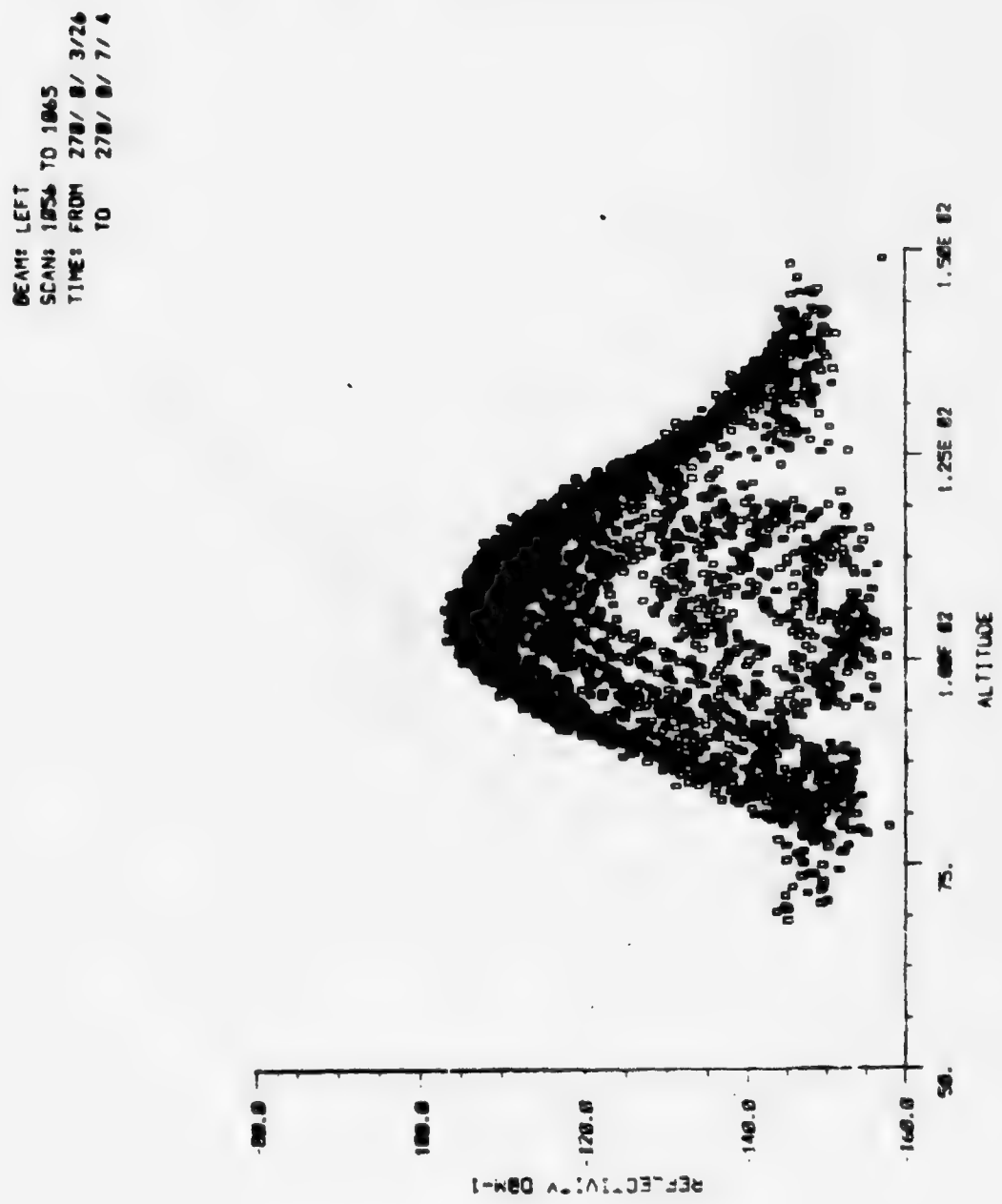


Figure 3-10

ASPECT RESPONSE CURVE FOR ALL ALTITUDES AT ONE POINTING ANGLE

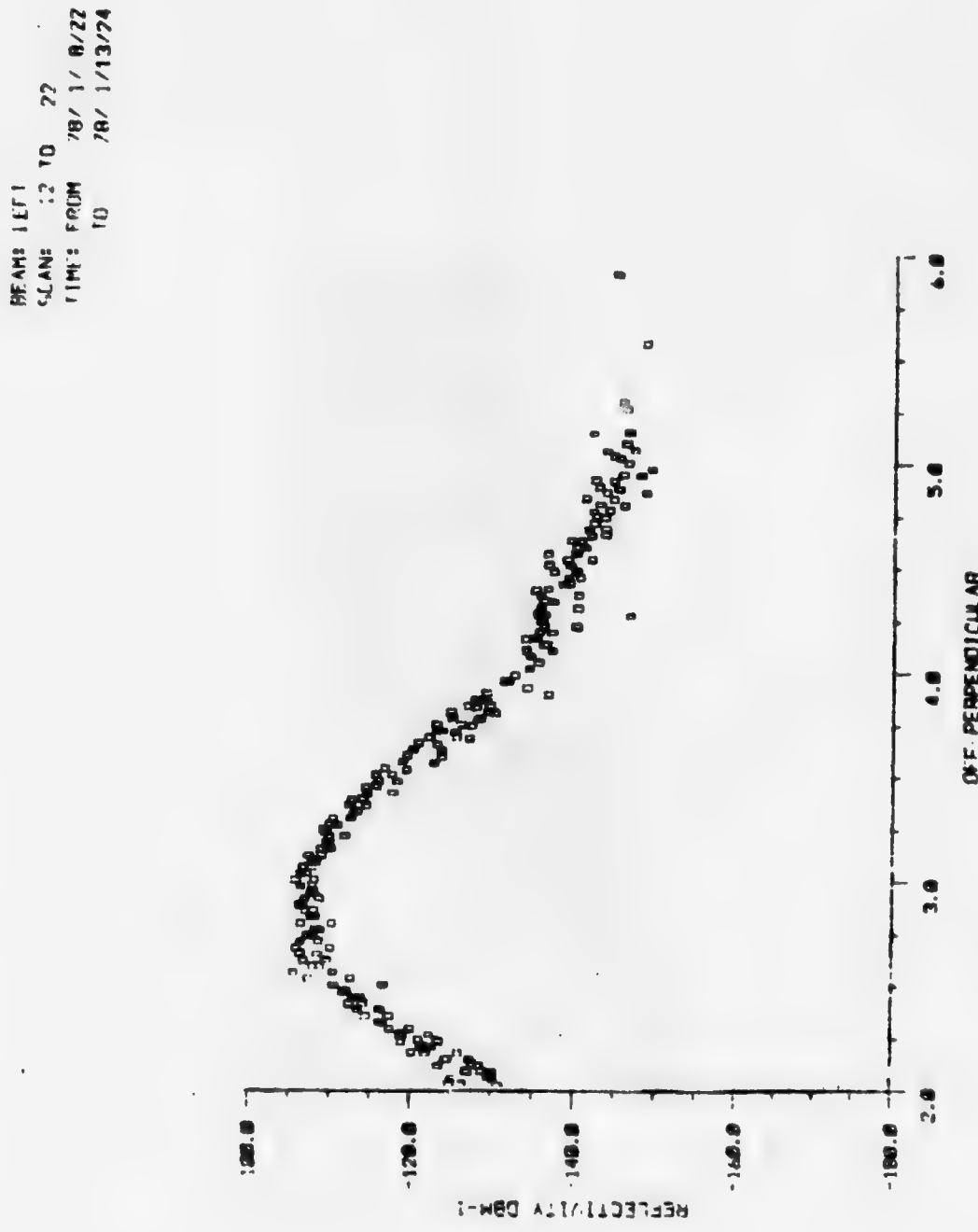


Figure 3-11

ASPECT RESPONSE CURVE FOR ALL ALTITUDES

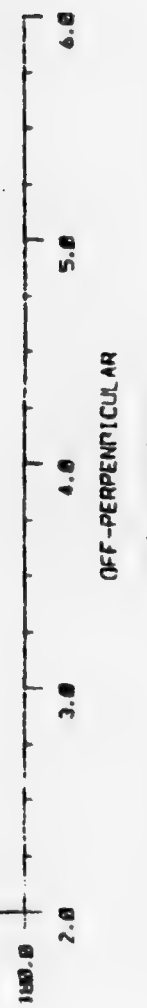


Figure 3-12

ASPECT RESPONSE FOR 105 - 106 km

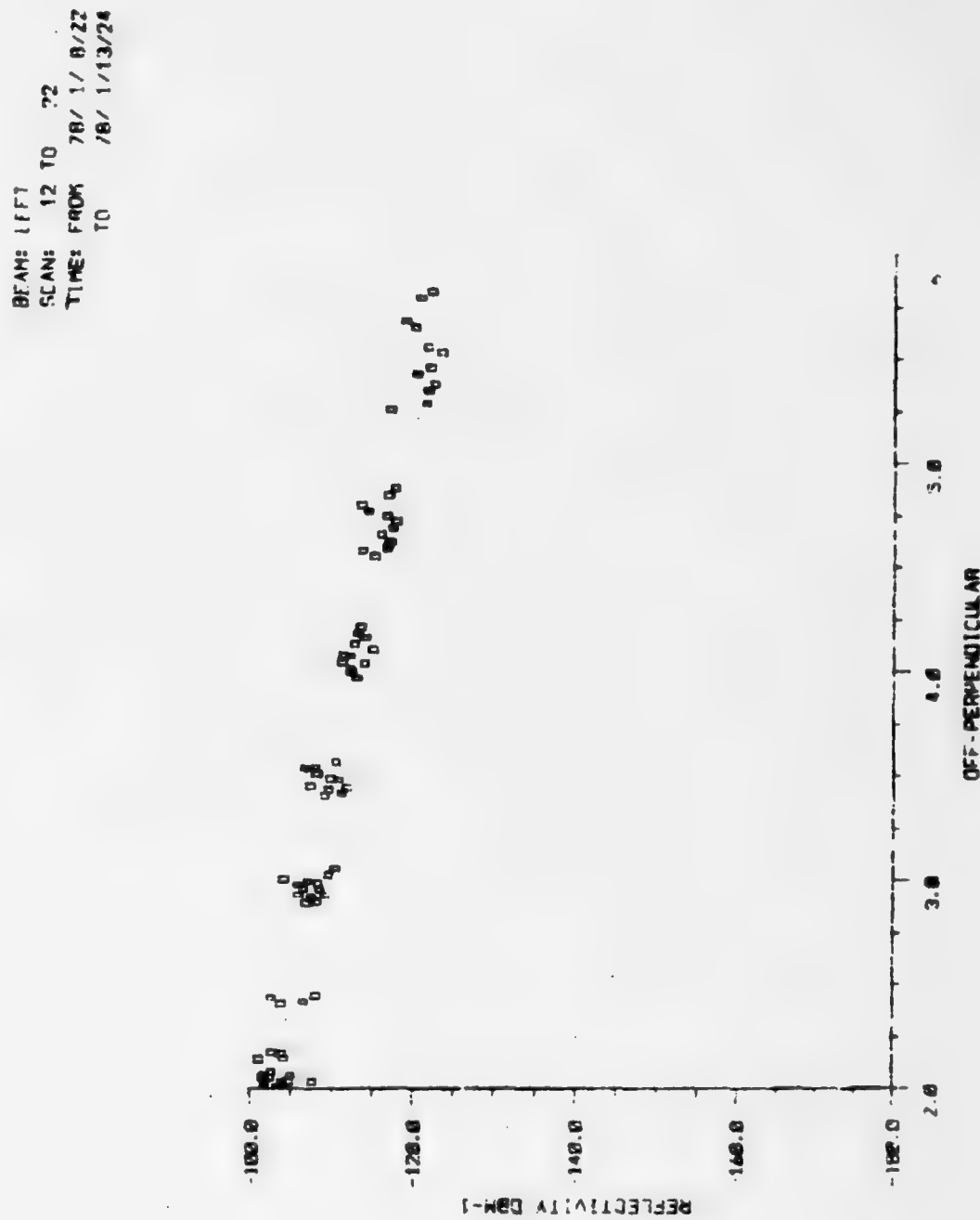


Figure 3-13

Another problem encountered in the aspect study results from regional variations in auroral reflectivity. These inconsistencies which appear as voids, edges, or overall shifts in reflectivity are not caused by the normal aspect relationship. An example of an auroral scan with gaps is shown in Figure 3-14. The off-perpendicular contours have been overlaid on this data providing a straightforward method for determining what magnetic aspects will be represented on the scatter plot. This figure shows the sharp regional changes in reflectivity which are often observed. The shifts in the overall reflectivity for another such scan are apparent in Figure 3-15. The scatter plot has a pattern containing three segments, each of which is obeying the same predictable aspect response function except that each is offset by an overall scale factor. Further investigation showed that each segment of this scatter plot was generated from echoes originating in widely separated regions.

In order to minimize this problem, care must be taken to select data from auroral forms which are as homogeneous as possible. This selection increases the probability that the changes in apparent reflectivity observed on the scatter plot truly represent the effects of the aspect response function. As a result of these observations, each scan used in the PAR aspect study was first plotted on a top-down map with off-perpendicular contour overlays as was shown earlier in Figure 3-14, and the data used to generate the scatter plots was taken from regions in which the auroral echoes appeared homogeneous. An important factor was to assure that the data was selected from a region including the widest range of off-perpendiculars within the smallest possible region. This minimized the degradation in the results due to the regional variations in auroral makeup which were discussed previously. This data selection was accomplished with the aid of a specially designed spatial filter and a special top-down overlay which shows the position at which each beam penetrates the altitude shell at the center of the arc. Using this overlay, shown in Figure 3-16, it was possible to select the exact steering angles from which to obtain data. By observing the top-down slice corresponding to the 105 km altitude, it was possible to pick the beam positions from which echoes were detected at extreme off-perpendicular angles while assuring elimination of voids, edges, etc.

One more problem inherent in this or any aspect study is determining whether the magnetic field model realistically represents the actual magnetic conditions which were valid at the time of that collection. Associated with an auroral arc is a strong current flow which distorts the local geomagnetic field.

Two techniques were employed to minimize field distortion-related errors for discrete arcs. The first was to examine the magnetometer data from Fort Churchill, Canada, participating research station located near the auroral arc being observed. The location of Fort Churchill is shown on the map in Figure 1-1. Backscatter data was not used for aspect calculations when the

TOP-DOWN REFLECTIVITY MAP SHOWING VOIDS

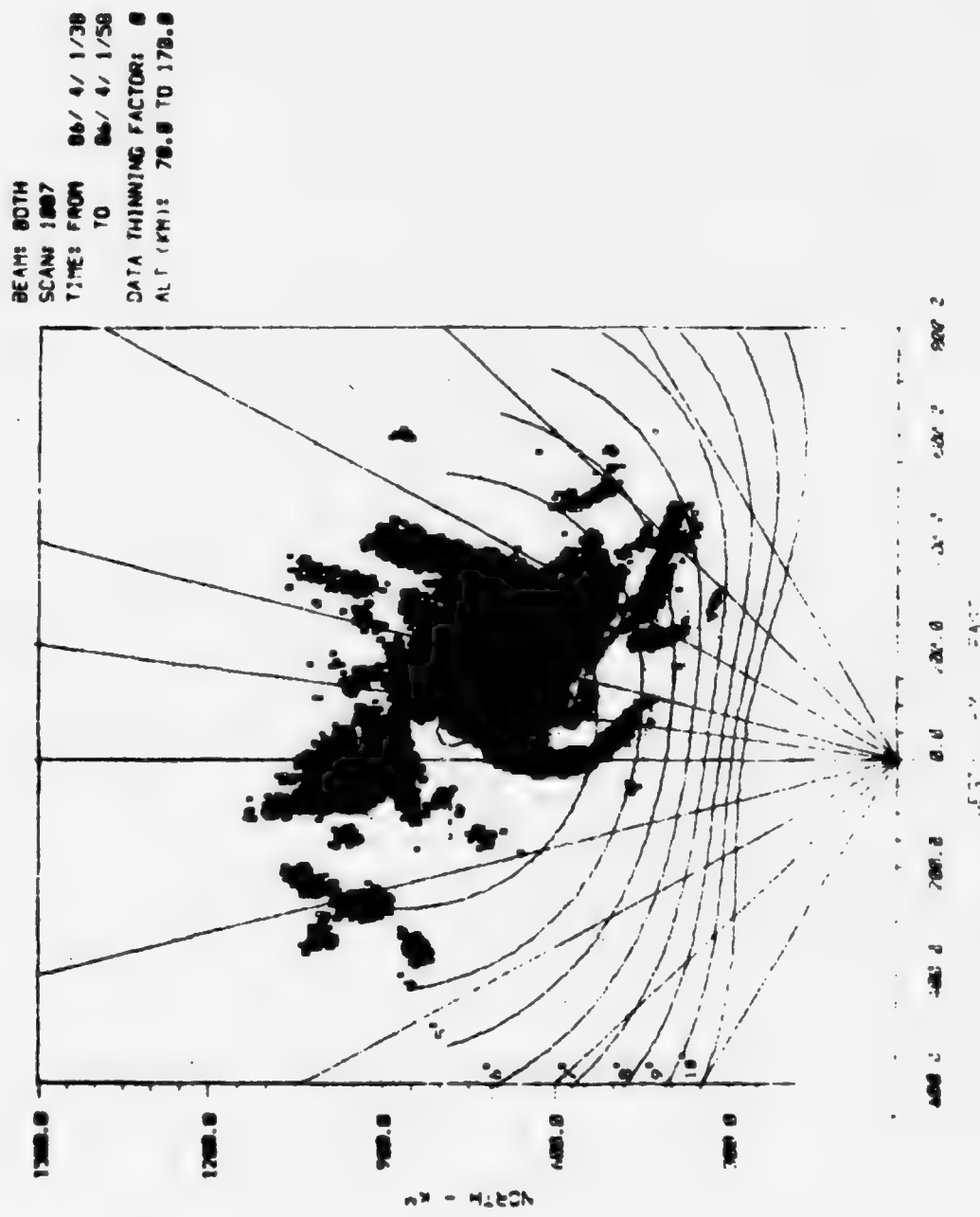
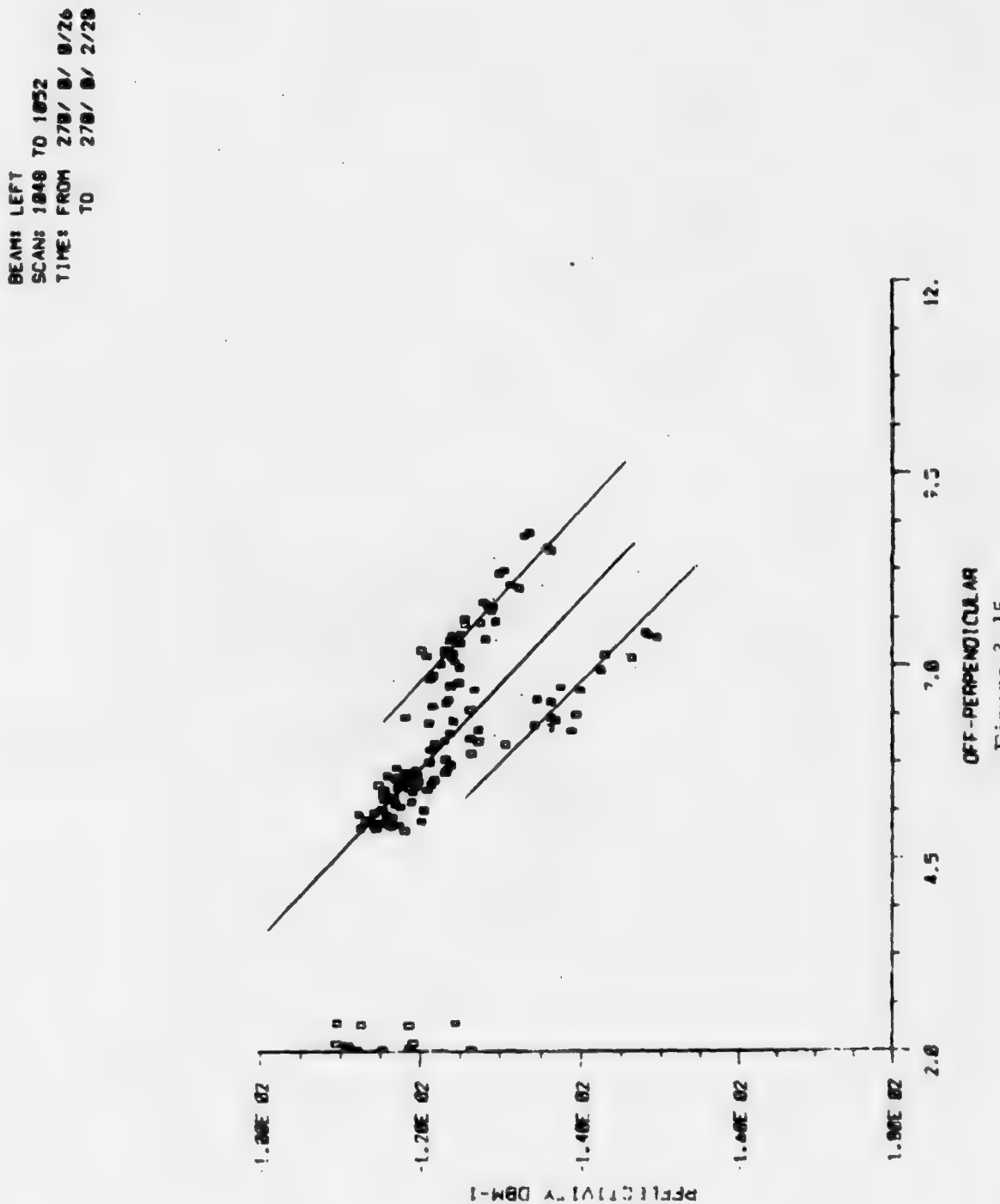


Figure 3-14

ASPECT RESPONSE SHOWING DISCRETE REFLECTIVITY SHIFT



TOP-DOWN OVERLAY WITH POINTING ANGLES AT INTERSECTIONS

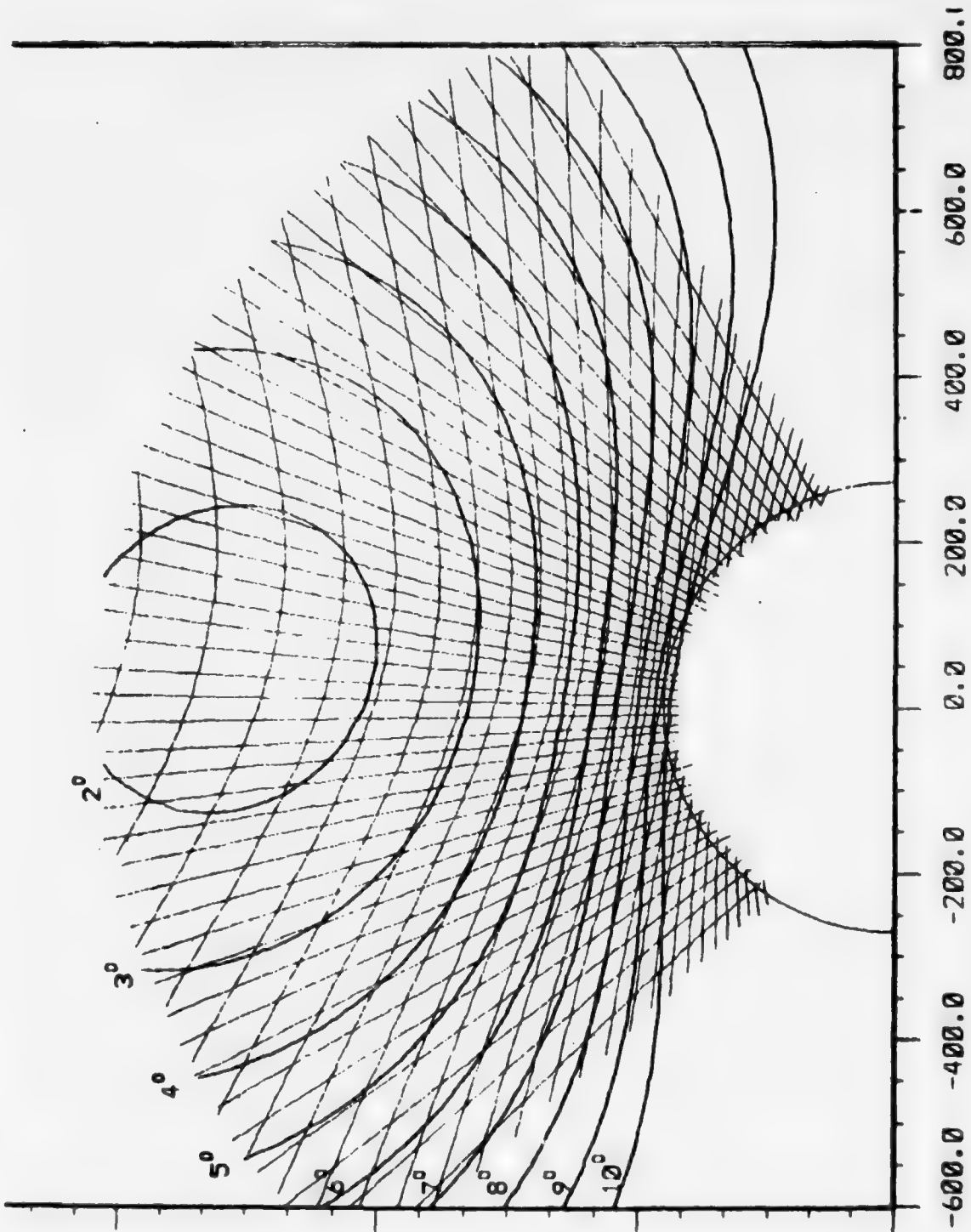
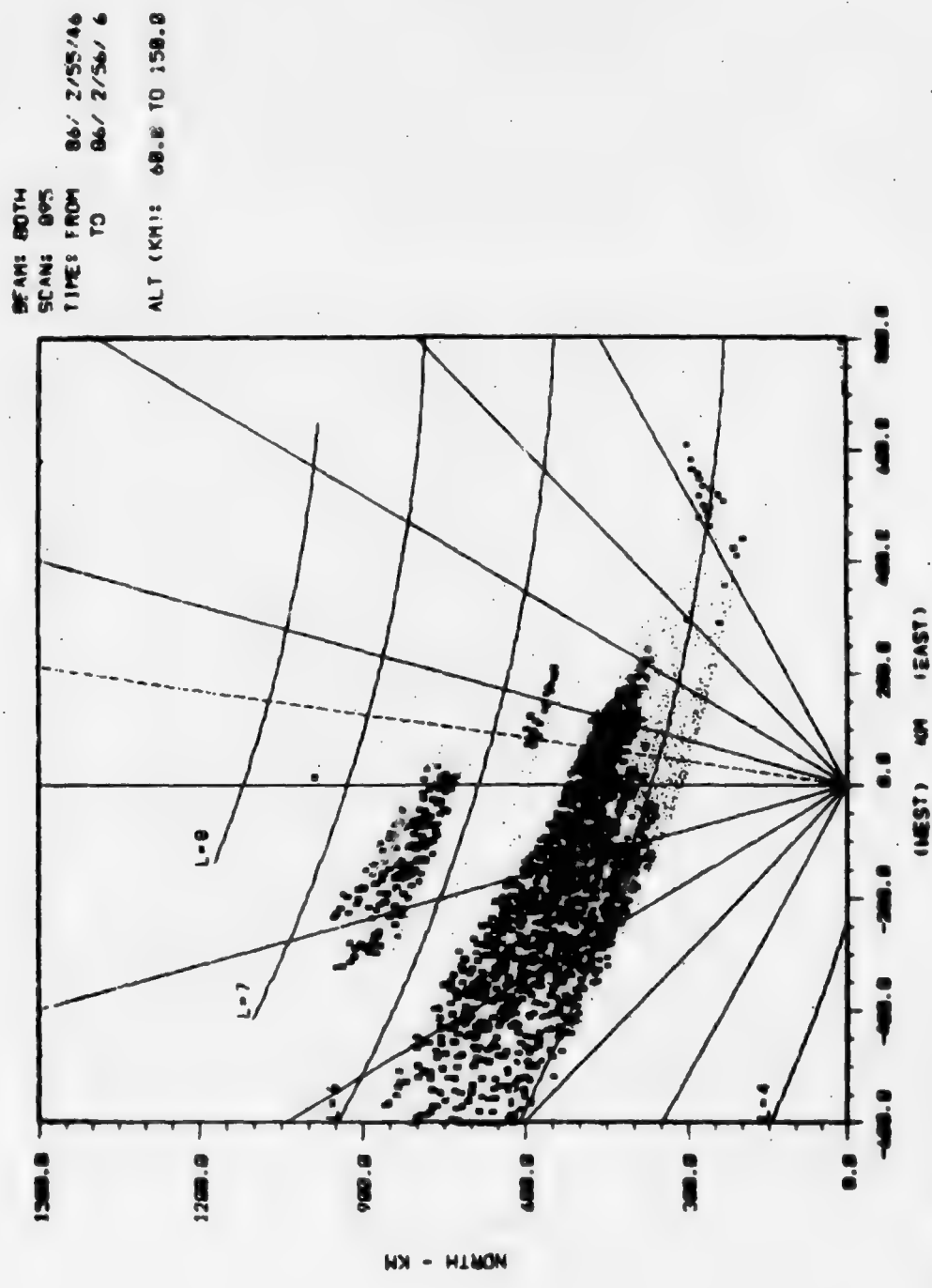


Figure 3-16

geomagnetic field was unstable or if any of the components had deviated by much more than 100 gammas from the nominal baseline.

The second technique is based on the fact that the auroral arc is normally aligned with the magnetic L-shells. This phenomenon can be used as an indicator of the magnetic distortion by plotting the L-shells on a top-down radar map of the arc as shown in Figure 3-17. In this study, only well-aligned arcs have been used to calculate the aspect response. Although this technique alone does not assure a minimization of effects from magnetic distortion, combining it with the magnetometer screening offers a measure of improvement in results, especially in repeatability over the use of randomly selected data. The results of the analysis reveal a phenomena associated with discrete arcs which suggest that, although the above technique may assure a degree of repeatability, a significant local magnetic distortion is inherent with these discrete forms. It appears that this distortion may result in an extreme shift in the magnetic aspect response characteristic. This phenomena will be discussed further in a later section.

TOP-DOWN REFLECTIVITY MAP WITH L-SHELL CONTOUR AT 105 km



COMPUTING

Figure 3-17

#### 4. DATA CASES USED IN THE ANALYSIS

Several test cases were carefully selected for the aspect study. They consist of both diffuse and discrete forms. A special distinction has been made between these two basic forms because of the recognition of a clear difference between the "apparent" aspect response characteristics of each type. Data represented in this study was collected on September 27, 1975, and on March 10, 18, 26, and 31, 1976. The next few sections show the results of the data reduction for each test case. Included is a top-down auroral map with overlaid 105 km off-perpendicular contours showing the region where the scatter plot data was selected. Two types of scatter plots are generally included. The first shows a reflectivity versus altitude plot used to locate the center of the reflecting arc as described in Section 3; the second shows the reflectivity versus off-perpendicular angle. A curve-fit has been performed on each of these scatter plots.

##### 4.1 Test Case 270/1058

The first test case occurred on September 27, 1976. A top-down auroral reflectivity map of this scan is shown in Figure 4-1. This auroral scan occurred during a period of relatively low magnetic activity as indicated by the nearby Fort Churchill, Canada, magnetometer data. The deviations, from their calibrated baseline of the three magnetic components, were 80% for the X component, 45% for the Y component, and 5% for the Z component. The three traces were essentially flat during the time of the scan. The riometer reading was also quiet and at a null. The peak signal-to-noise ratio of these echoes was 60 dB and they averaged about 30 dB. The map shows a typical quiet diffuse form or possibly the south edge of an arc. Good aspect data may be expected due to low magnetic field distortion within the region covered. The reflectivity versus altitude plot in Figure 4-2 shows the center of the arc to be near 105 km, so aspect sensitivity data was selected only from within the 105-106 km band. By examining the relationship of the off-perpendicular contours to the aurora, shown in Figure 4-1, it can be seen that the off-perpendicular angles from which echoes originated range from  $2^{\circ}$  to  $8^{\circ}$ . To determine the aspect sensitivity, Figure 4-3 was generated using echo data from the small region A shown in Figure 4-1. Data for the second scatter plot (Figure 4-4) came from region B. These two cuts were made in order to evaluate any differences in the apparent aspect response when data was sampled approximately parallel to the L-shell as in region A or perpendicular to the L-shells as in region B.

The two scatter plots demonstrate a clear difference in apparent aspect sensitivity. When the data points are selected along region A, a 7.34 dB/deg slope was measured, but from the region perpendicular to the L-shells (region B), a 16.3 dB/deg slope was found.

TOP-DOWN REFLECTIVITY MAP OF SCAN 1058

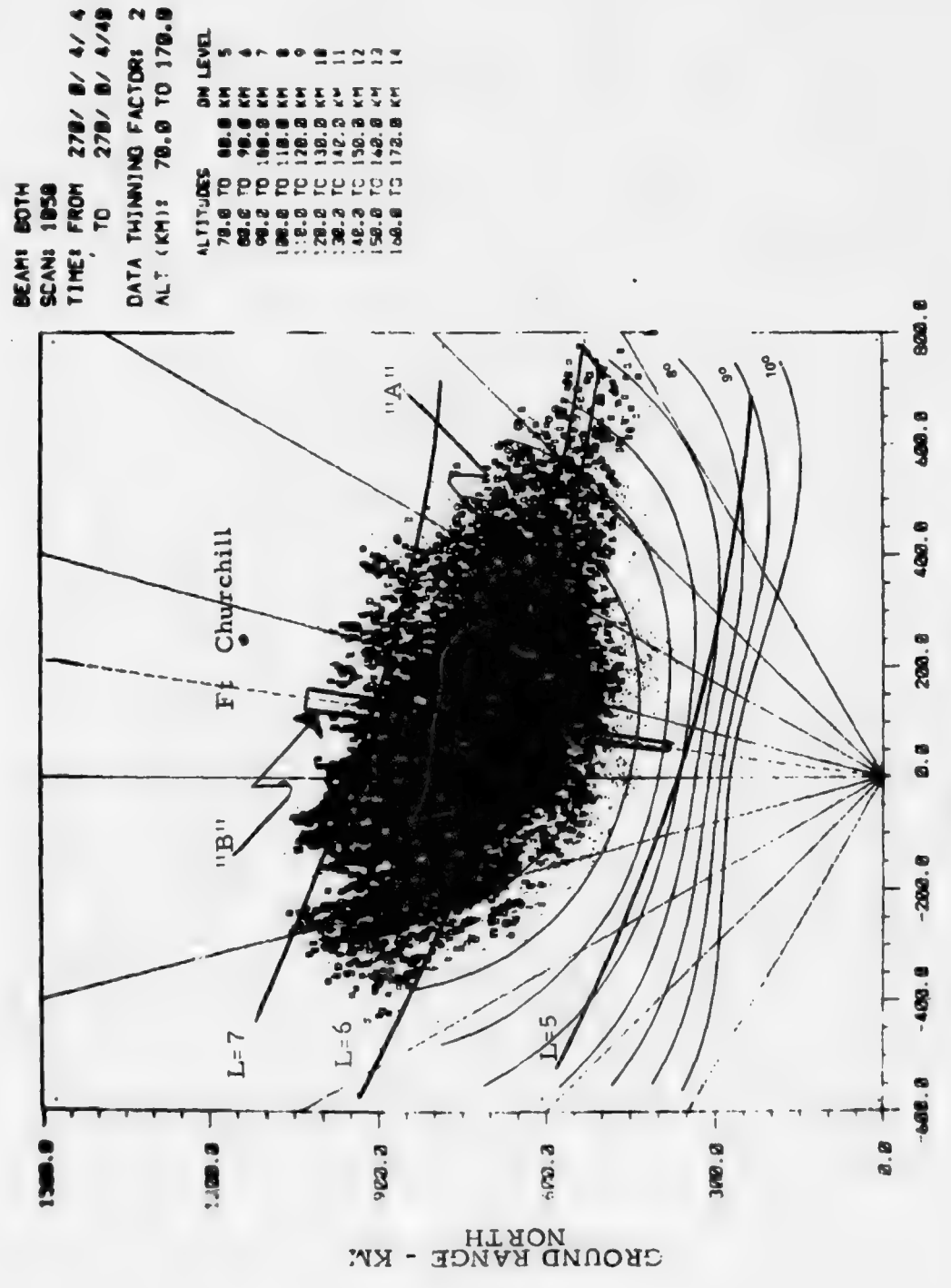


Figure 4-1

SCATTER PLOT SHOWING ARC CENTER

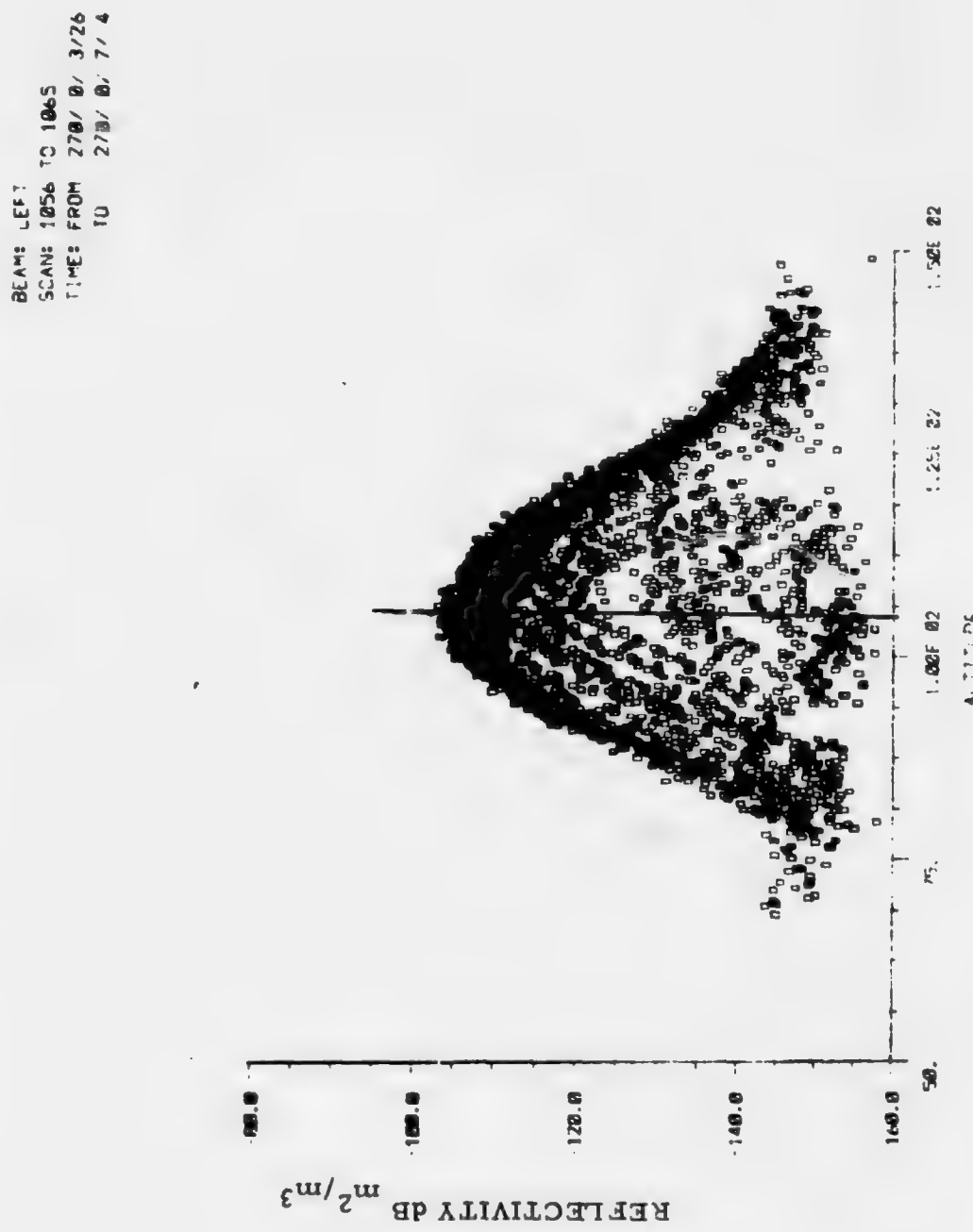


Figure 4-2

SCATTER PLOT FROM REGION "B"

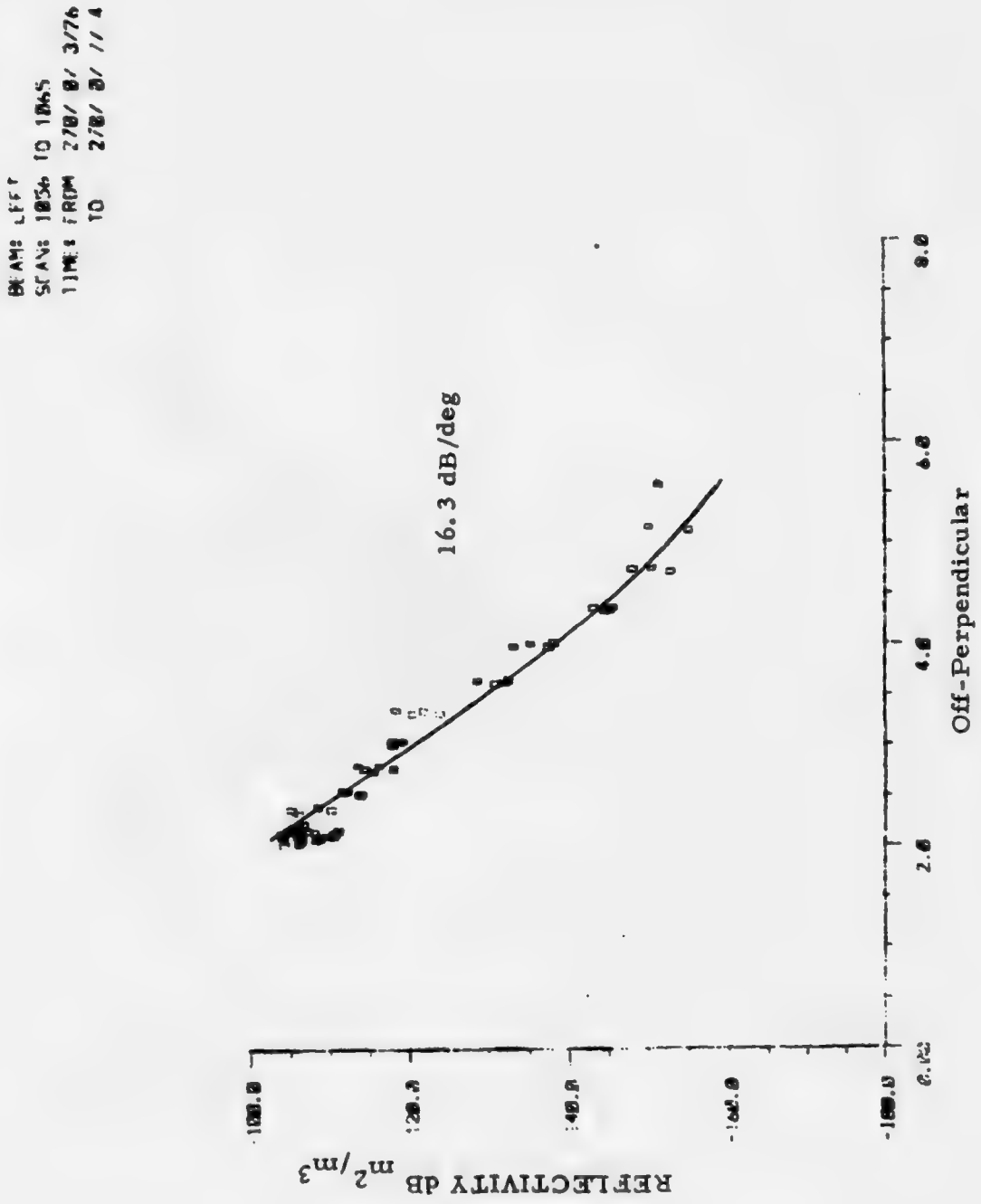


Figure 4-3

## SCATTER PLOT FROM REGION "A"

BEAM: LEFT  
SCAN: 1056 TO 1265  
TIME: FROM 270° 0' 3.76  
TO 370° 0' 1.4

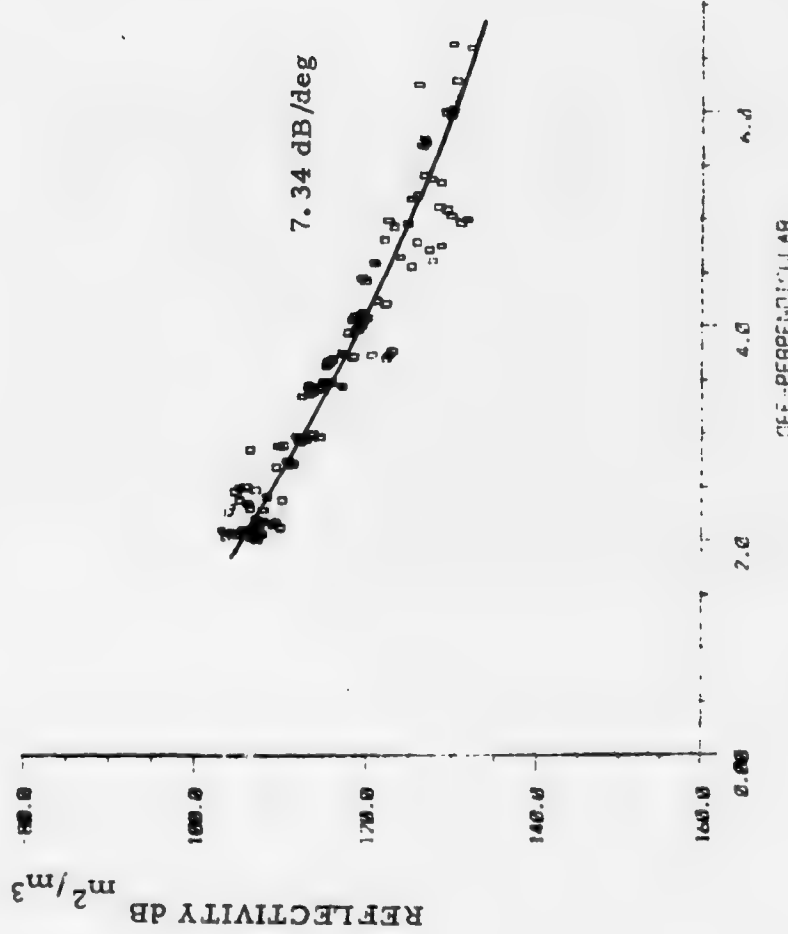


Figure 4-4

#### 4.2 Test Case 70/666

This test case involves a discrete arc as shown in Figure 4-5. This arc consists of the main reflecting band shown in the lower portions of the figure and a smaller band above it. The only magnetic data available was at 14:14 UT when the  $A_p$  index was about 33 and a minor geomagnetic storm was in progress. The absence of magnetometer data from Fort Churchill makes it impossible to estimate the instantaneous geomagnetic distortion; however, there is good alignment of the arc with the L-shell contours. The peak s/n was 54 dB, the average about 24 dB. Two scatter plots were generated using data from the 105-106 km band as indicated by the peak of the altitude versus reflectivity profile of Figure 4-6. The scatter plot shown in Figure 4-7 was generated from data selected from region A in Figure 4-5. The scatter plot shown in Figure 4-8 resulted from data selected in region B. A distinct difference in the aspect response characteristics of these two plots is readily apparent. One unusual observation is the very high (20 dB/deg) slope at the low off-perpendicular angles as seen in Figure 4-7.

#### 4.3 Test Case 78/12

This is a homogeneous and clearly defined discrete arc from which echoes were measured with signal-to-noise ratios as great as 64 dB and averaging about 46 dB. The magnetic activity was low with an  $a_p$  of only 16 reported at 14:14 UT. Figure 4-9 shows that echoes were detected throughout the range of angles from  $2^\circ$  to  $8^\circ$  off-perpendicular. Figure 4-10 shows the center of the arc at about 105 km. The aspect response curve shown in Figure 4-11 was created from data parallel to the L-shells (region A in Figure 4-9). The curve in Figure 4-12 was created from echoes along region B.

The slopes of these curves, which were manually fit to the data, reveal again the gross differences noted when attempting to determine aspect sensitivity from different sets of data. The differences in the shape of these aspect response curves will be discussed in more detail in a later section, but the differences are felt only to be apparent, but are in fact the result of magnetic distortion from the current flow in the discrete arc.

TOP-DOWN REFLECTIVITY MAP OF SCAN 667

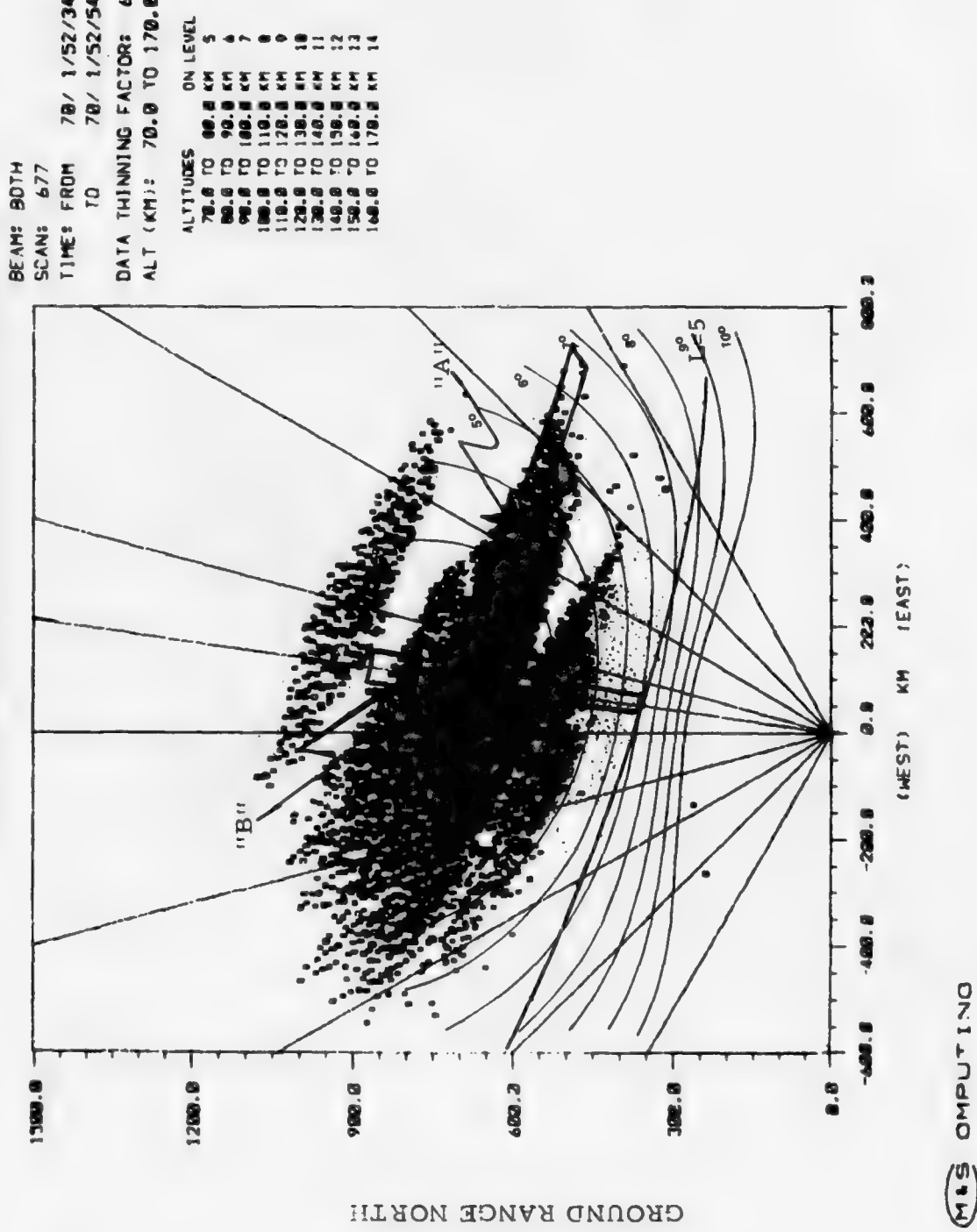


Figure 4-5

ALTITUDE PROFILE FOR ALL ASPECT ANGLES

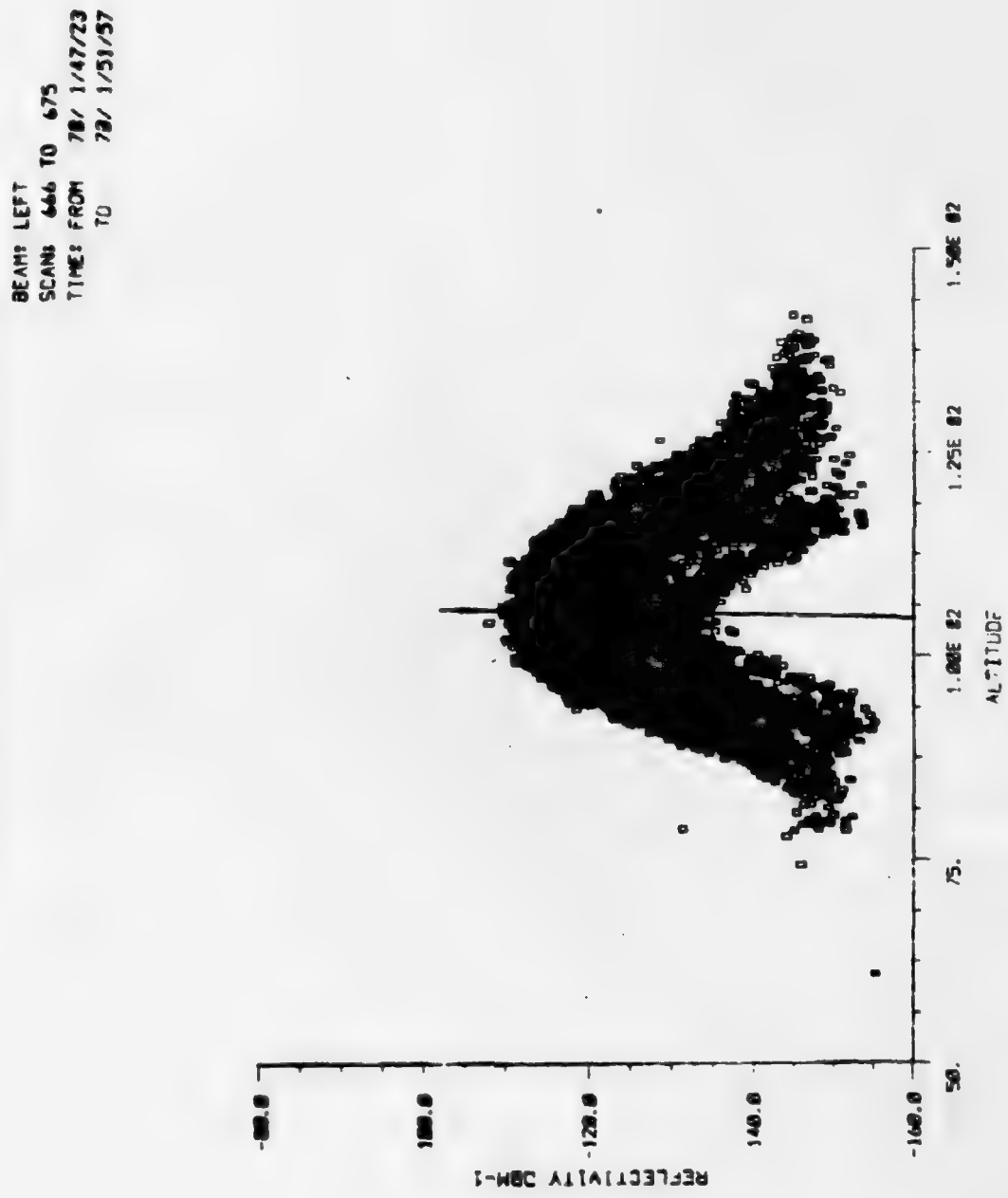


Figure 4-6

SCATTER PLOT FROM REGION "A"

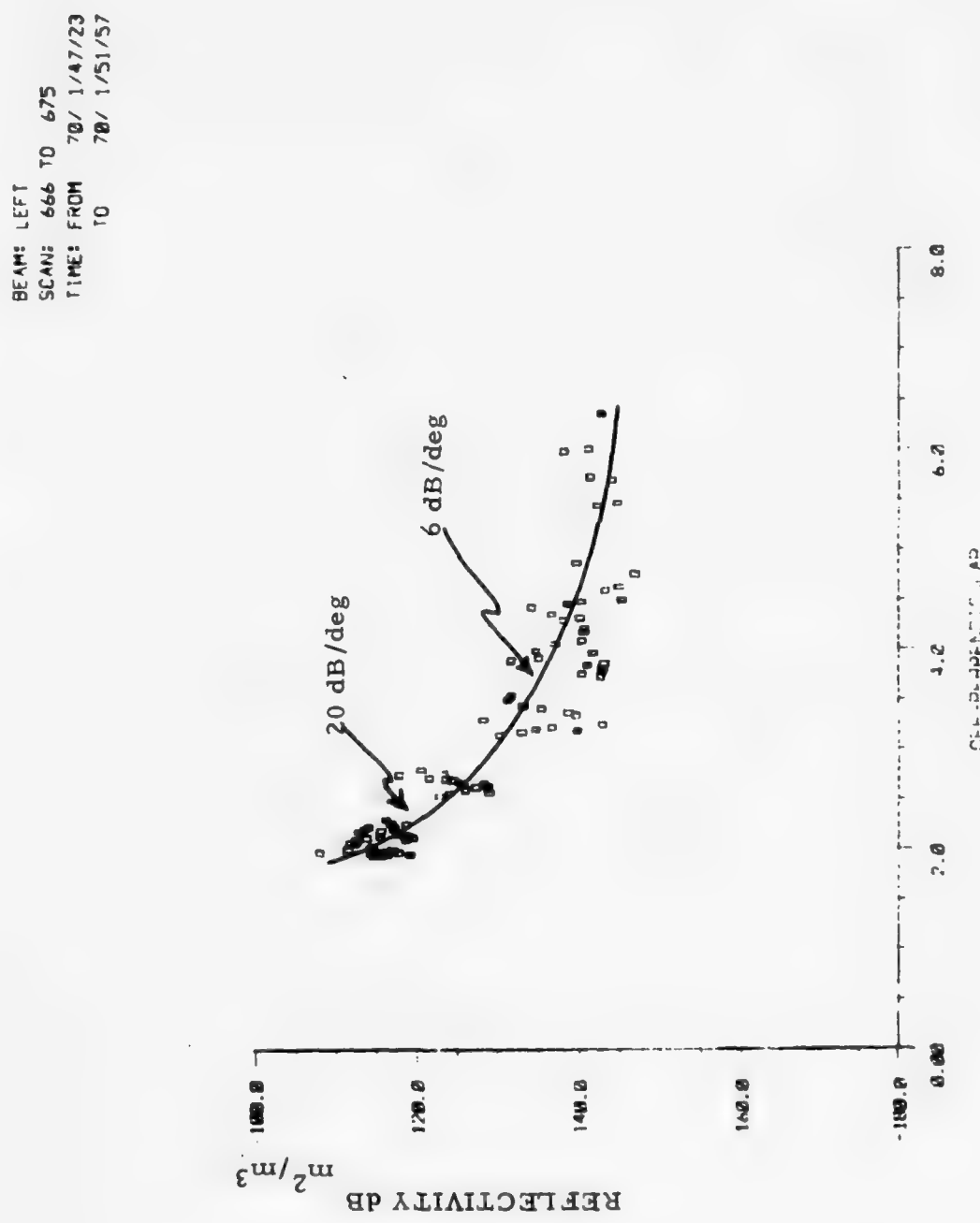


Figure 4-7

SCATTER PLOT FROM REGION "B"

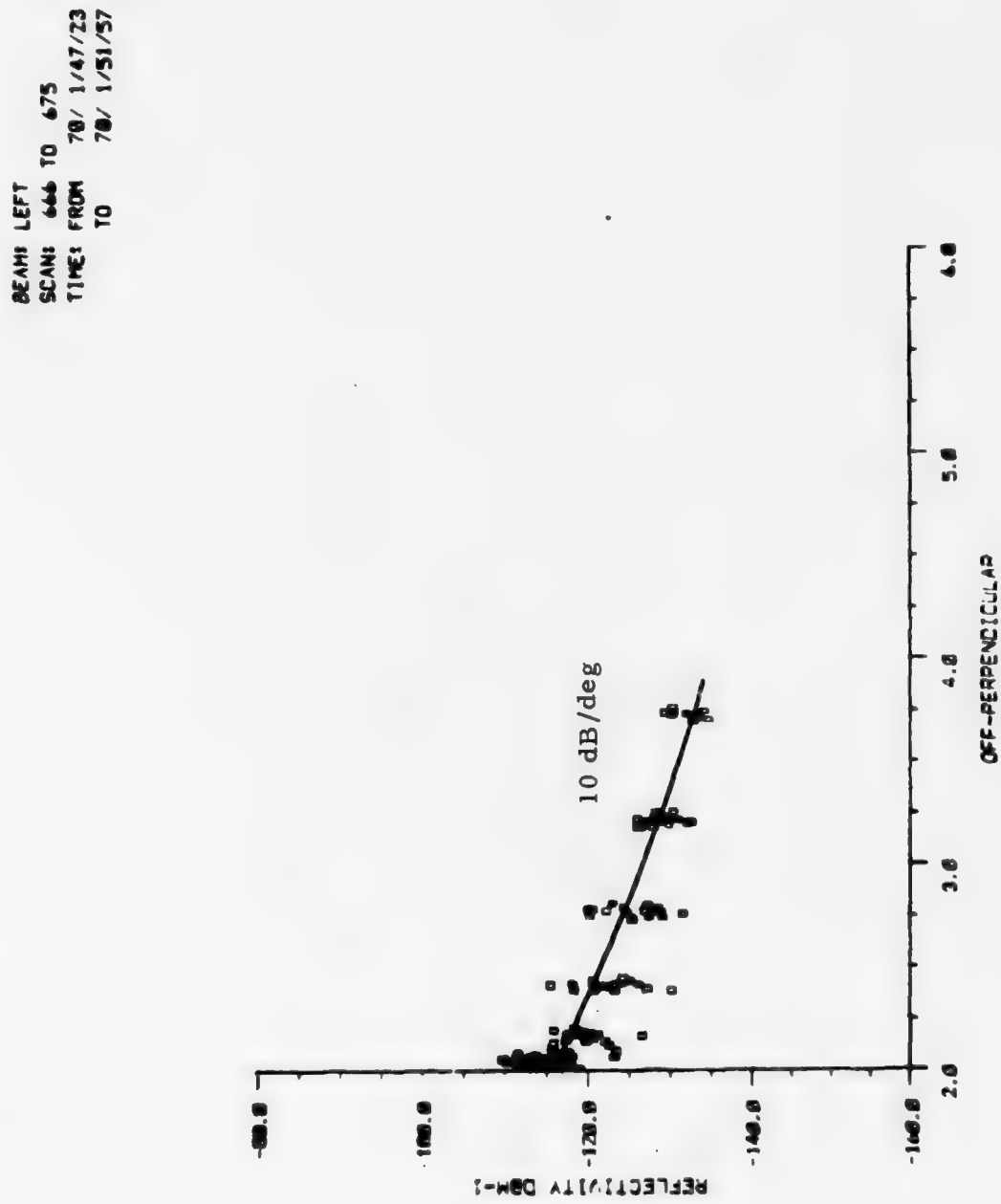


Figure 4-8

TOP-DOWN REFLECTIVITY MAP OF SCAN 12

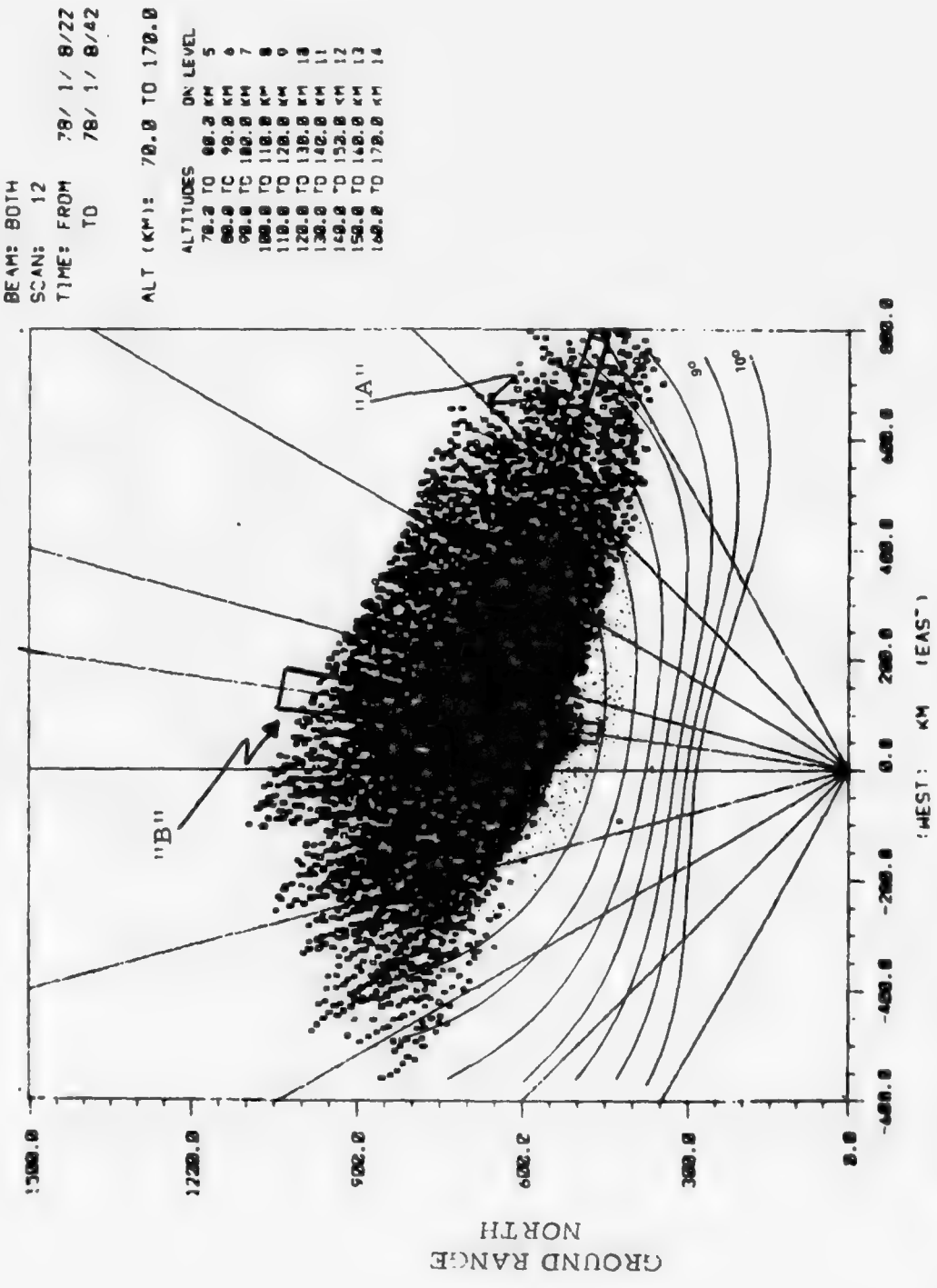


Figure 4-9

SCATTER PLOT SHOWING ARC CENTER

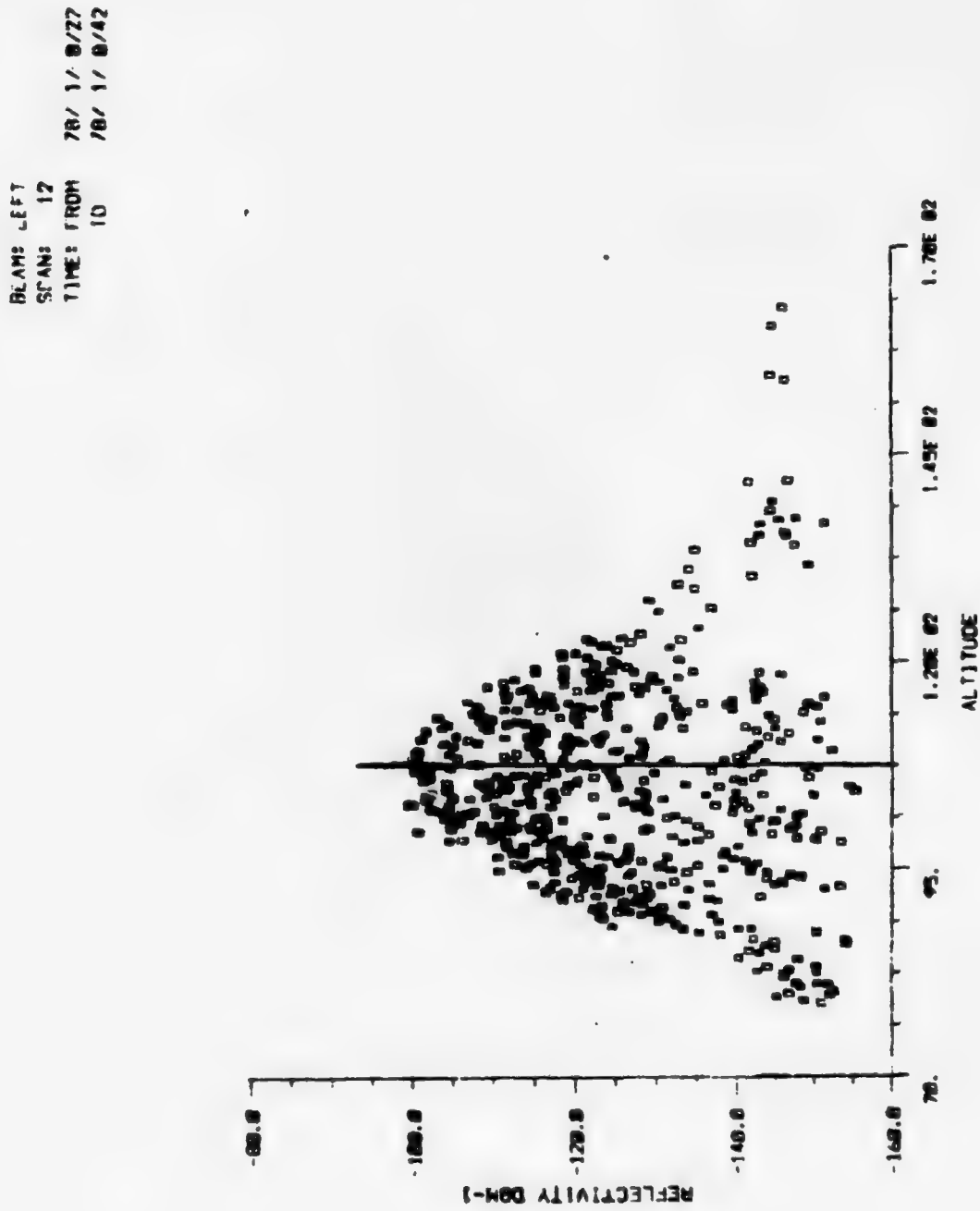


Figure 4-10

ASPECT SCATTER PLOTS OF SCANS 12-22 FROM REGION "A"

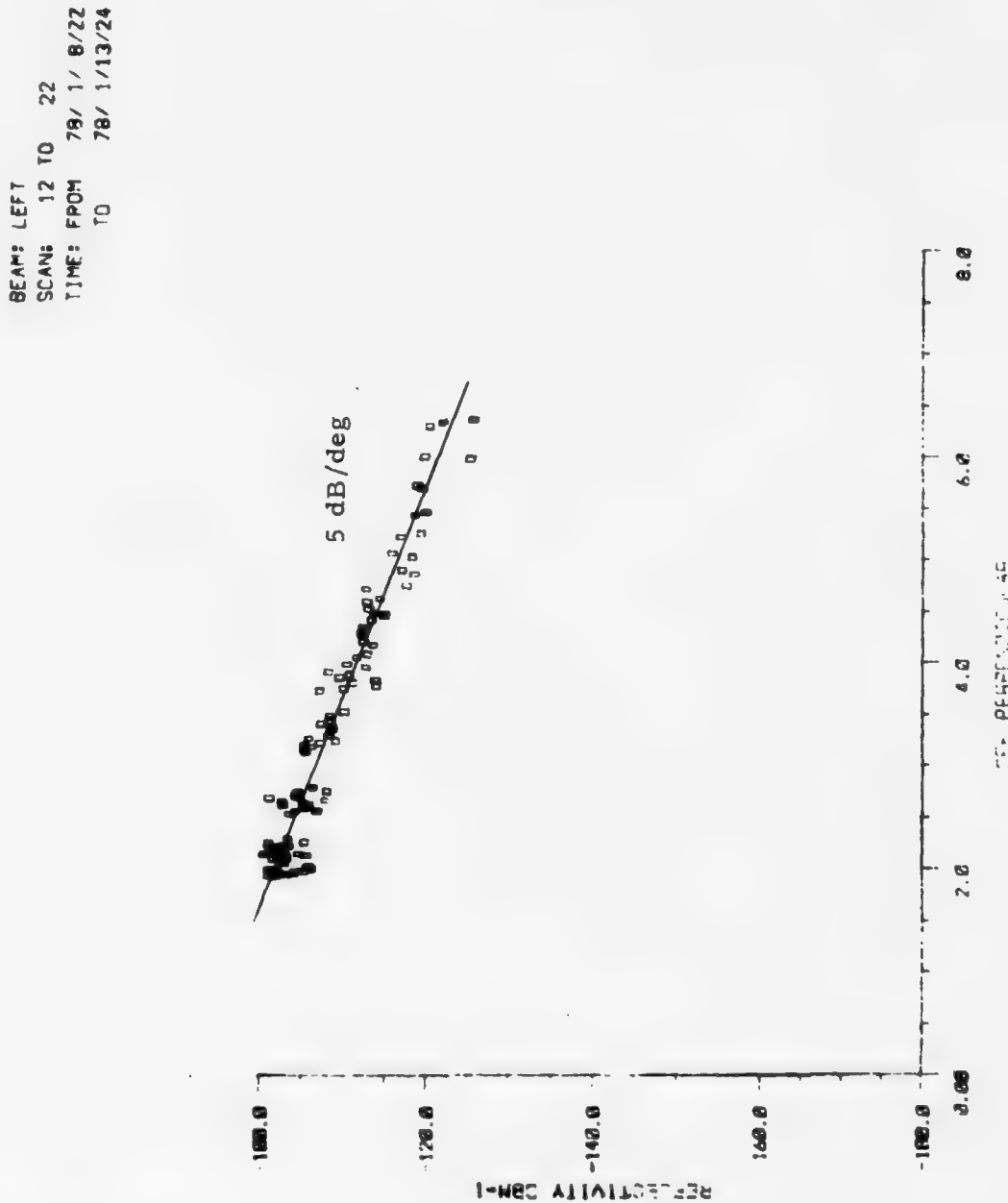


Figure 4-11

SCATTER PLOT FROM REGION 'B'

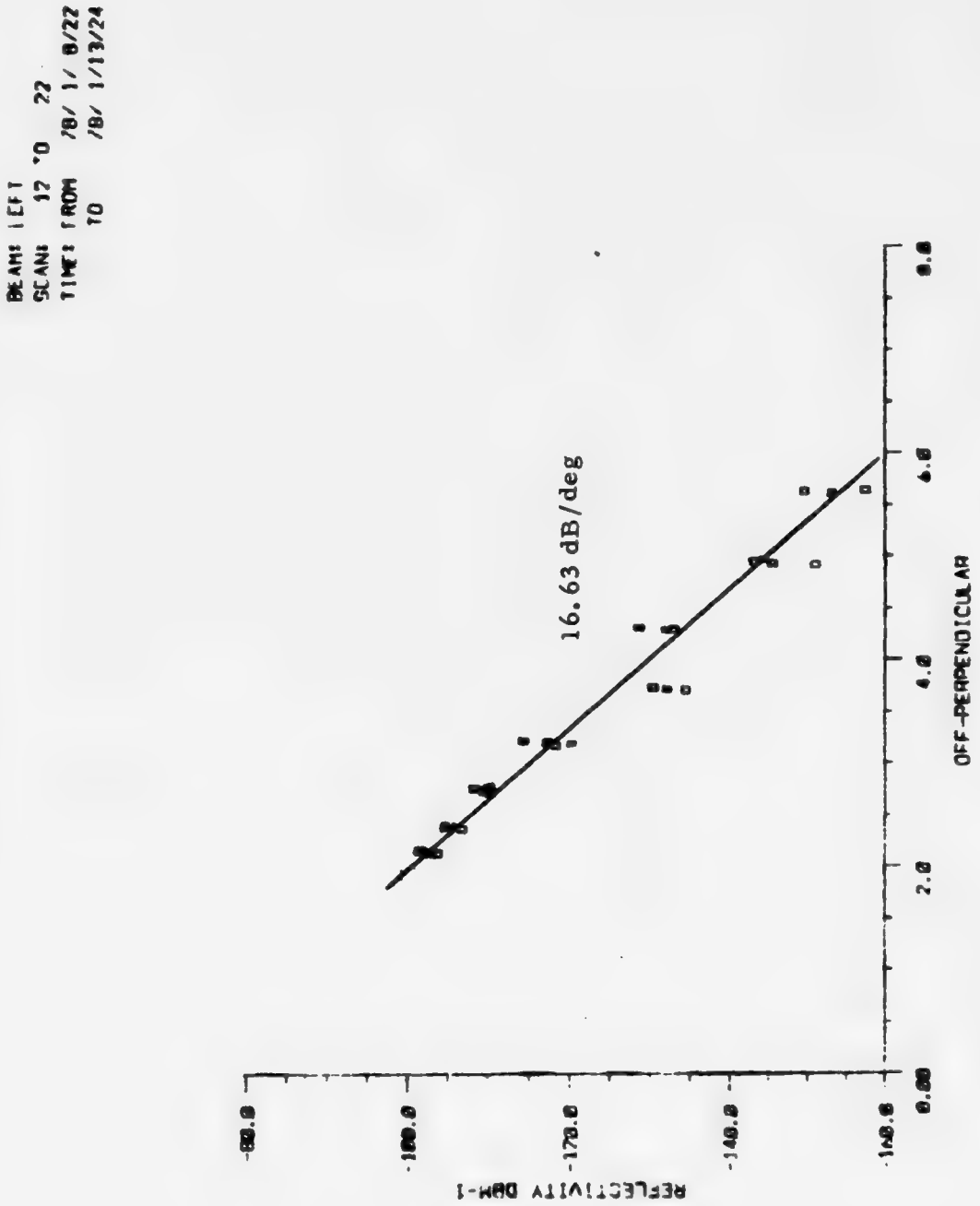


Figure 4-12

#### **4.4      Test Case 86/576**

The scan representing this test case is shown in Figure 4-13. The map shows this discrete arc including off-perpendicular angles from  $2^\circ$  to  $8^\circ$ . The Churchill magnetometer was steady, showing a deviation from baseline of  $+60\gamma$  for the X component,  $+5\gamma$  for the Y component, and  $-80\gamma$  for the Z component. The arc was well-aligned with the L-shells as shown in Figure 4-14. Figure 4-15 shows the arc to be centered near 105 km.

Sample regions parallel and perpendicular, respectively, to the L-shell, shown as region A and region B in Figure 4-13, yield the scatter plots given in Figures 4-16 and 4-17. The contrast between the apparent aspect sensitivity of the two samples is again evident. A slope of only  $5.83 \text{ dB/deg}$  was calculated for the region approximately parallel to the L-shell contour (region A) and  $11.4 \text{ dB/deg}$  for the data from the perpendicular region (region B). The curve-fit used in the figure required manual screening of the points on either end of the scatter plot because the severe reflectivity dropoff noted on either end is a direct result of the sample region crossing the arc boundaries shown as C and D on Figure 4-13. At these boundaries there is a sharp transition from relatively strong reflectivity to zero reflectivity. This results in the effects noted and is especially clear near the  $2^\circ$  off-perpendicular angle in Figure 4-13. These edge effects are not representative of the aspect response and must be manually detected and eliminated in the curve-fit and analysis process.

#### **4.5      Test Case 86/632**

This discrete arc, shown in Figure 4-18, occurred during quiet magnetic conditions nearly identical to the previous test case. The two scatter plots were generated from the two cuts along region A and region B and from the 105-106 km altitude band as indicated by the altitude profile of Figure 4-19. The scatter plot in Figure 4-20 was generated from data within region A of Figure 4-18, or generally parallel to the L-shells. The scatter plot of Figure 4-21 was generated from data along region B, perpendicular to the L-shells.

It should be noted that only three scans were available for averaging. This fact is evident in the more than usual dispersion of the scatter plots, especially notable in Figure 4-20. The curve-fit to the scatter plot of Figure 4-21 required manual correction to eliminate the edge effects. By studying how the off-perpendicular contours fit the map on Figure 4-18, it can be seen that only the region from about  $2.5^\circ$  to  $3.75^\circ$  off-perpendicular can yield echoes free of edge effects.

Again, the sample region B perpendicular to the L-shell produces a steeper aspect response slope than does the data from region A.

TOP-DOWN REFLECTIVITY MAP SHOWING ASPECT CONTOURS

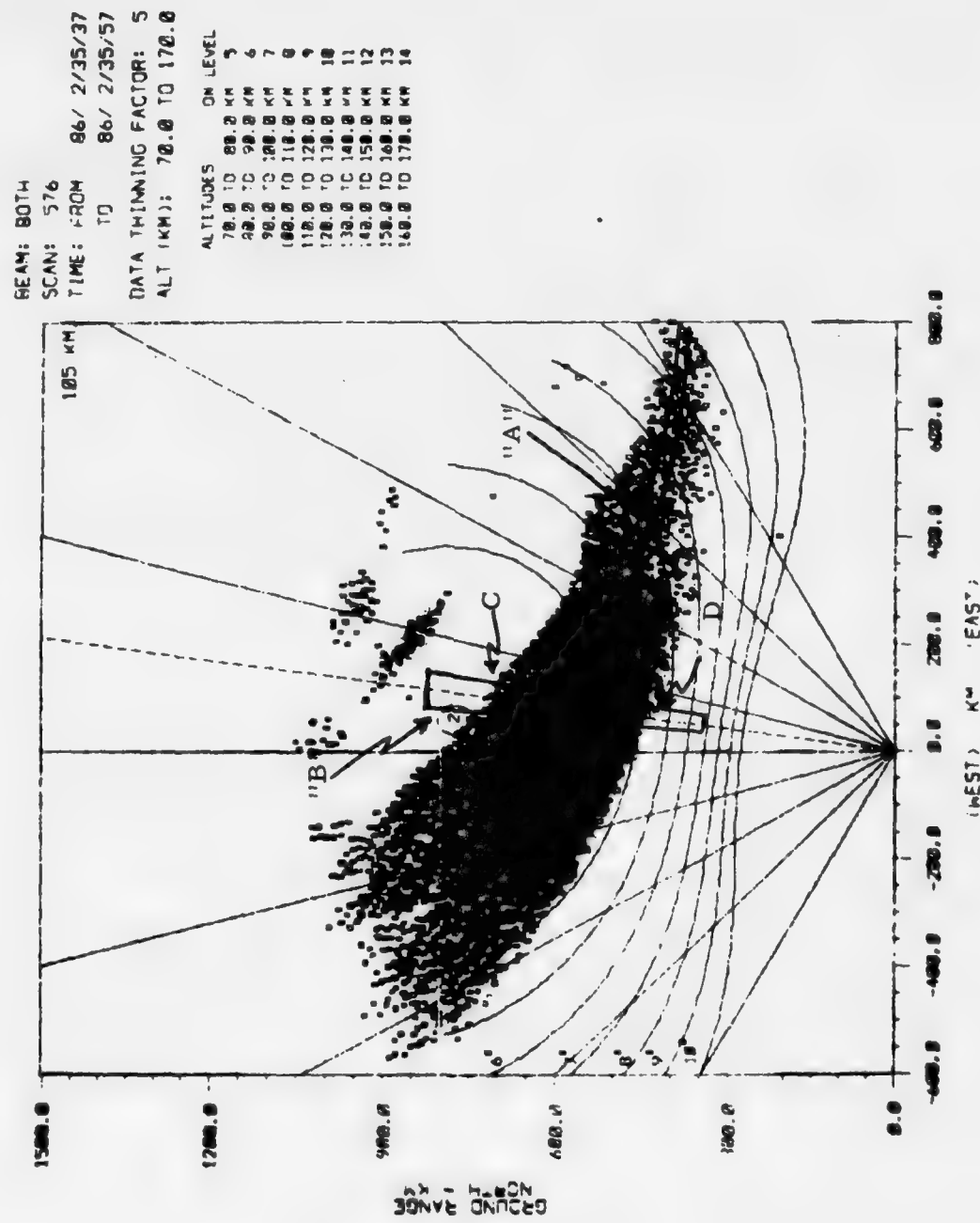
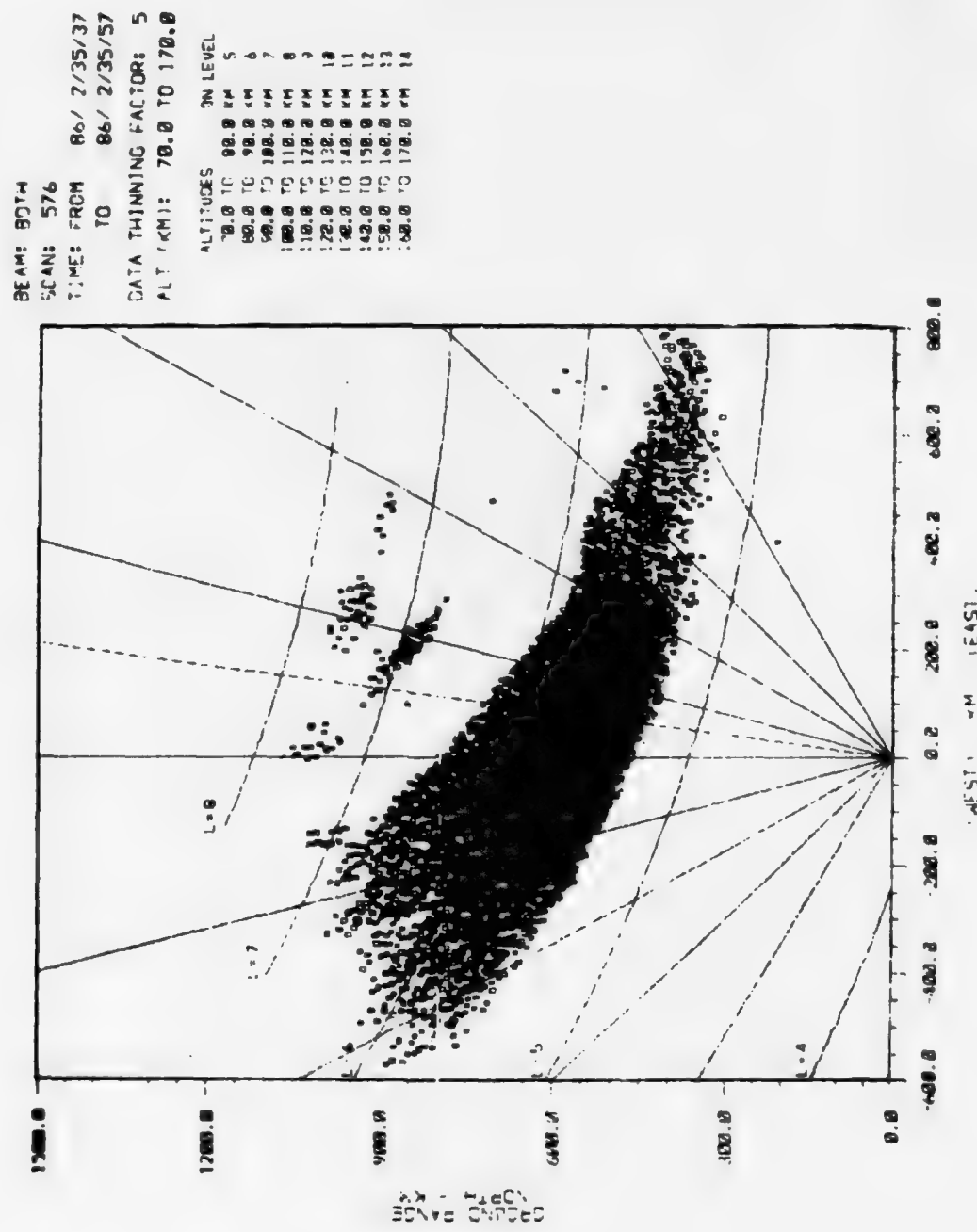


Figure 4-13

MAP OF SCAN 576 SHOWING L-SHELL CONTOURS AT 105 KM



-55-

Reproduced from  
best available copy.

Figure 4-14

SCATTER PLOT SHOWING ALTITUDE VERSUS REFLECTIVITY

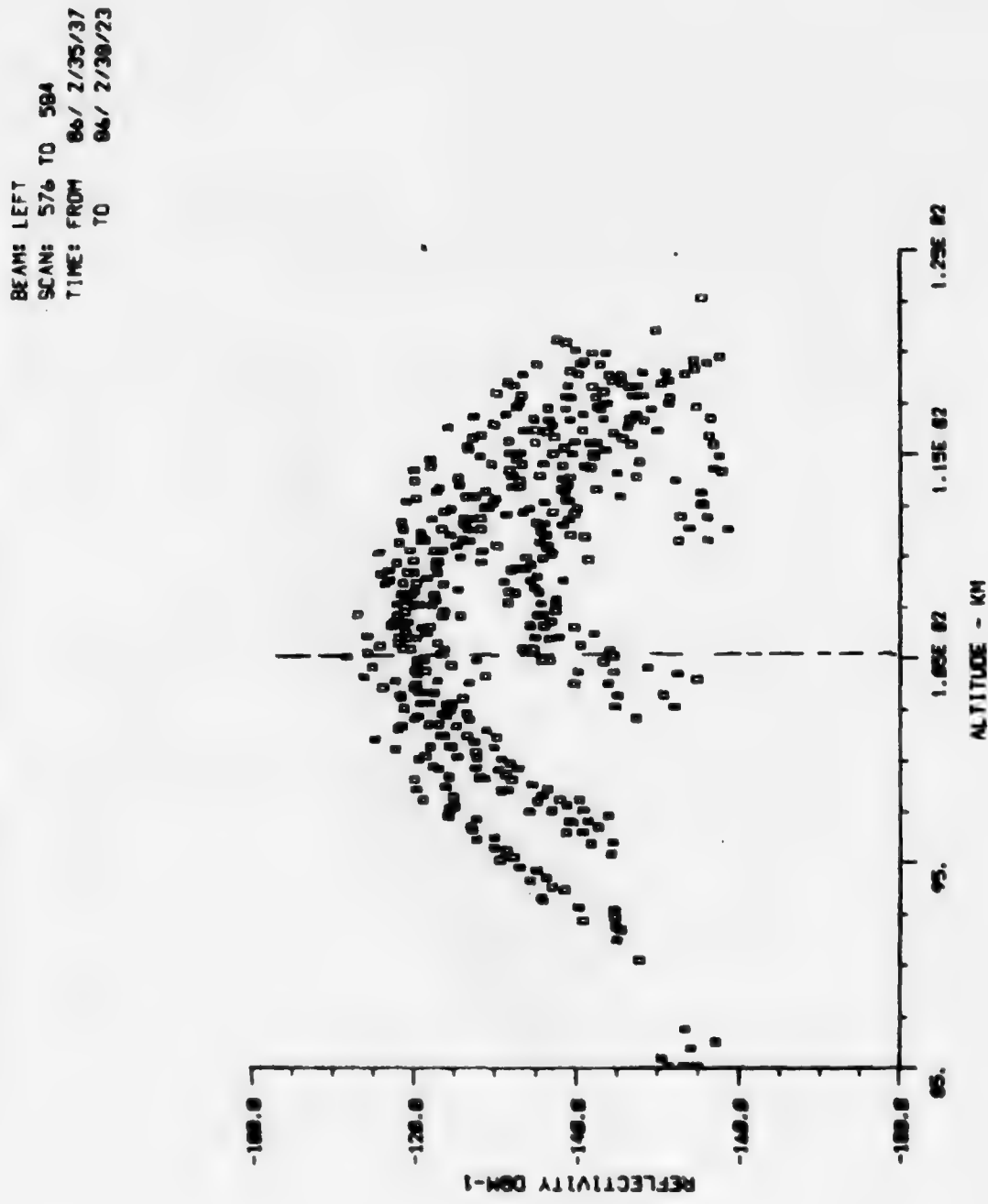


Figure 4-15

SCATTER PLOT FROM REGION "A"

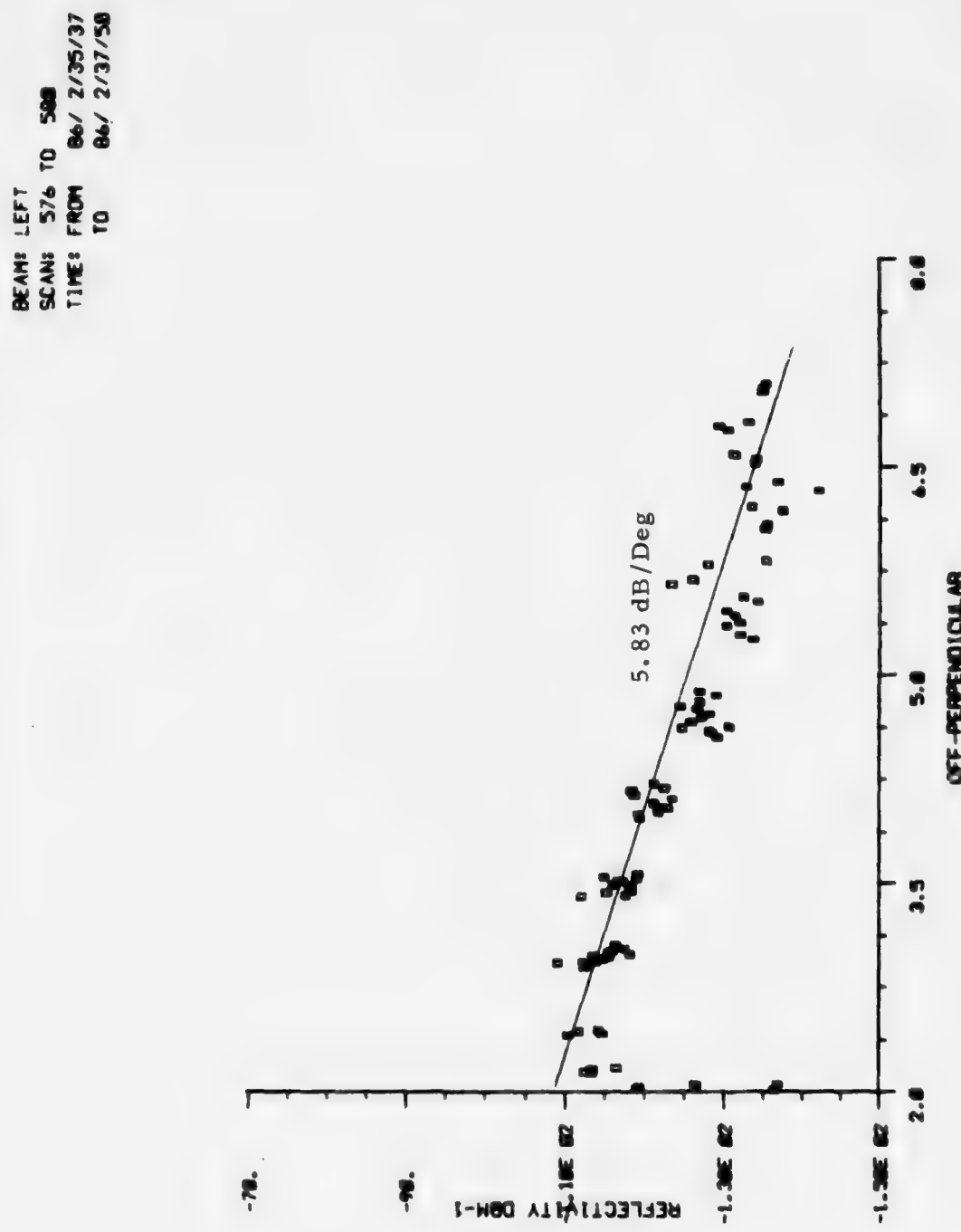


Figure 4-16

ASPECT RESPONSE FROM REGION "B"

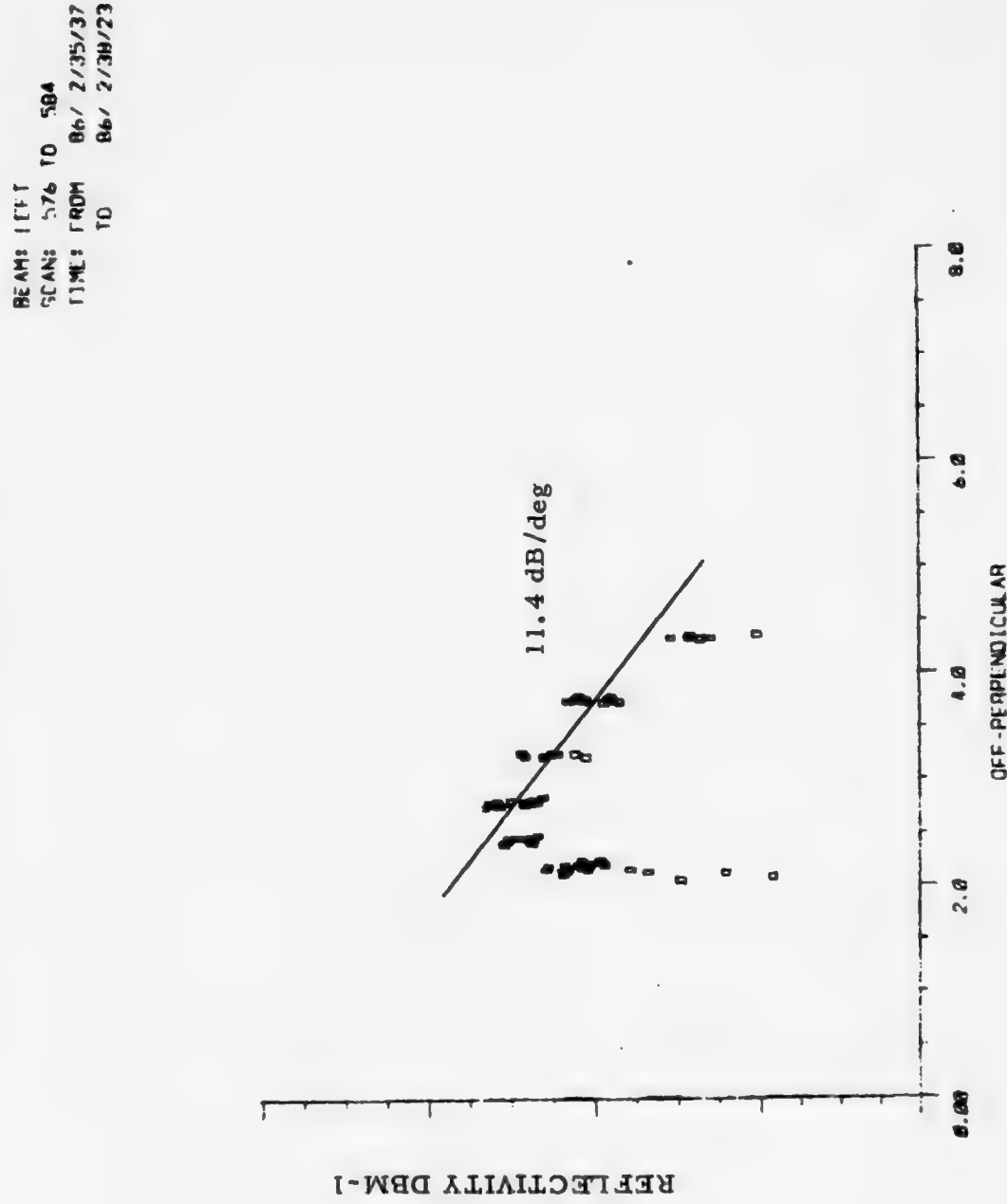


Figure 4-17

TOP-DOWN MAR OF SCAN 633

BEAM: BOTH  
 SCAN: 633  
 TIME: FROM 86/2/39/29  
 TO 86/2/39/49  
 DATA THINNING FACTOR: 4  
 ALT (KM): 70.0 TO 170.0  
 ALTITUDES ON LEVEL

Figure 4-18

ALTITUDE REFLECTIVITY PROFILE SHOWING CENTER OF ARC

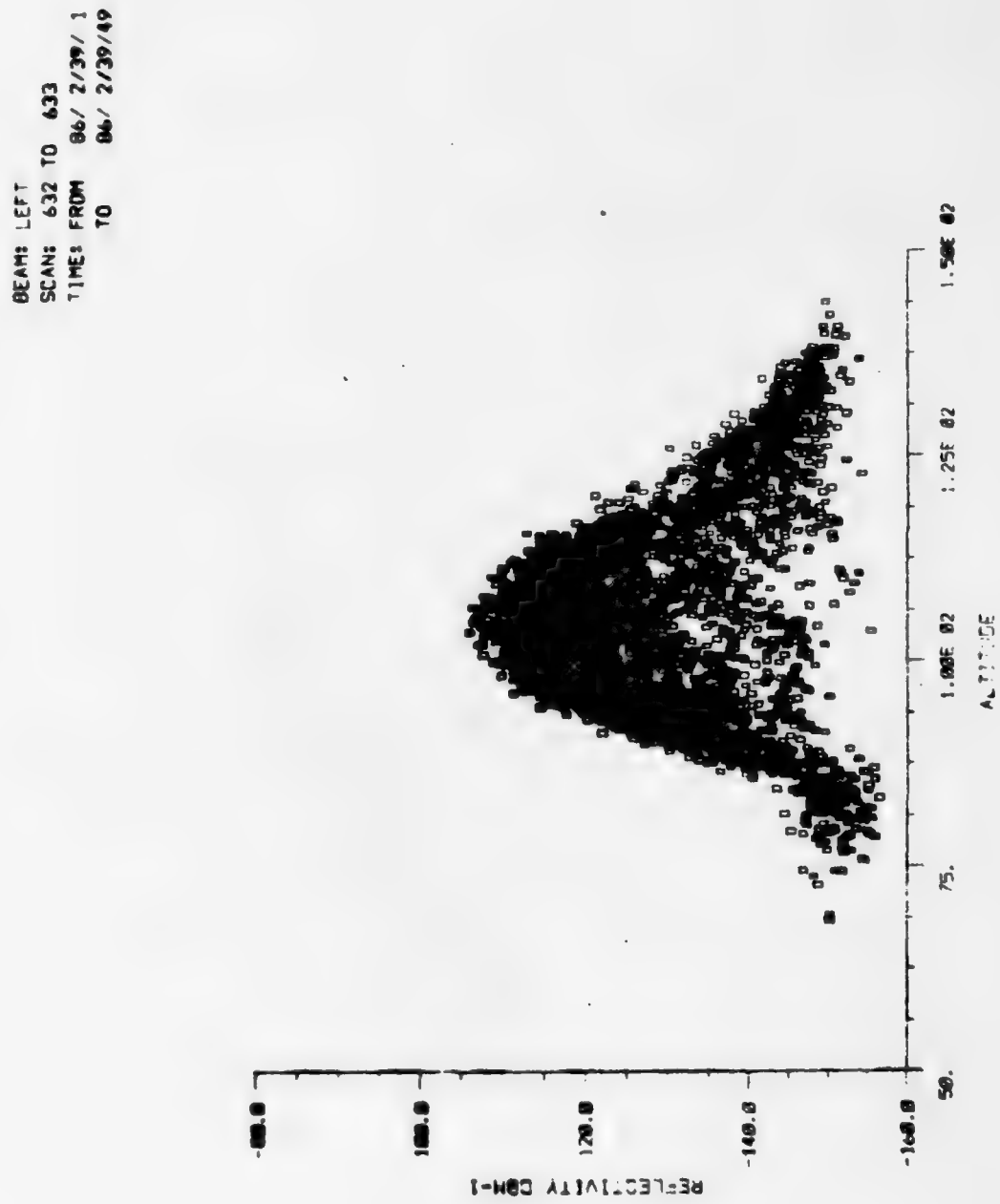


Figure 4-19

SCATTER PLOT FROM REGION 'A'

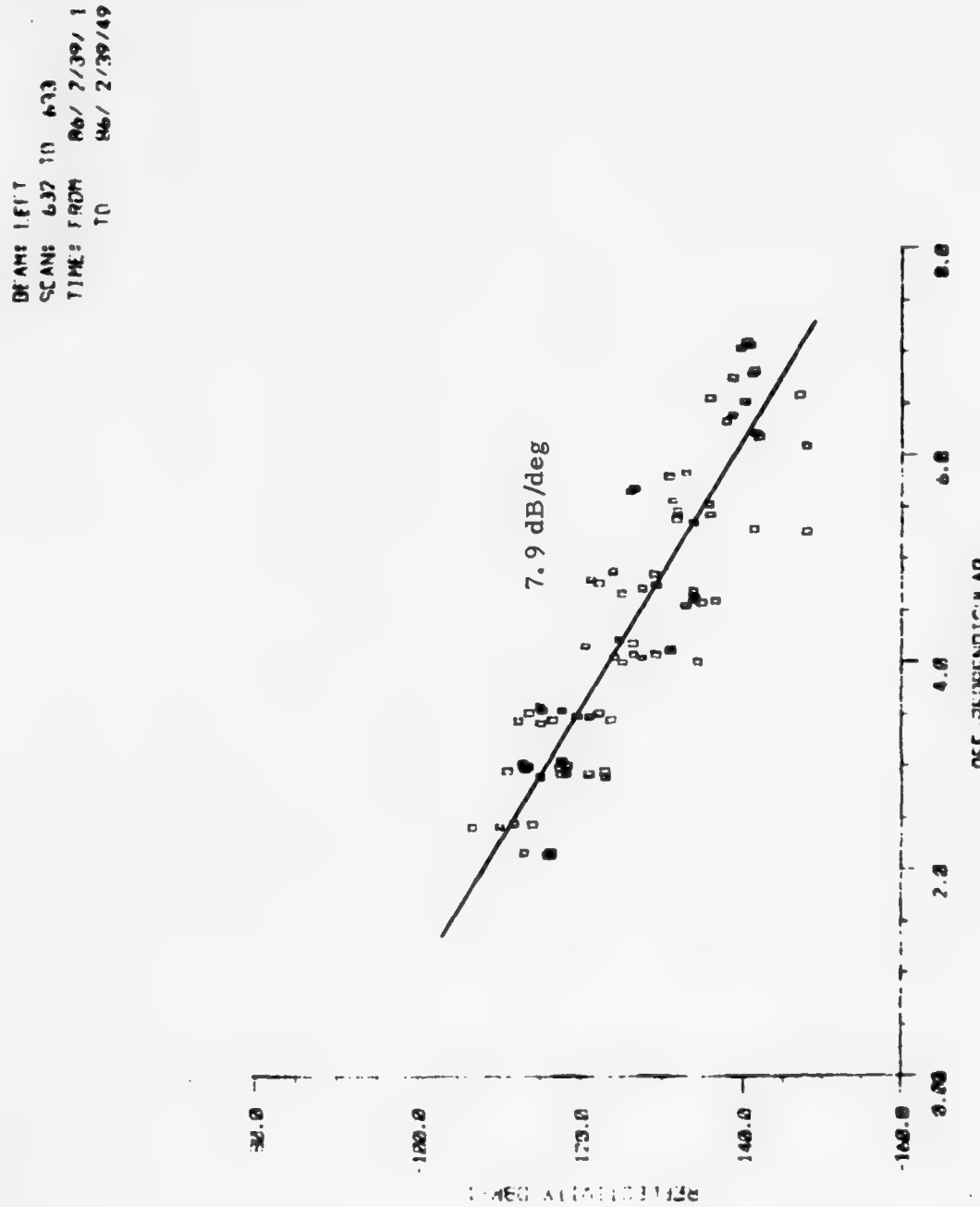


Figure 4-20

ASPECT SCATTER PLOT FROM REGION "B"

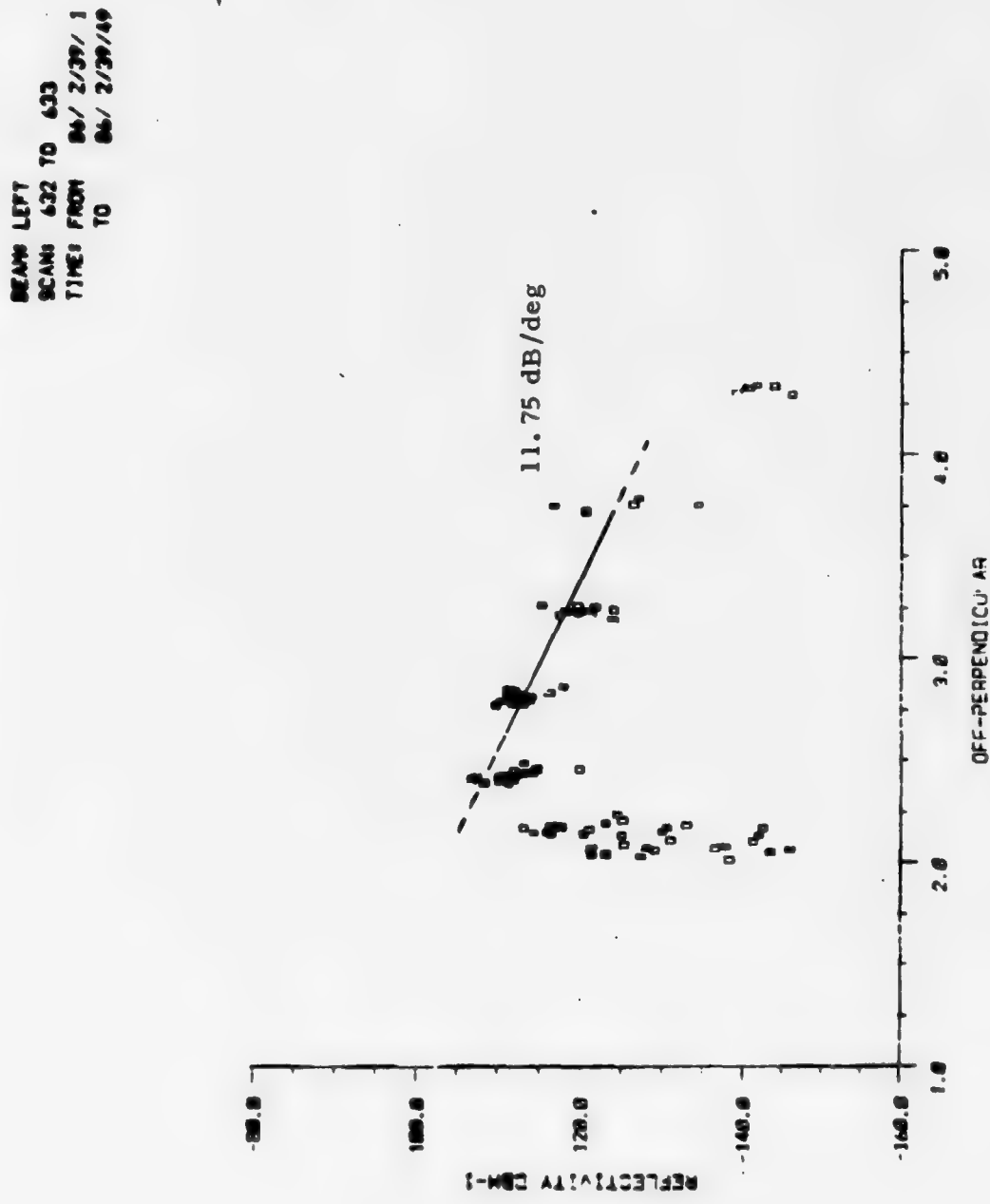


Figure 4-21

#### **4.6    Test Case 86/5557**

As indicated in Figure 4-22, this map shows a large diffuse auroral form. The poleward limits of the reflection region are determined by the radar horizon, and the boundary near the radar results from the minimum range of the sensor. Reports from the Finley Air Force Radar Station, south of the PAR, confirmed that the equatorial edge of the arc extended far south of the PAR. Magnetic activity at Fort Churchill was very steady at this time. The magnetometer was steady and showed a deviation of  $-40\gamma$  in the X component,  $-75\gamma$  in the Y component, and  $-140\gamma$  in the Z component.

The center of the reflectivity arc is located near 105 km as shown by Figure 4-23. The altitude profile is, however, unusual because of the gaps on either side of the primary plot. No attempt will be made to explain this phenomenon. Three aspect response scatter plots have been generated, one from each of the three regions, labeled A, B, and C in Figure 4-22. The first scatter plot, Figure 4-24, comes from region A; the slope is 5.5 dB/deg. The second scatter plot, shown in Figure 4-25, was generated with data from region B; its slope is 4.84 dB/deg. The final scatter plot was generated from a combination of data from regions B and C. Region C includes data from the maximum attainable off-perpendicular angles. The resultant scatter plot of Figure 4-26 covers a wide range of aspect angles and shows how the slope flattens at high aspect angles. This effect was described earlier and has been noted by others [6, 9].

This test case is the first clearly diffuse large-scale aurora investigated in the study. It should be noted that for the first time the aspect response slope was lower when the data was selected perpendicular to the L-shells, than when selected parallel to them, as evidenced by Figures 4-24 and 4-25. In fact, there are no significant differences in the two curves.

#### **4.7    Test Case 86/5571**

The data set which generated the auroral map in Figure 4-27 was collected near in time to the previous scan and the apparent geomagnetic conditions were nearly identical. The arc was assumed to be centered near 105 km. The three scatter plots, shown in Figures 4-28, 4-29, and 4-30, were generated with data from regions A, B, and C, respectively (see Figure 4-27). Comparing Figures 4-28 and 4-29 again shows the aurora appears more aspect-sensitive when sampling perpendicular to the L-shells than when selecting data along a line generally parallel to the contours. The scatter plot in Figure 4-30 was generated from region C data and displays very little aspect sensitivity. All the curves demonstrate a decreasing slope with increasing aspect angle.

TOP-DOWN REFLECTIVITY MAP OF SCAN 5558

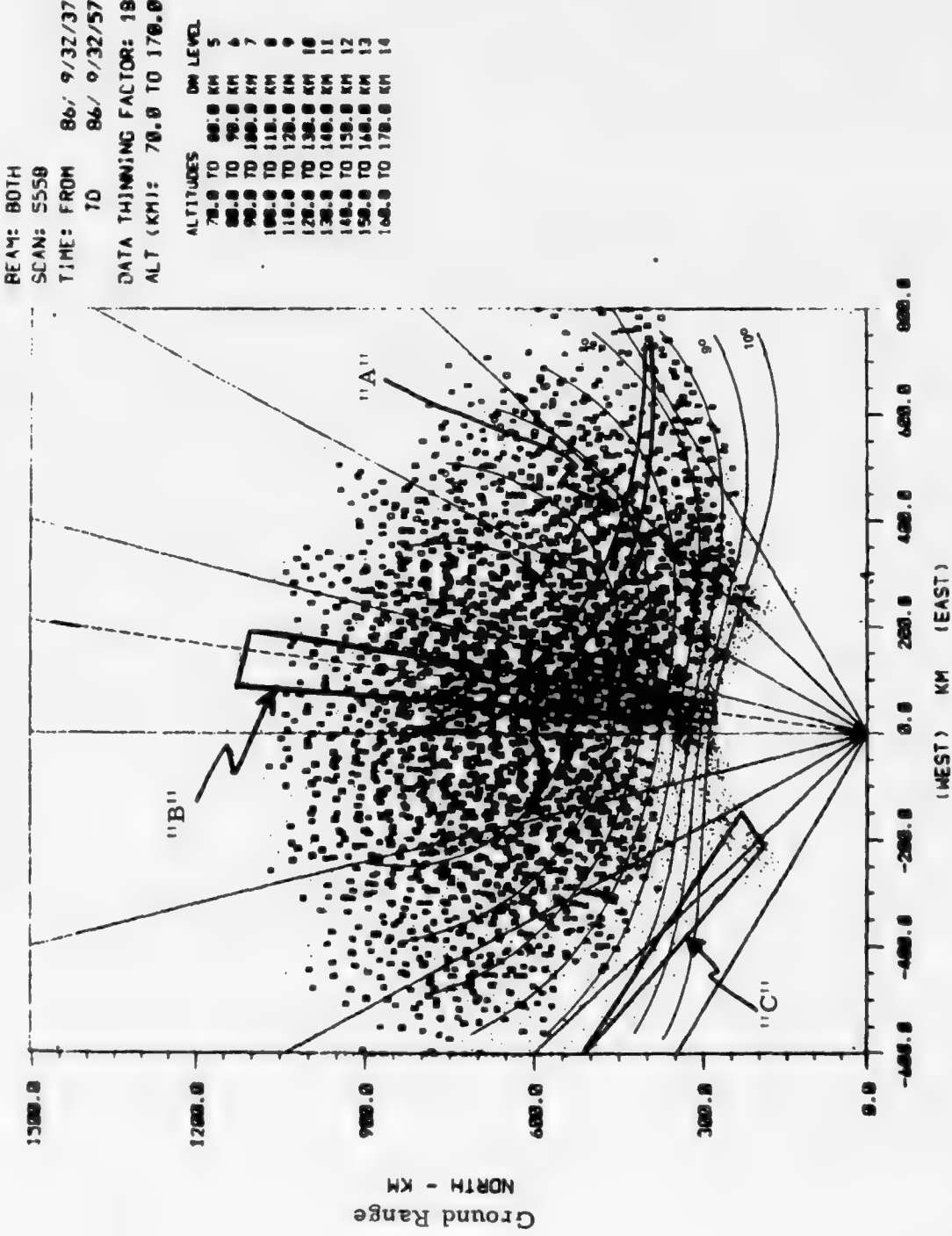


Figure 4-22

SCATTER PLOT SHOWING ALTITUDE PROFILE

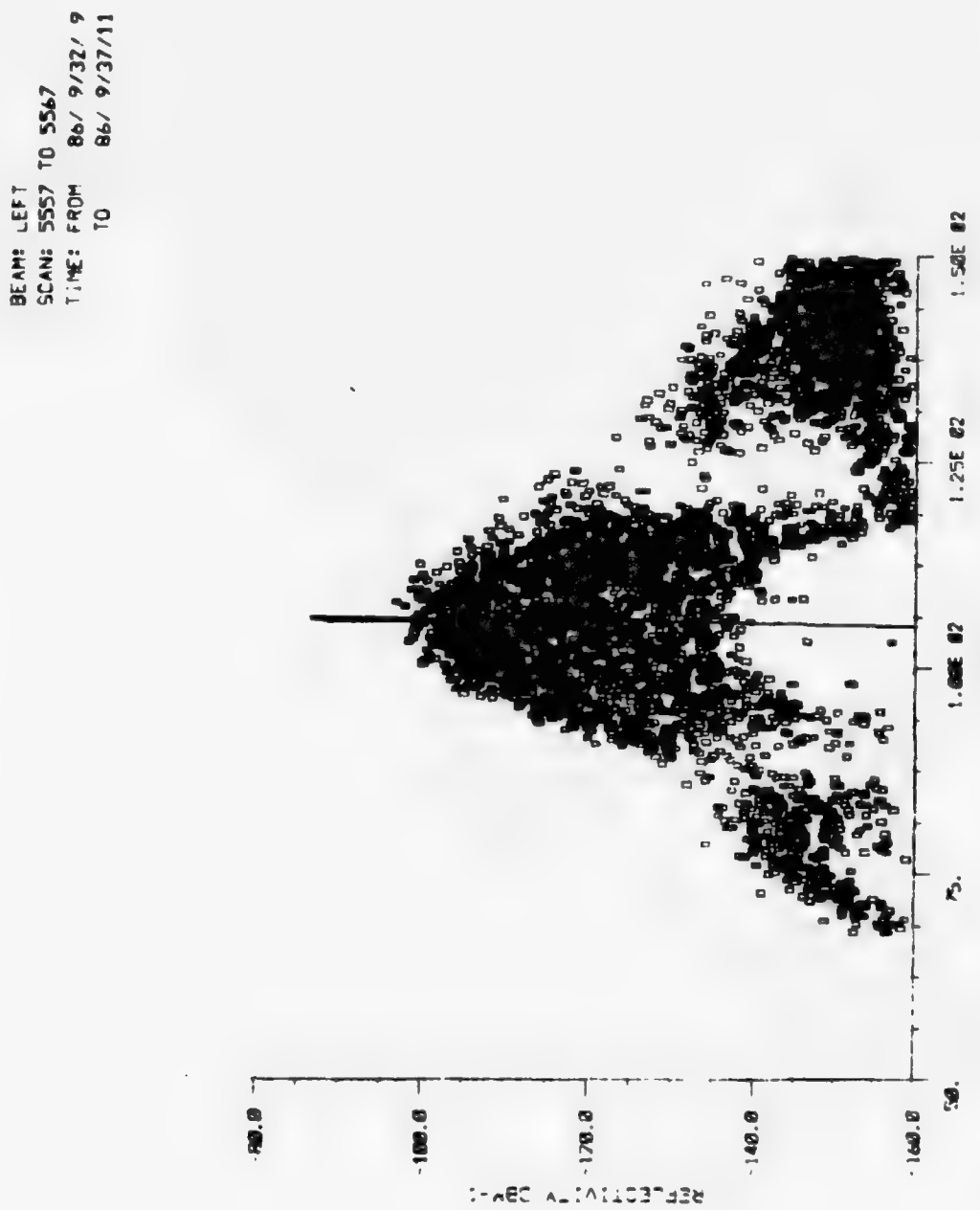


Figure 4-23

SCATTER PLOT SHOWING ASPECT RESPONSE ALONG "A"

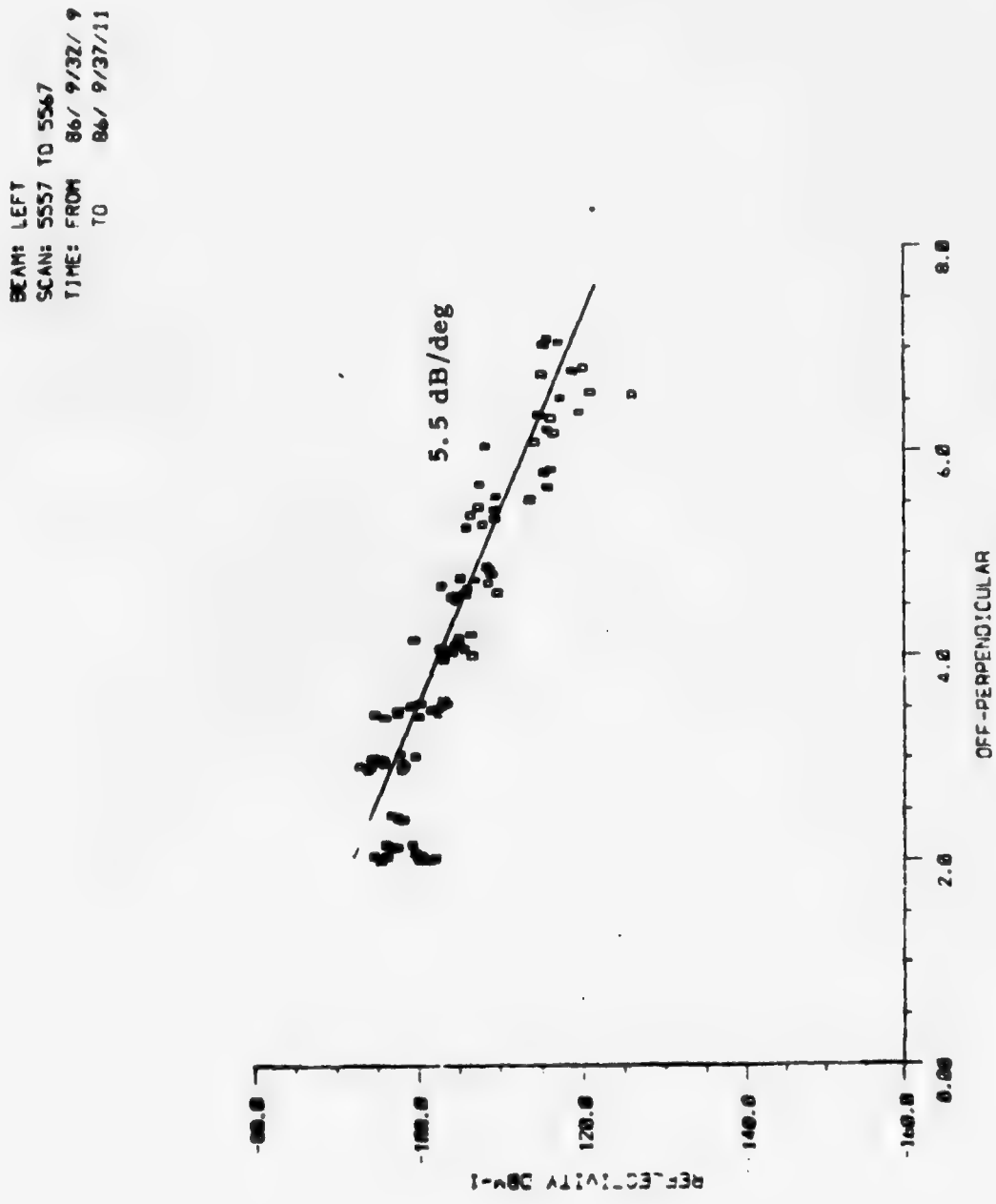


Figure 4-24

SCATTER PLOT FROM REGION "B"

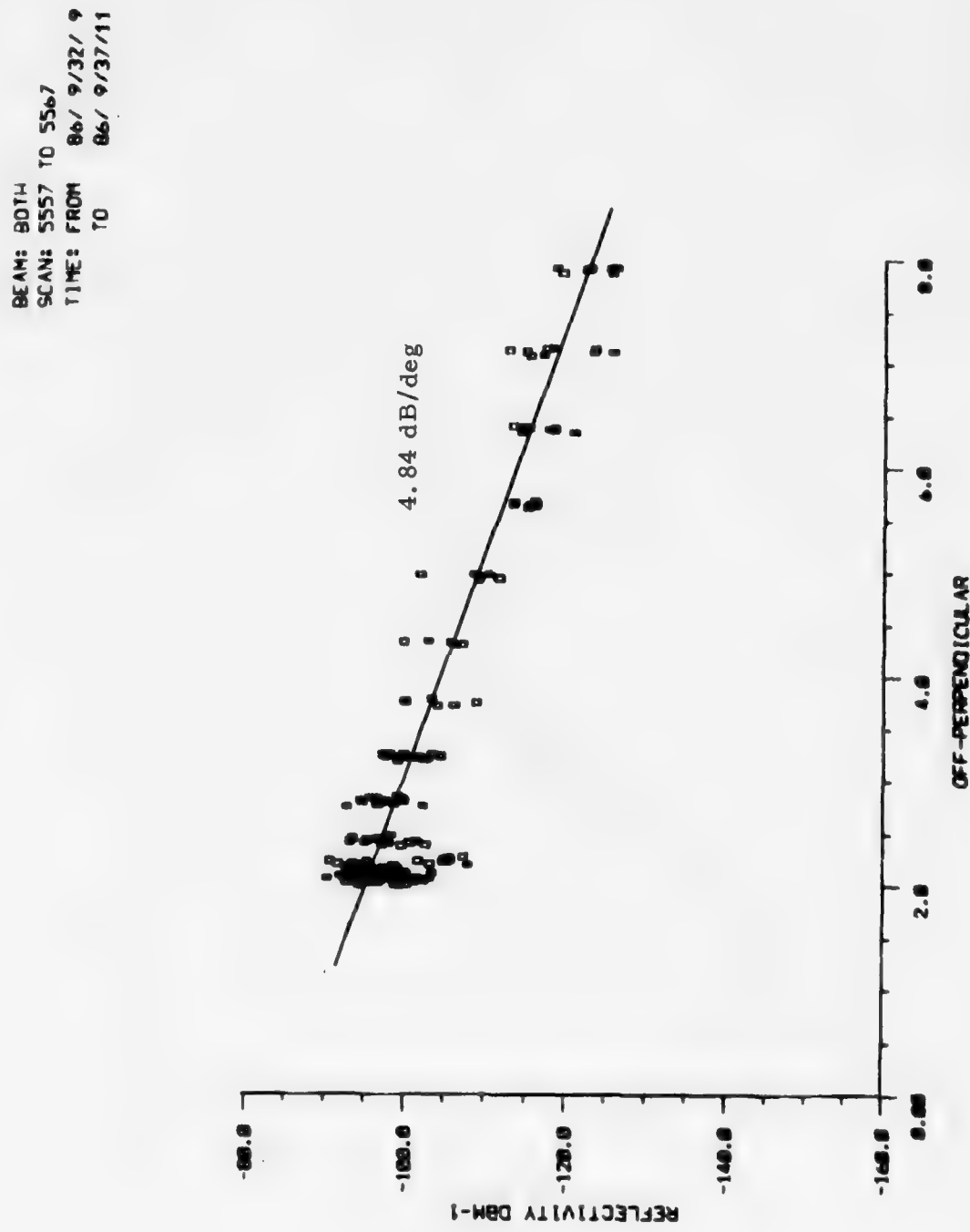


Figure 4-25

SCATTER PLOT FROM REGIONS "B" AND "C"

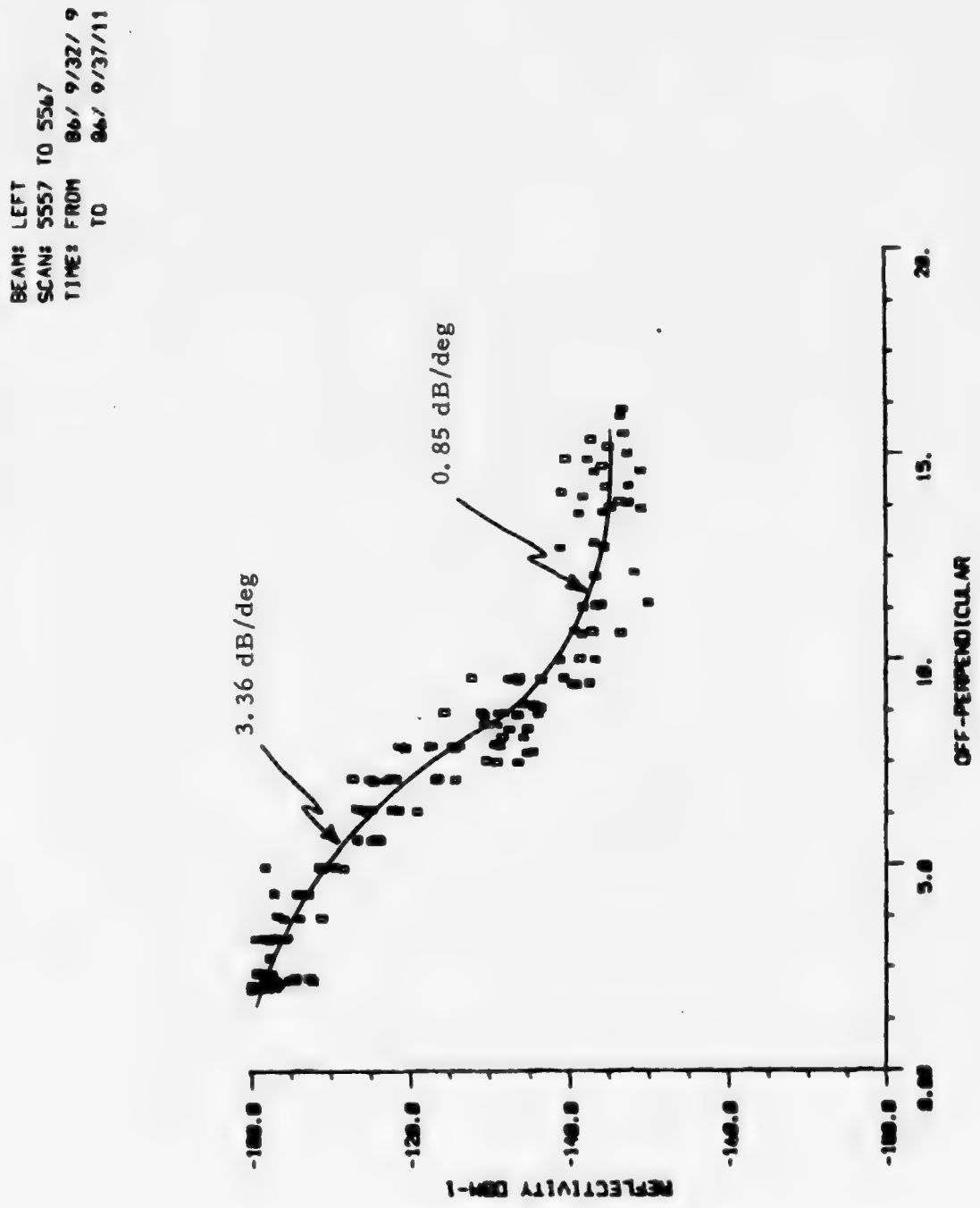
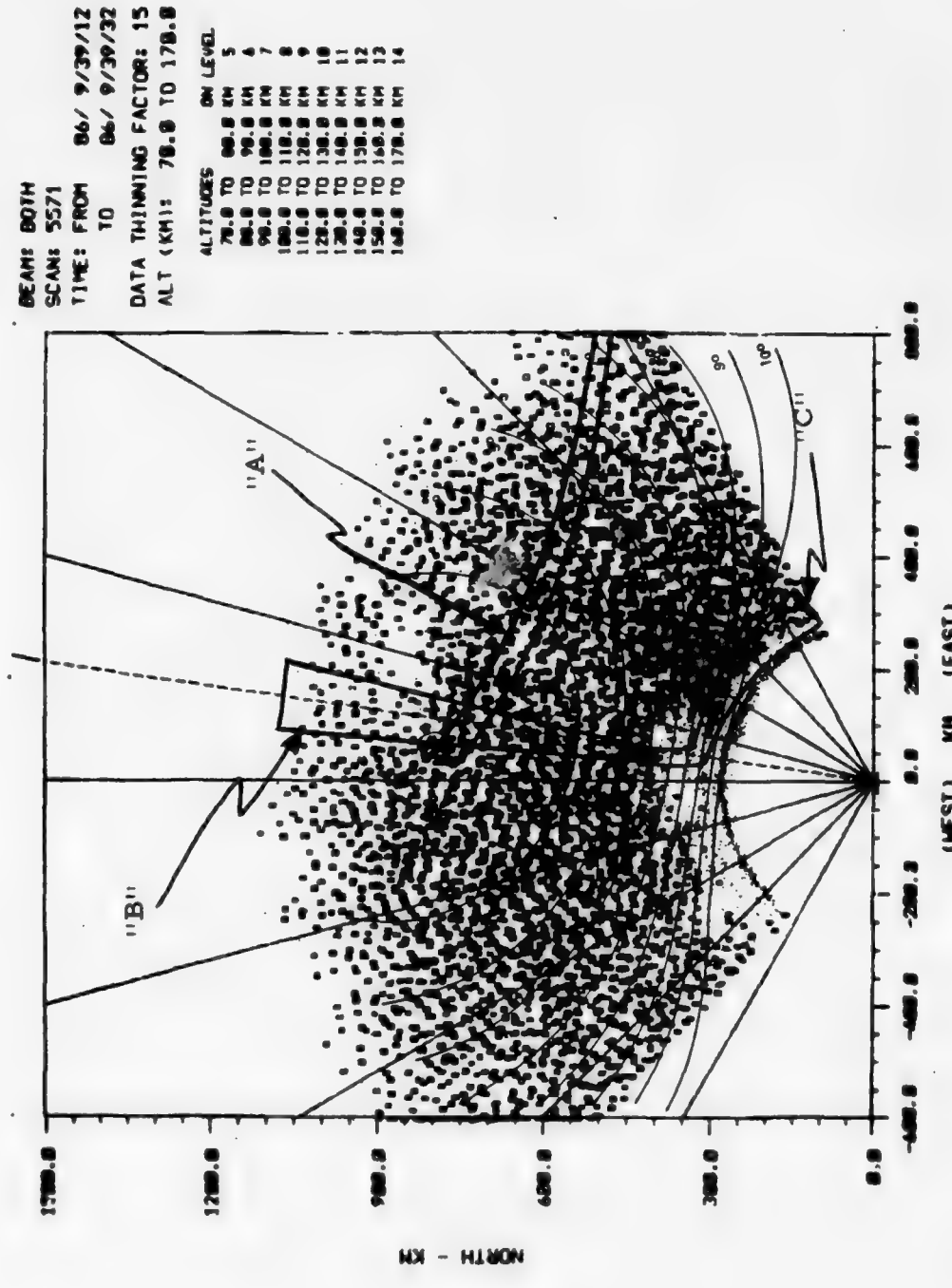


Figure 4-26

TOP-DOWN MAP OF AURORAL REFLECTIVITY FOR SCAN 5571



(180) COMPUTING

Figure 4-27

ASPECT RESPONSE ALONG REGION "A"

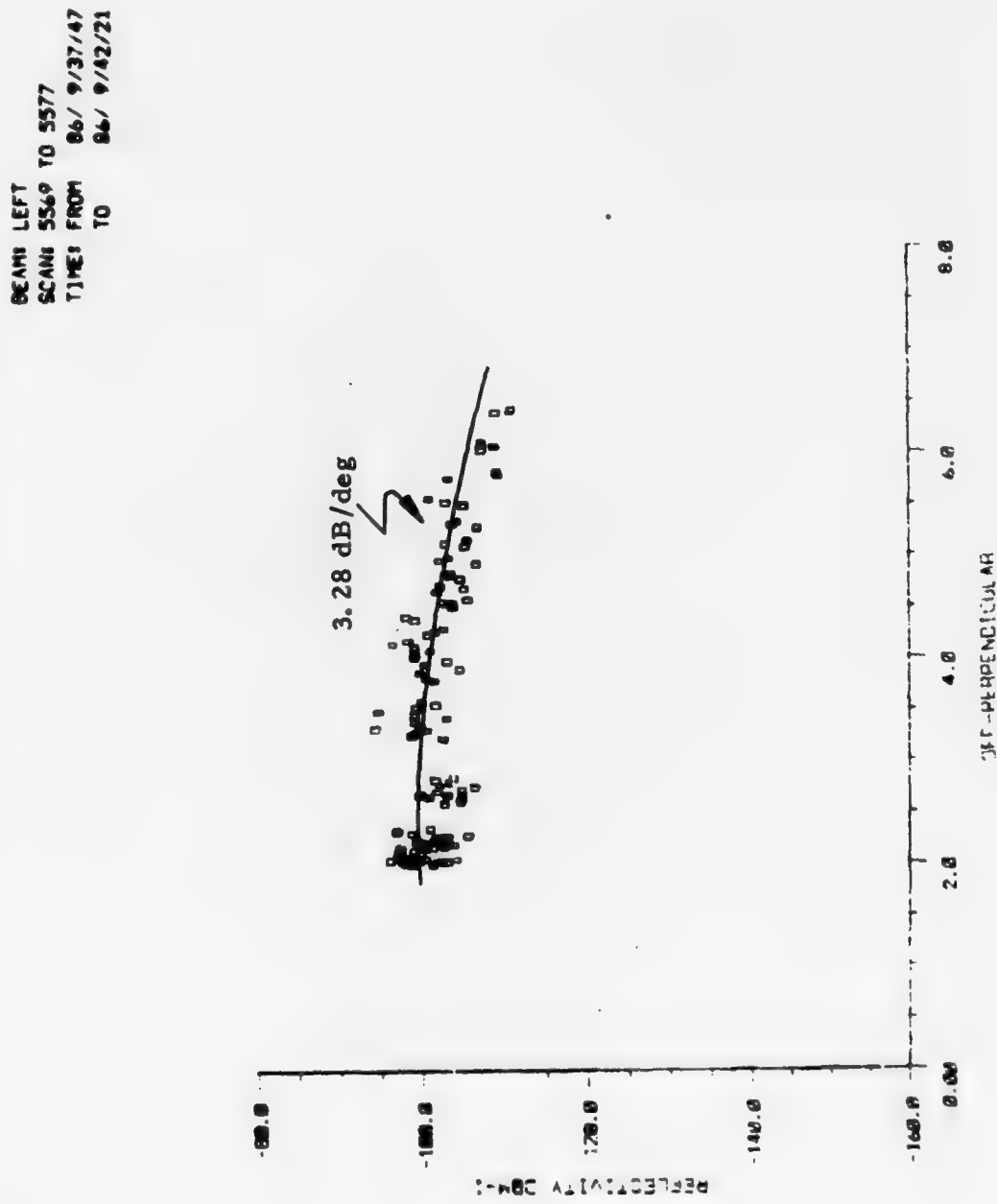


Figure 4-28

ASPECT SCATTER PLOT ALONG REGION "B"

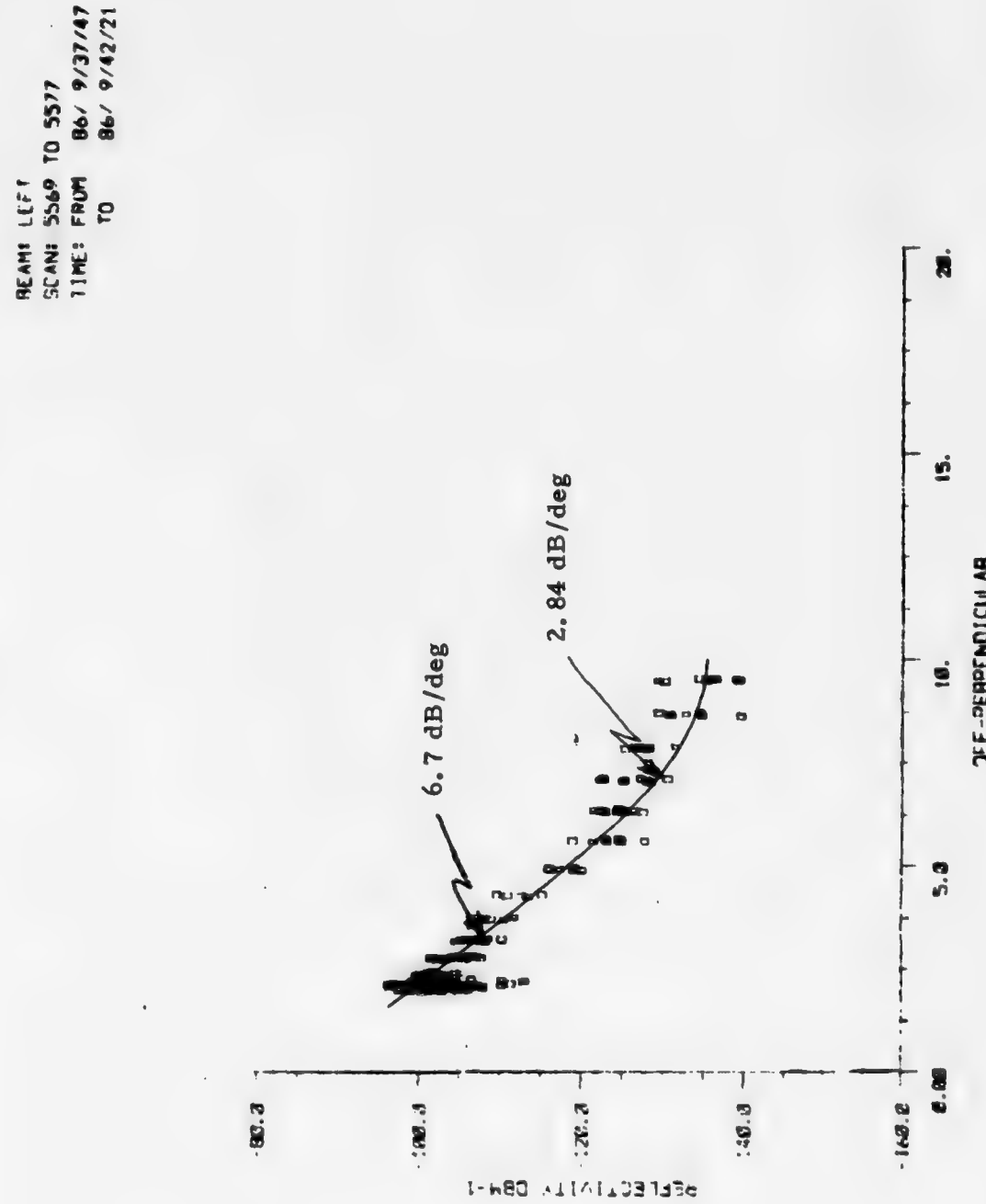


Figure 4-29

ASPECT RESPONSE FROM REGION "C"

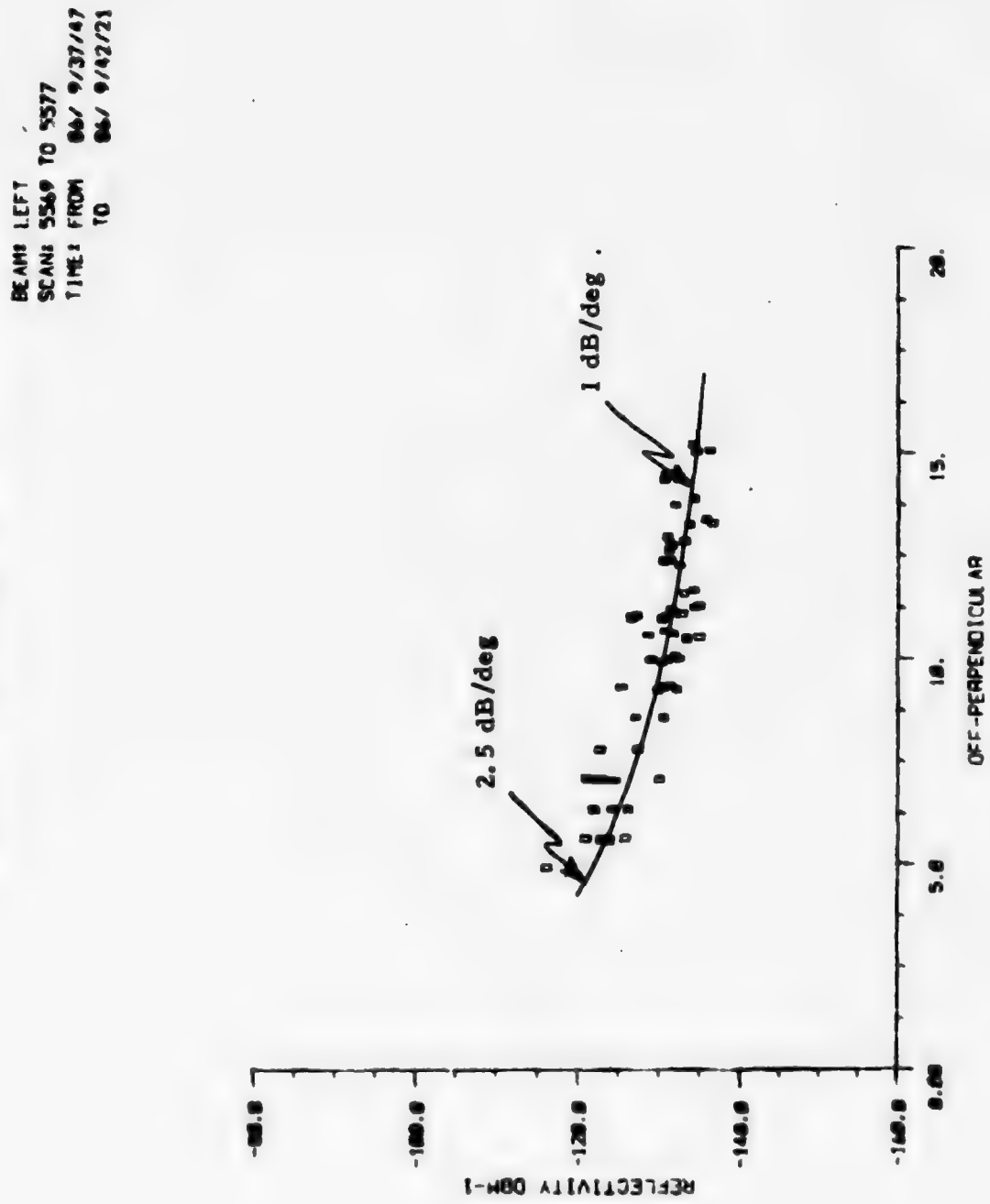


Figure 4-30

#### 4.8 Test Case 86/5622

This scan shows a large blanketing diffuse form, very much like the previous examples. The  $a_p$  index was 234 during the observation, but the magnetometer at Fort Churchill was steady showing about the same deflections as test case 86/5557. The off-perpendicular contours in Figure 4-31 show again echoes detected from over a wide range of magnetic aspect angles, out to about  $18^\circ$ . Figure 4-32 shows the center of the arc to be located near the center of the 105-106 km altitude band, from which all data for the three scatter plots was selected.

The first scatter plot, shown in Figure 4-33, was created from data taken along region A in Figure 4-31. Due to its distorted appearance, the slope is given at only one point. The scatter plot shown in Figure 4-34 was created with the data from region B, and the third scatter plot, shown in Figure 4-35, represents the aspect response obtained by combining data from regions B and C. This aspect response demonstrates a steady decrease in slope from about 6 dB/deg to 1.9 dB/deg. Although the last two scatter plots demonstrate a well-behaved aspect response, there was apparently a high level of magnetic field distortion aligned in some way with the L-shells which resulted in the distortion seen in Figure 4-33. Explaining this phenomena is beyond the scope of this report, but such an effect could result from a localized current component directed perpendicular to the L-shell contours.

TOP-DOWN REFLECTIVITY MAP OF SCAN 5626

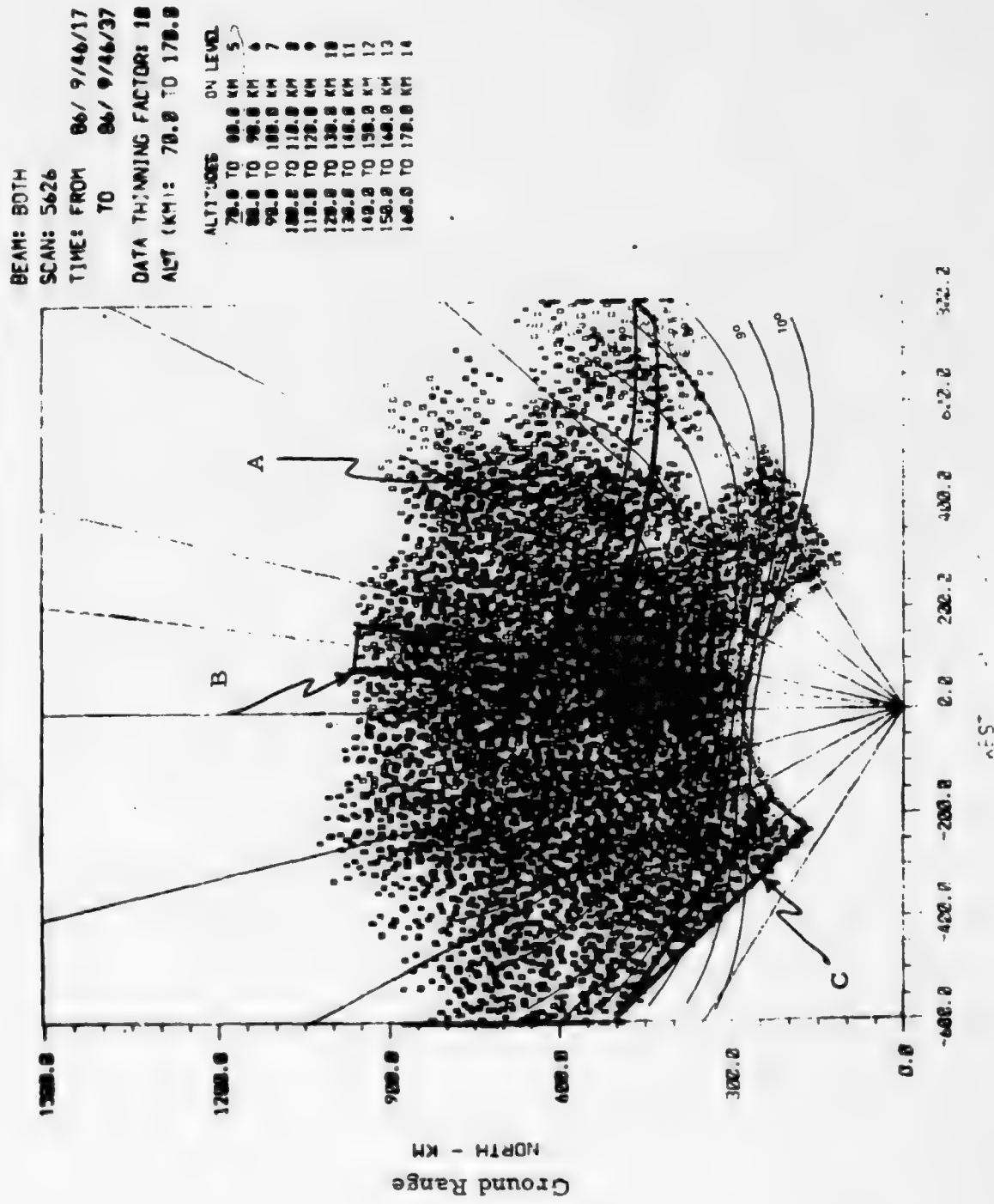


Figure 4-31

ALTITUDE PROFILE SHOWING ARC CENTER

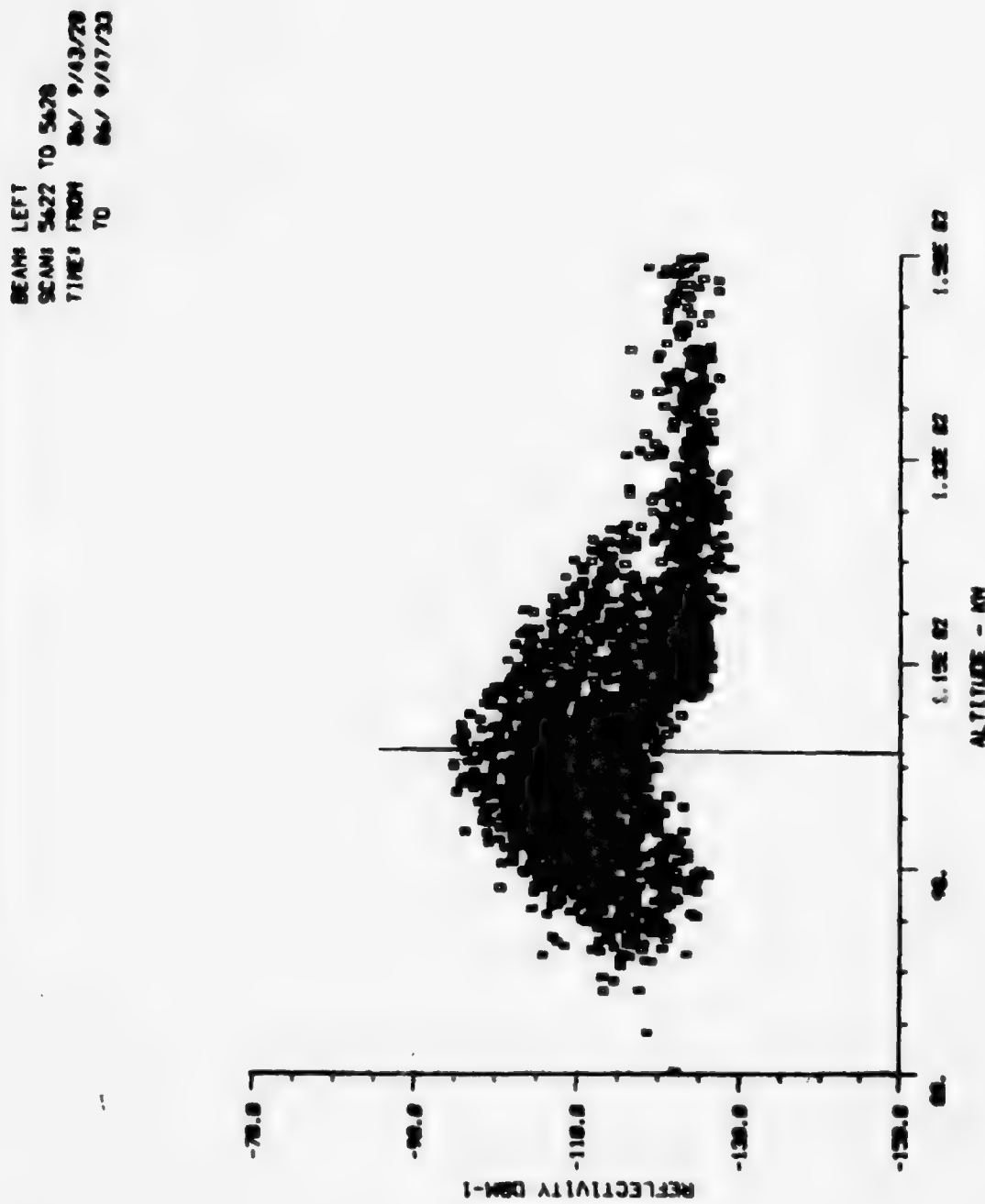


Figure 4-32

ASPECT RESPONSE FROM REGION "A"

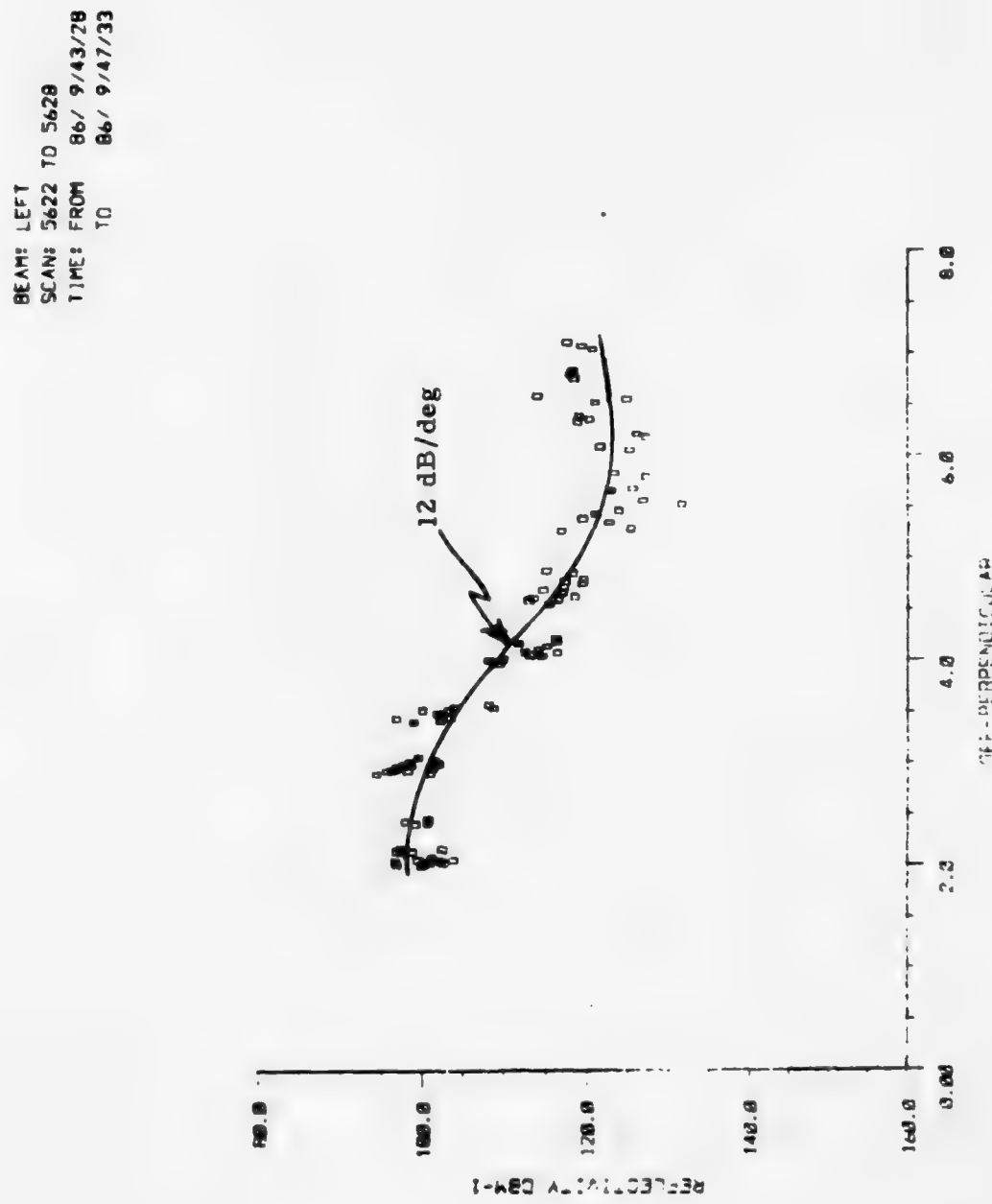


Figure 4-33

ASPECT RESPONSE FROM REGION "B"

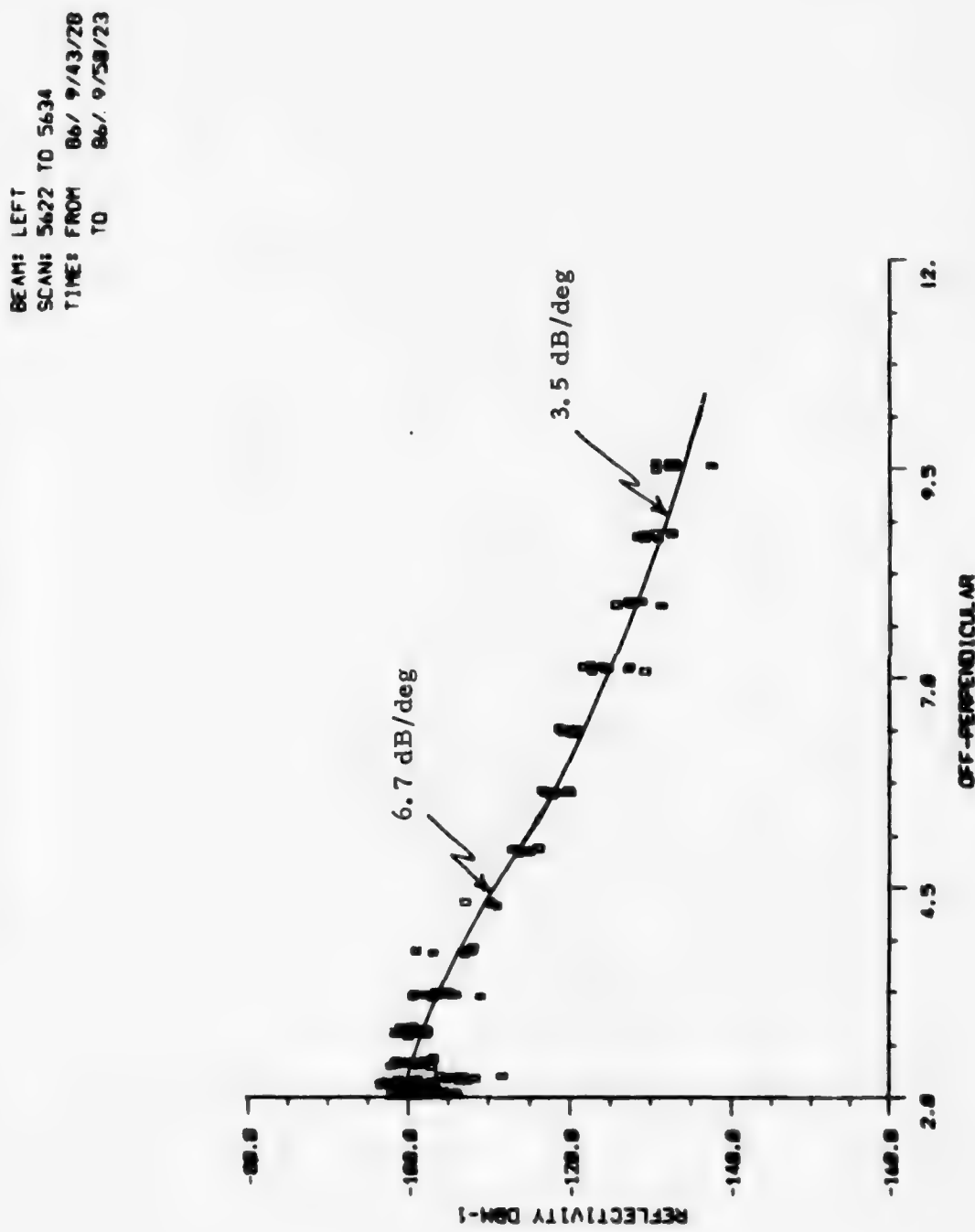


Figure 4-34

ASPECT RESPONSE FROM REGIONS "B" AND "C"

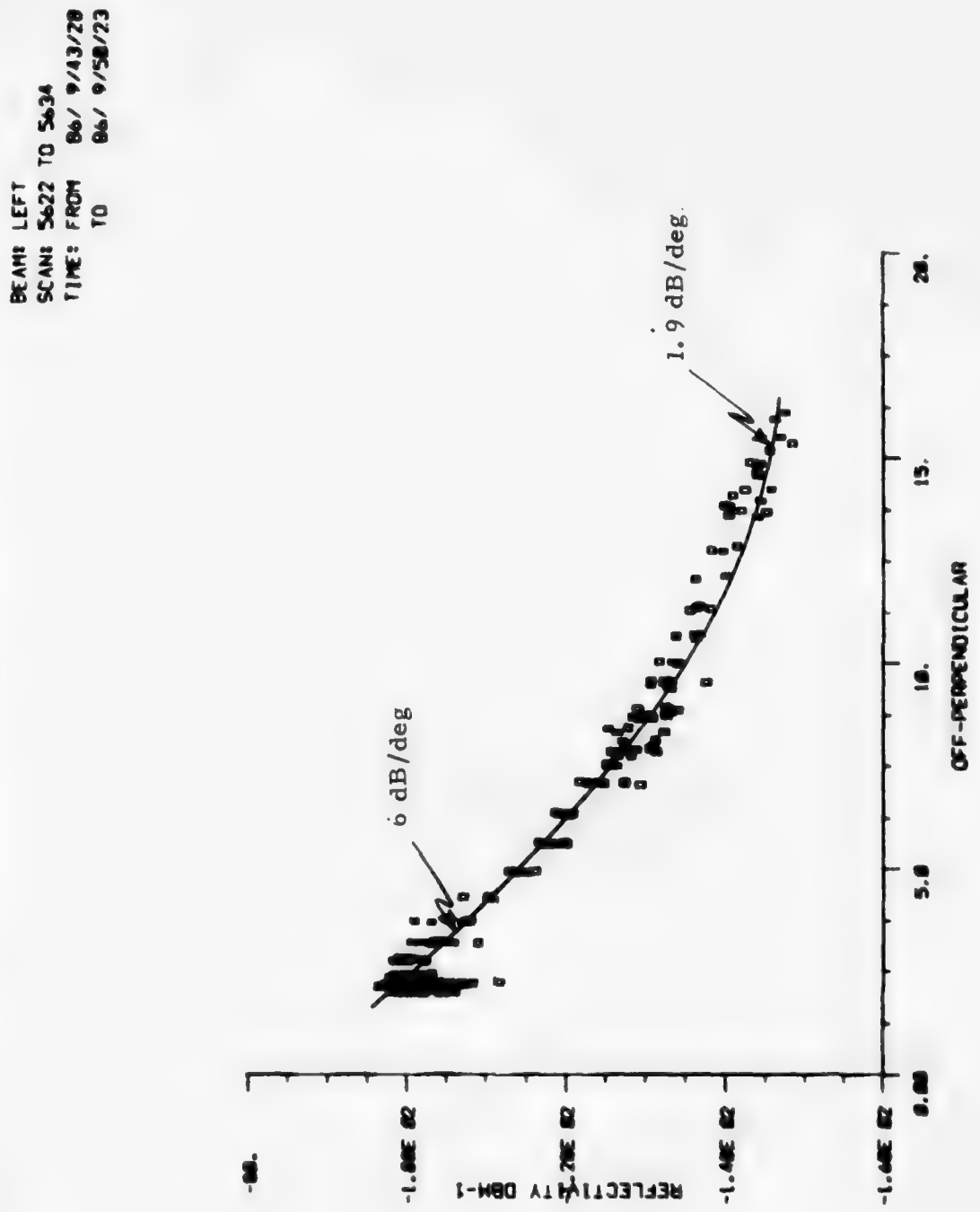


Figure 4-35

#### 4.9 Test Case 92/681

Although diffuse, the structure of the reflecting region was changing quite rapidly during the 10 volume scans used in this test case. This fact is evident from the scans in Figures 4-36 and 4-37, the scans at the beginning and end of the observation period. Unfortunately, magnetometer data from Fort Churchill was not available, and the  $a_p$  index was over 200, so the local magnetic conditions are not clear. However, at the PAR, diffuse aurora has usually been noted only during steady local magnetic activity.

Figure 4-38 shows the reflecting arc to be centered near 105 km as indicated by the altitude versus reflectivity plot. The first aspect response curve of Figure 4-39, created from data in region A, is given in Figure 4-36. This sample region is generally parallel to the magnetic L-shells and demonstrates almost no aspect sensitivity up to about  $5^\circ$  off-perpendicular where the slope rapidly changes to nearly 12 dB/deg. More evidence of this unusual phenomena can be seen in the top-down map of Figure 4-37. Notice the strongly reflecting central region and the sudden dropoff in reflectivity starting between  $4^\circ$  and  $5^\circ$  off-perpendicular. It was immediately suspected that this may have resulted from saturation of the radar receiver, but subsequent checks assured that no such problem occurred. The apparent aspect response was thus properly represented. Of course, this does not eliminate the effects of magnetic field distortion during this extremely active auroral occurrence.

The second aspect response curve is associated with region B, perpendicular to the L-shell. This plot, shown in Figure 4-40, demonstrates a more conventional characteristic, but it still shows an apparent increase in aspect sensitivity at greater off-perpendicular angles. The third scatter plot includes data from regions B and C. The response curve, shown in Figure 4-41, has a well-behaved slope out to about  $12^\circ$  off-perpendicular where it flattens and even appears to become positive. This flattening or slope reversal has been observed in other test cases and may be a result of radar limitations rather than an actual change in aspect sensitivity.

The final aspect response curve, shown in Figure 4-42, was generated from data in regions B and D. Aspect data is shown covering angles from  $2^\circ$  to about  $17^\circ$  off-perpendicular. The slope shift at about  $5^\circ$  is still noticeable, and the data distribution becomes less well-defined at angles from  $7^\circ$  to  $17^\circ$ . Most of these data points came from region D which was apparently somewhat perturbed at that time.

TOP-DOWN REFLECTIVITY MAP OF SCAN 681

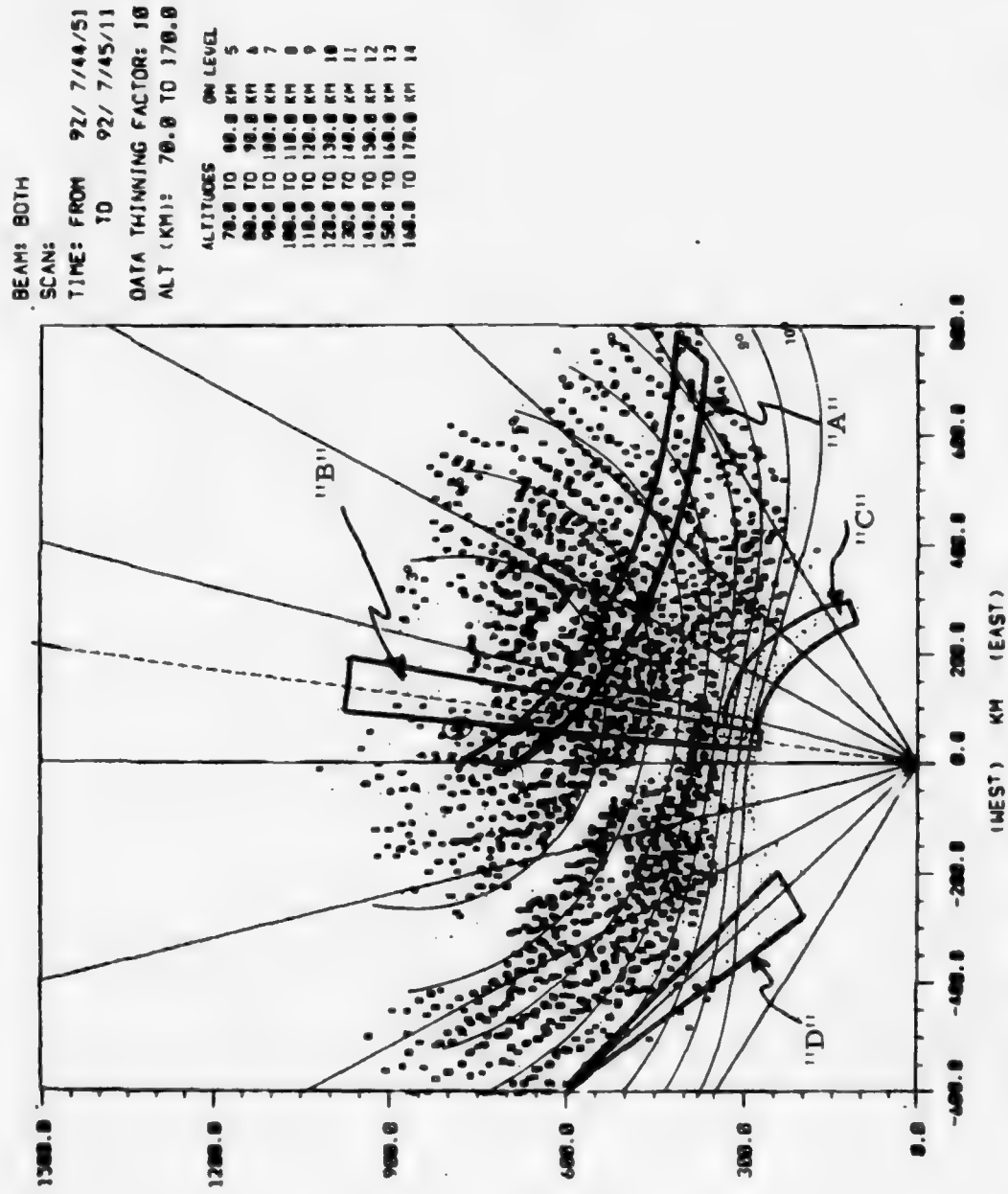


Figure 4-36

TOP-DOWN REFLECTIVITY MAP OF SCAN 690

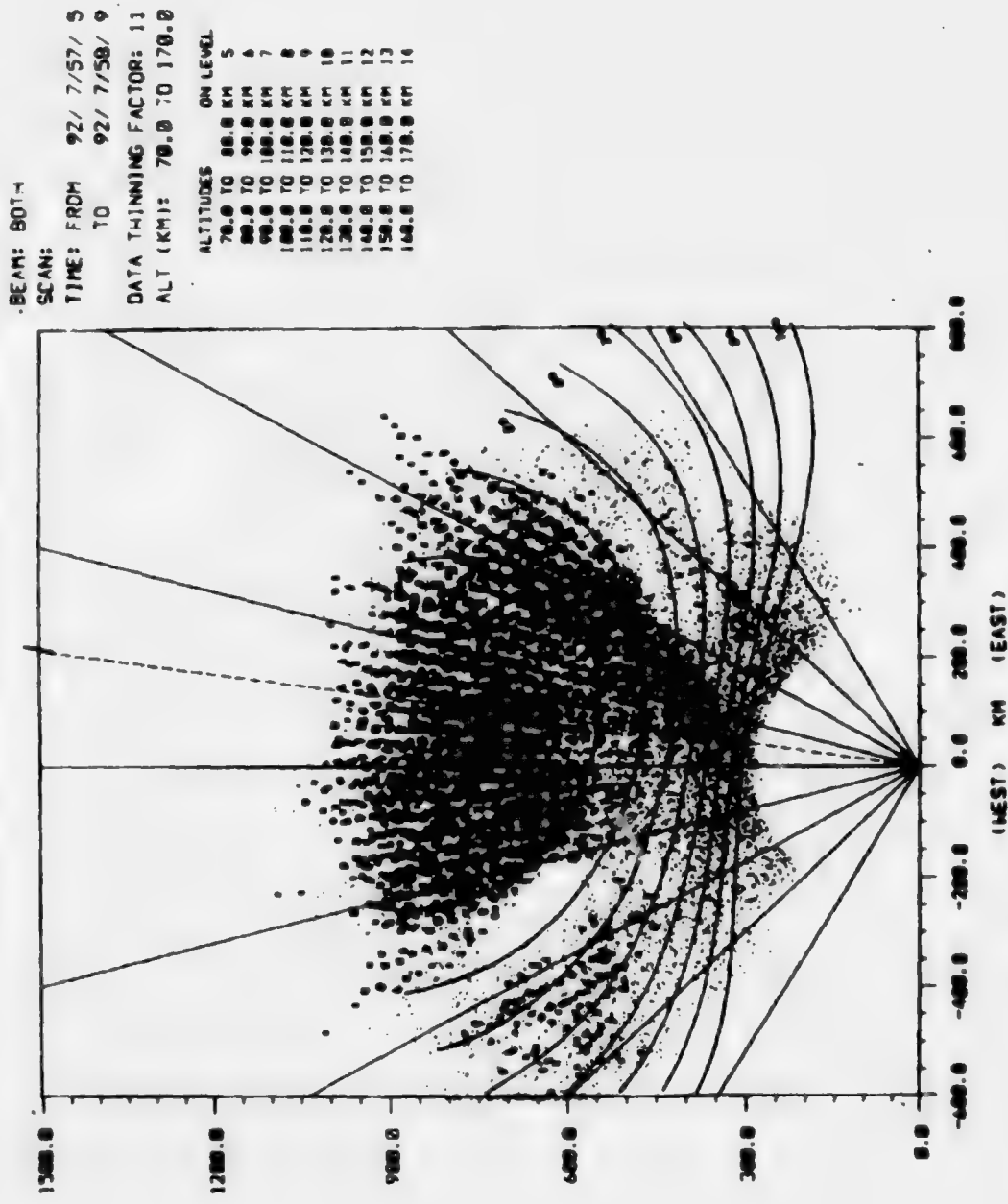


Figure 4-37

ALTITUDE PROFILE SHOWING ARC CENTER

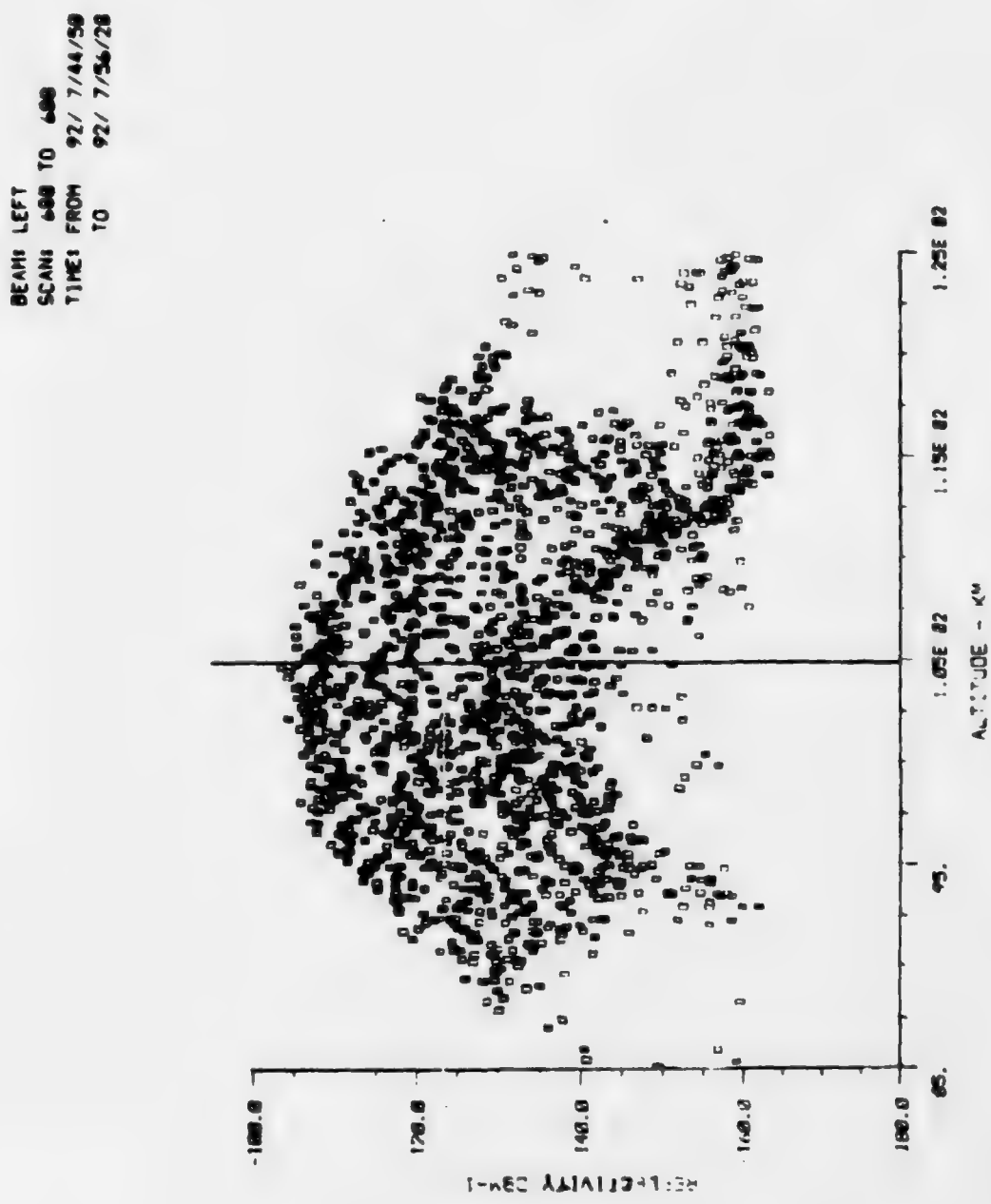


Figure 4-38

ASPECT RESPONSE FROM REGION "A"

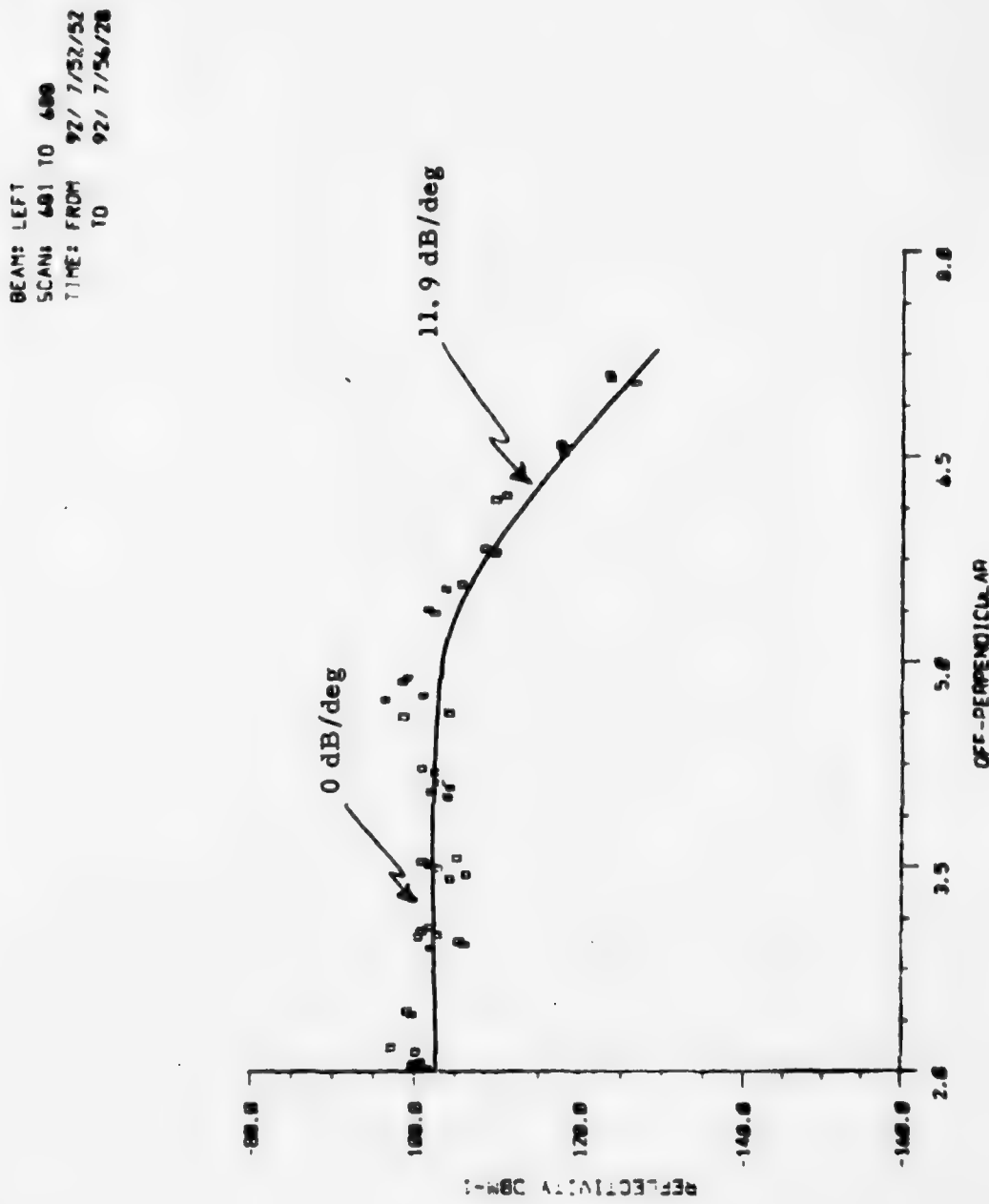


Figure 4-39

ASPECT RESPONSE ALONG REGION "B"

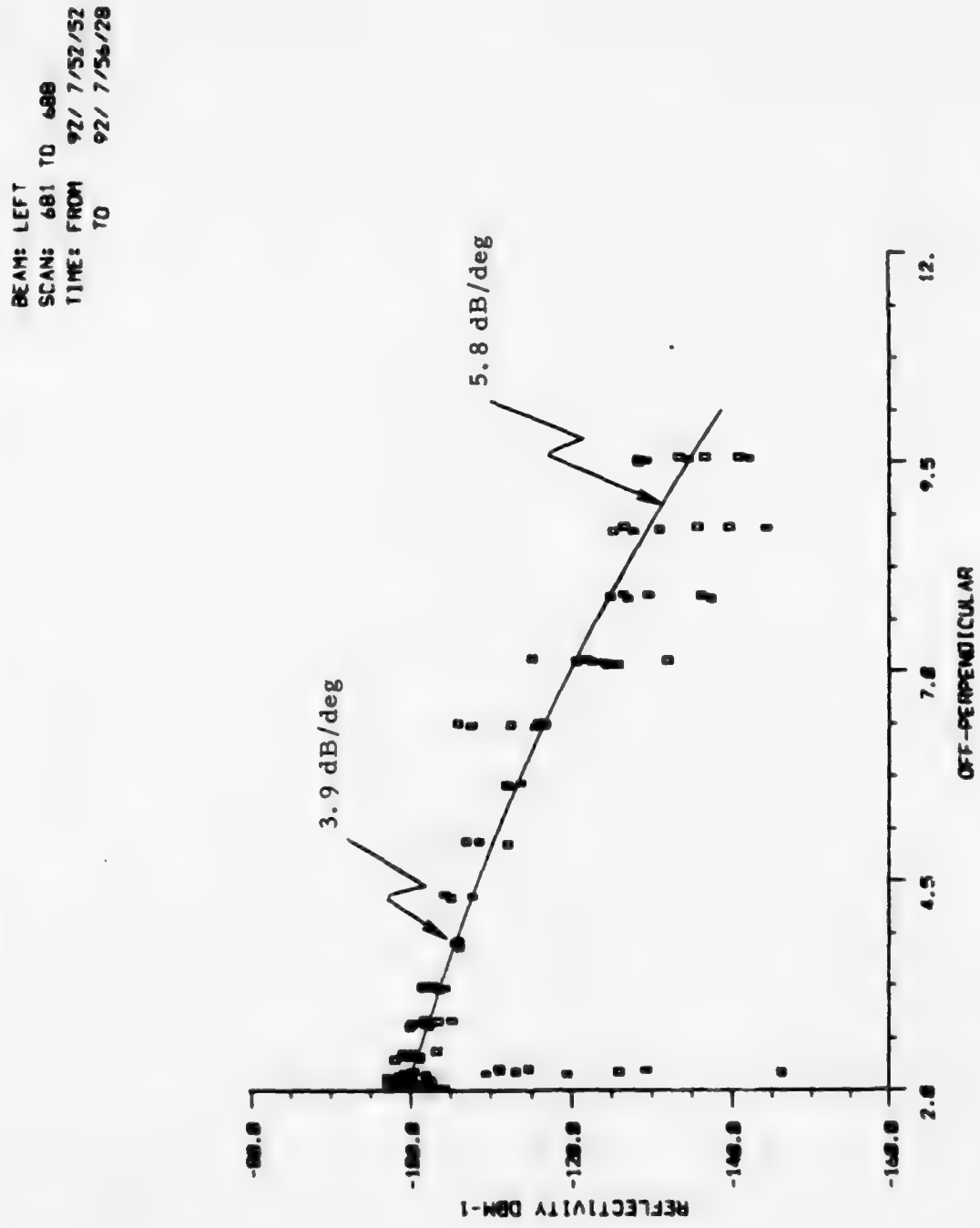


Figure 4-40

ASPECT RESPONSE FROM REGIONS "B" AND "C"

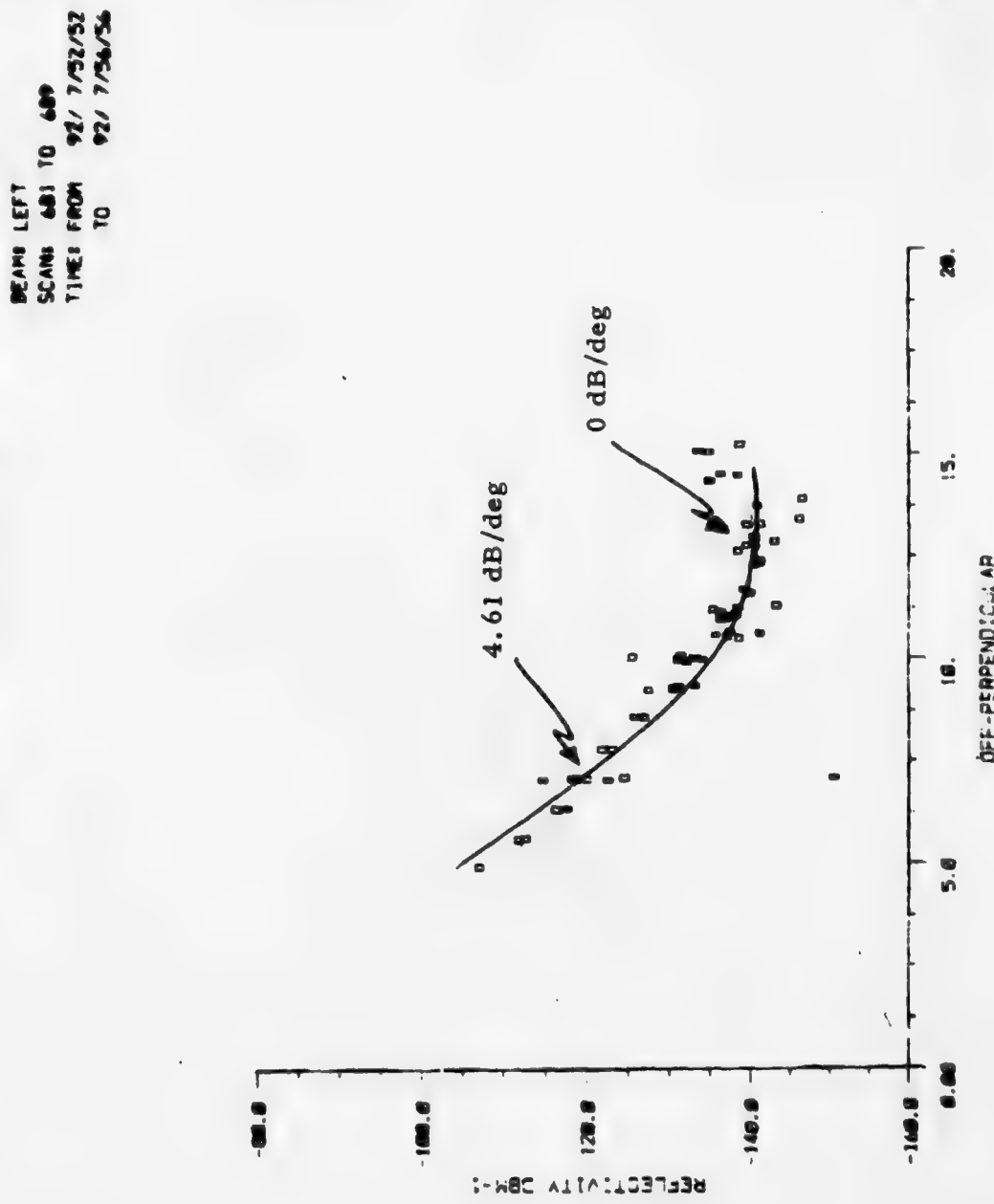


Figure 4-41

COMPOSITE ASPECT RESPONSE FROM REGIONS "B" AND "D"

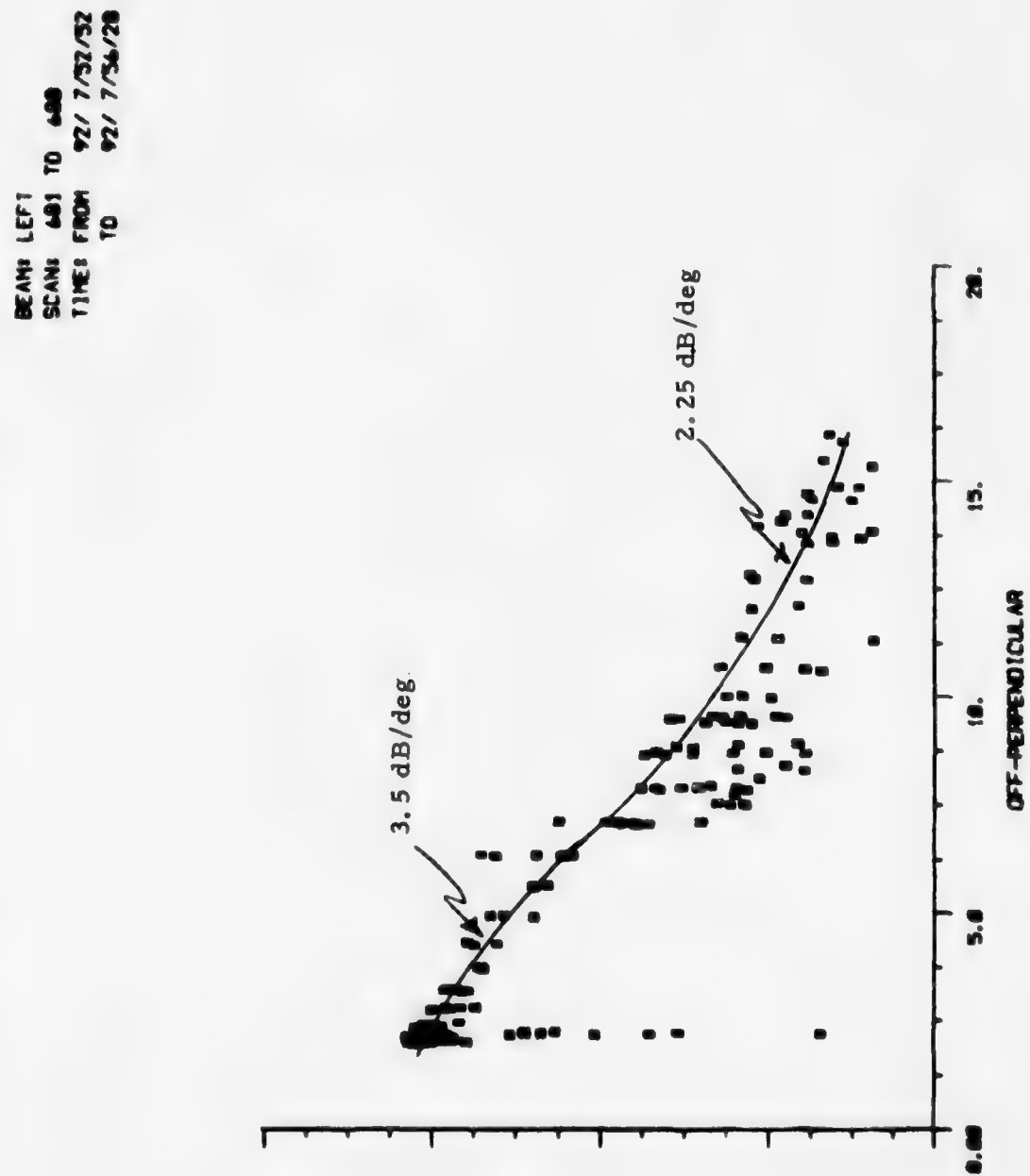


Figure 4-42

#### 4.10 Test Case 92/723

This test case has been included because the scan includes echoes with signal-to-noise ratios near 100 dB. These may be among the strongest auroral echoes ever detected by a radar. The strongest echoes measured by PAR somewhat earlier exceeded 101 dB signal-to-noise ratio with a reflectivity of about  $-70 \text{ dB m}^2/\text{m}^3$ . The distribution of reflectivities, after 11 scans were averaged, is shown in the histogram in Figure 4-44. This histogram was generated with data from region B in Figure 4-43.

The ap index was very high at this time ( $\approx 200$ ) and no local geomagnetic data is available. The scatter plots for this test case were generated from the 105-106 km altitude band. The first of these was created with data from along region A of Figure 4-43. The data from this region, which is generally parallel to the L-shells, results in the scatter plot in Figure 4-45. Evidence of some type of distortion is apparent at about  $2^\circ$  off-perpendicular, but the function is quite well-defined at other aspect angles and has a slope of 6.68 dB/deg. The second aspect response function, shown in Figure 4-46, was generated with data from regions B and C. More distortion is evident in this data, but the slope of the aspect response was clearly quite low and measured about 2.25 dB/deg. One point of special interest in this case is that the apparent slope of the aspect did not decrease as drastically as in other cases. This may be because the reflectivity was greater than for other cases so that there was a high mainbeam-to-sidelobe power ratio. This supports the author's theory that the apparent decrease in slope may be due to sidelobe returns as will be discussed in Section 5.

TOP-DOWN REFLECTIVITY MAP OF SCAN 727

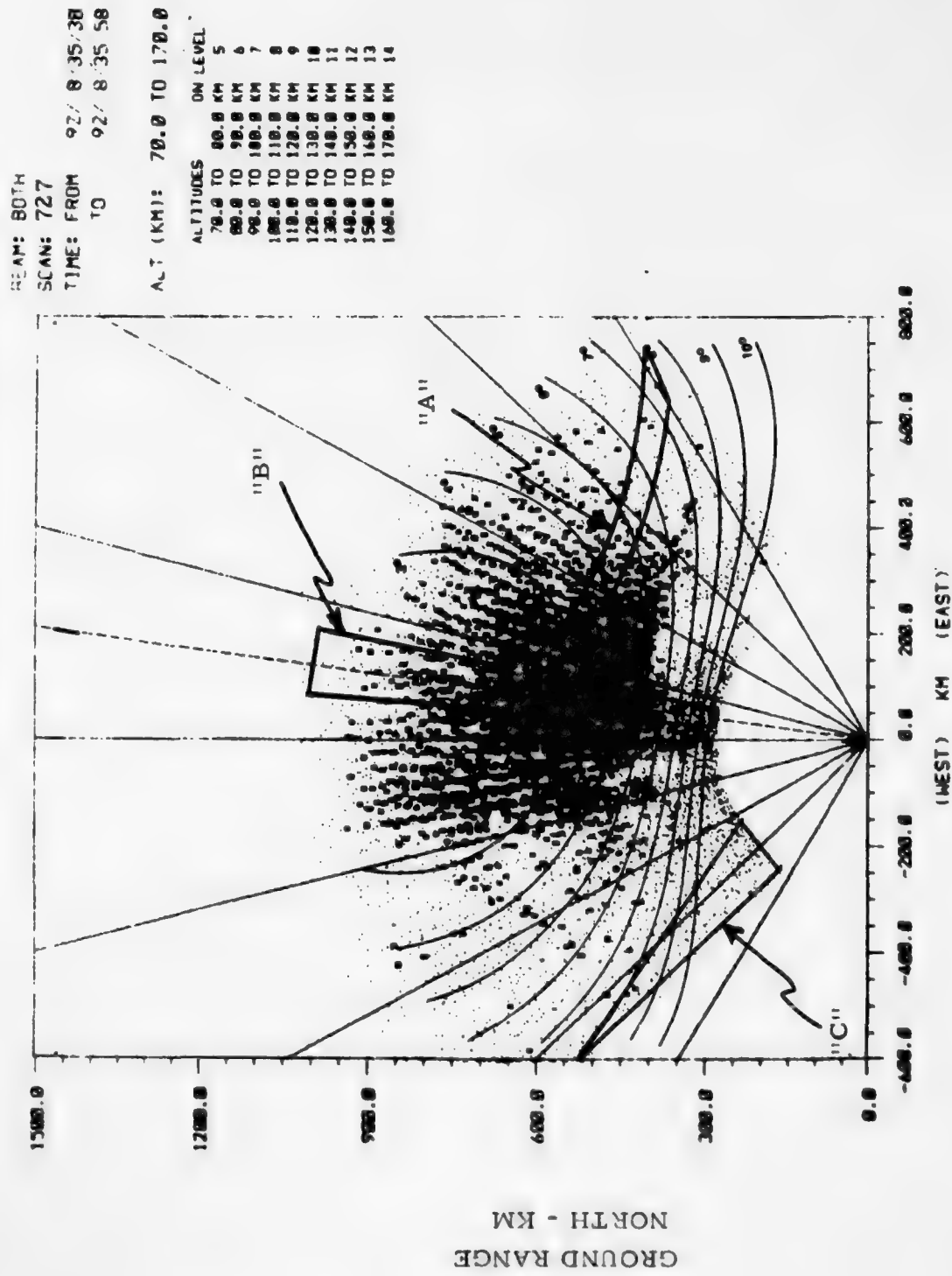


Figure 4-43

AD-A034 505 M AND S COMPUTING INC HUNTSVILLE ALA  
PAR AURORAL STUDY. VOLUME V. RADAR AURORAL MAGNETIC ASPECT SENS--ETC(U)  
OCT 76 M J MITCHELL, J L BROWN F/G 17/9  
DASG60-74-C-0026  
UNCLASSIFIED NL

2 OF 2  
ADA  
034 505

END  
DATE  
FILMED  
3-7-77  
NTIS

DISTRIBUTION OF ECHO REFLECTIVITIES AFTER AVERAGING

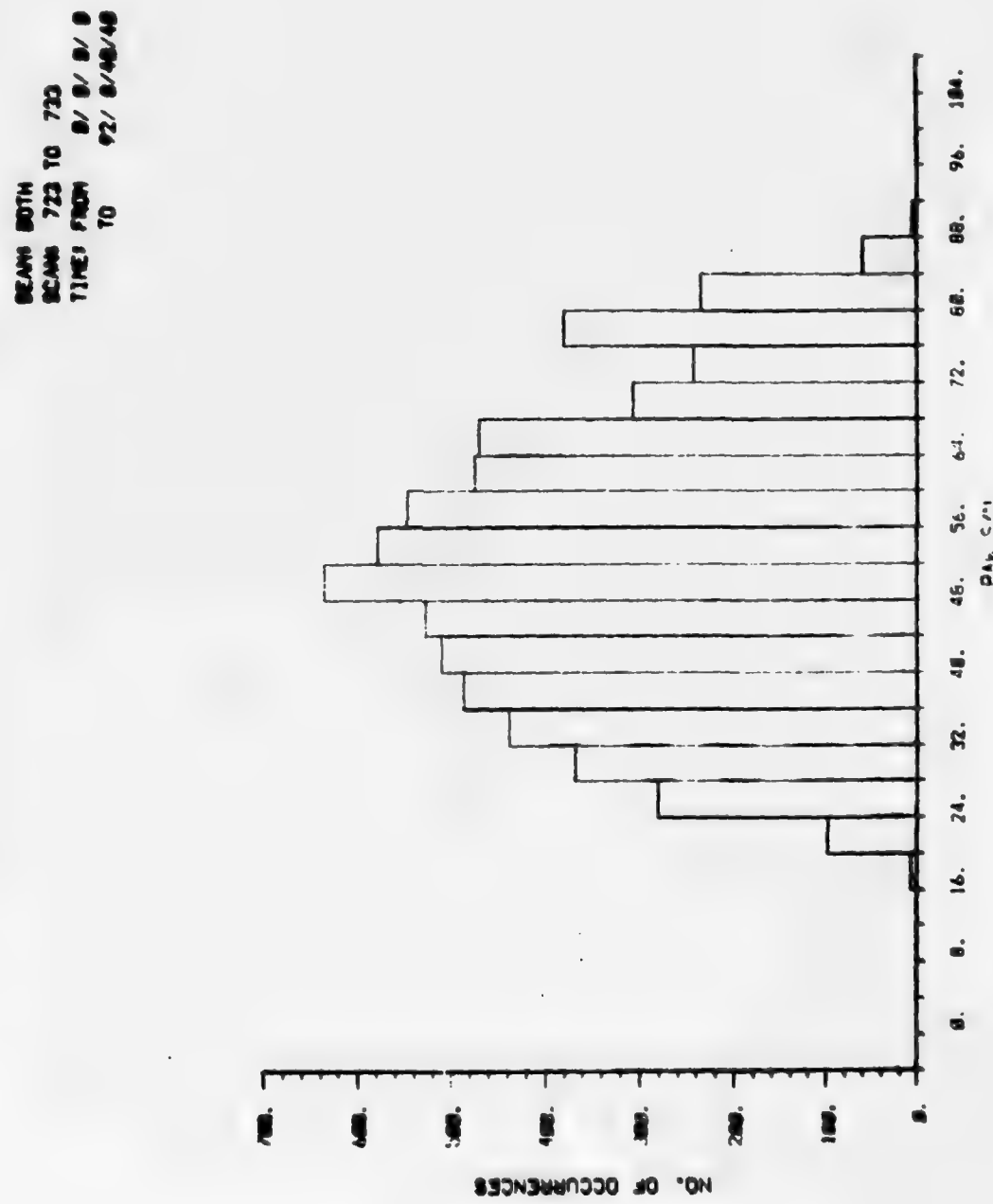


Figure 4-44

ASPECT RESPONSE FROM ALONG REGION "A"

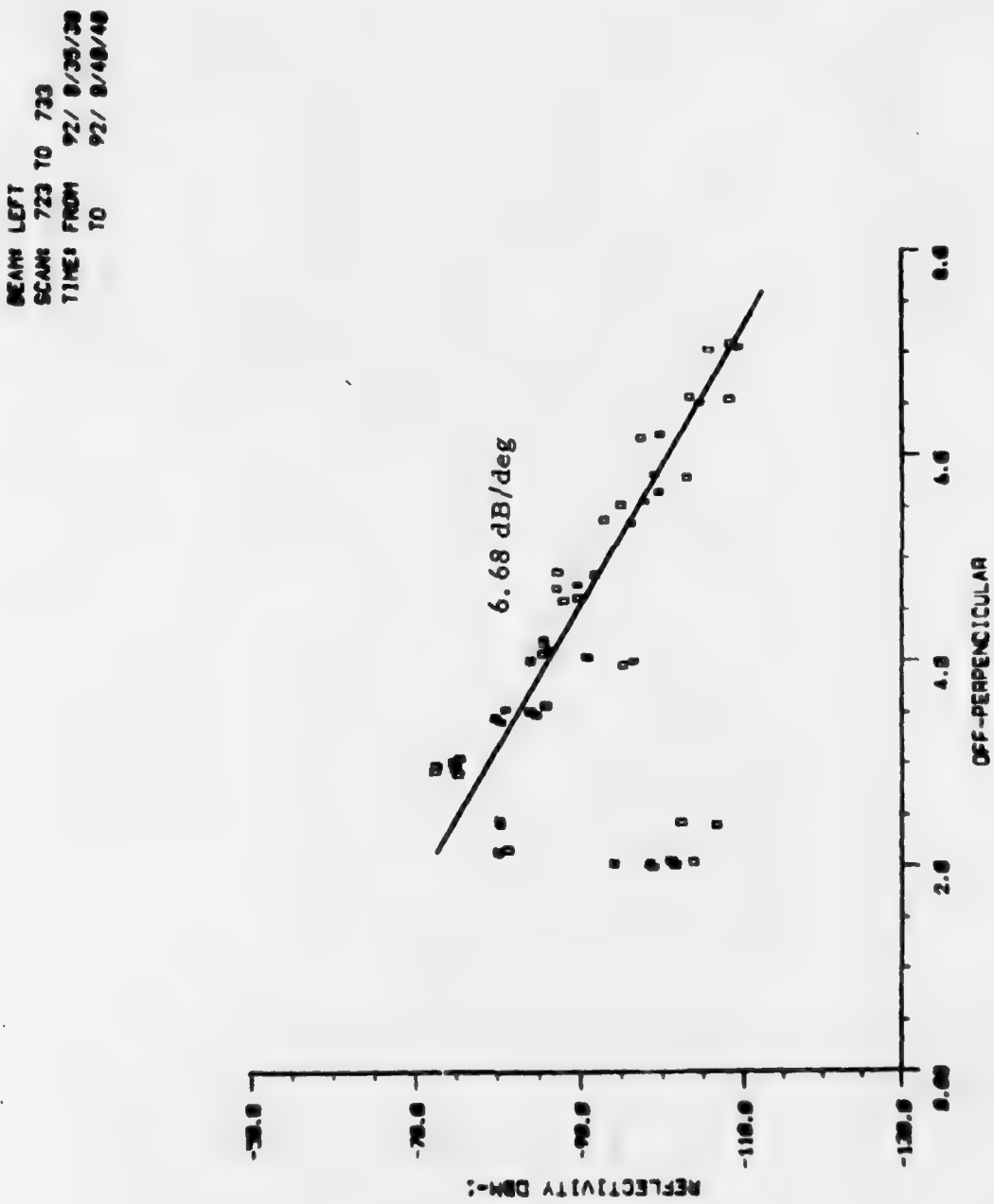


Figure 4-45

ASPECT RESPONSE ALONG "B" AND "C"

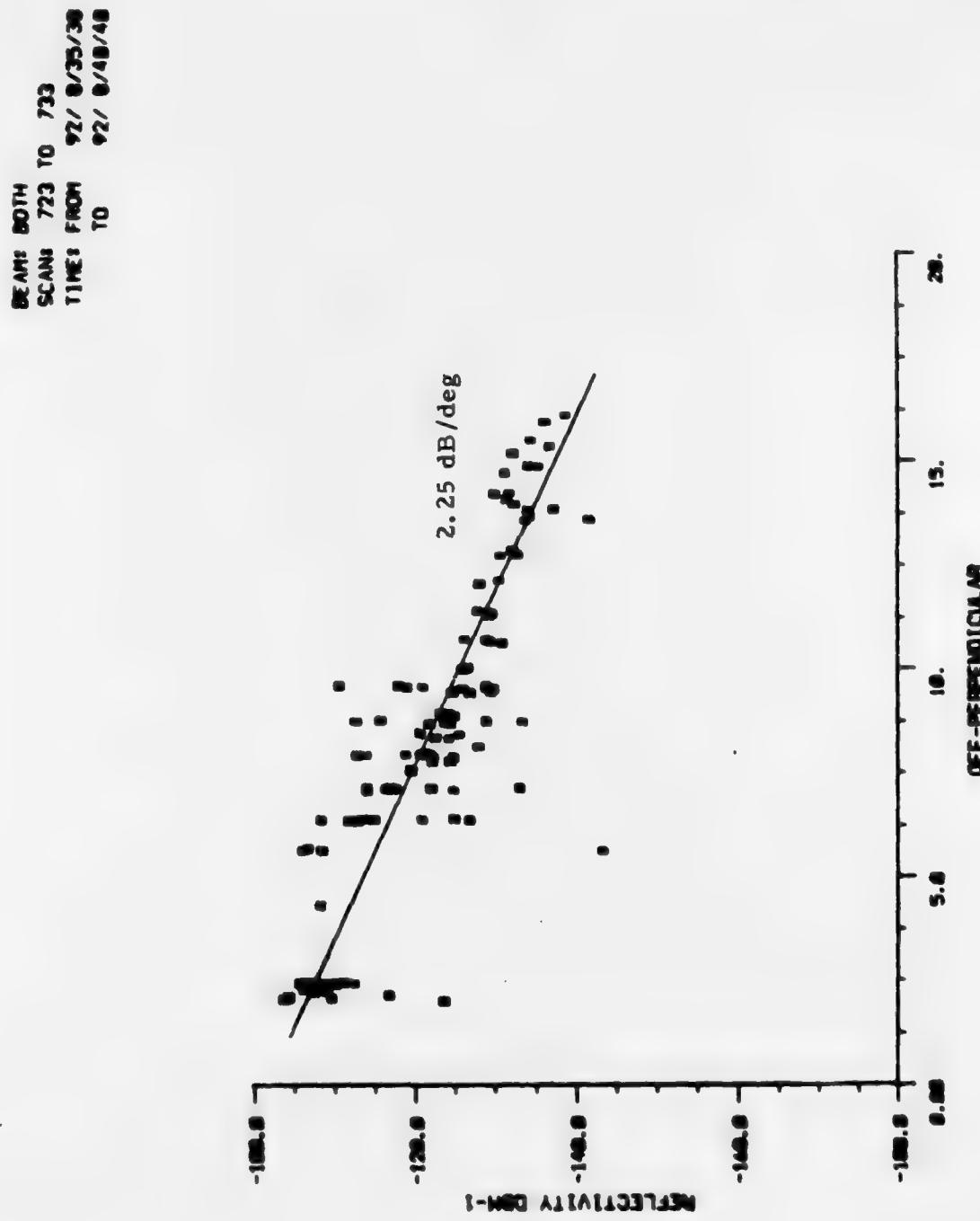


Figure 4-46

## 5. ANALYSIS RESULTS

Even though very little discussion was included with the test cases, many of the indications are obvious upon observation of the data. The most salient point, however, is that in spite of all the safeguards employed to minimize the ambiguities in the processing of auroral magnetic aspect data, an array of aspect response curves has been generated. The primary information from the test cases has been compiled in Table 5-1, which clearly shows some of the effects noted. It is evident from the individual test cases that the mechanism responsible for the apparent aspect sensitivity relationship is a highly dynamic phenomena. The marked differences in the aspect response curves from the different sample regions suggest that there may be only a very small volume of validity for the true aspect response characteristics. Depending on the sampling method, each scan will probably yield innumerable aspect curves.

It is clear that discrete arc forms "appear" to have a steeper aspect sensitivity slope than do diffuse forms. This phenomena may, however, be only an apparent effect, since the current systems associated with discrete arcs can create distortion in the local magnetic field, which is somewhat different than that for diffuse aurora. It appears that the mechanism which results in aspect sensitivity may be more complex than originally thought because of the apparent difference in the aspect sensitivity relationship of samples from different regions of a scan. Another reason for suspecting a more complex aspect phenomena is that in a number of cases, the magnetic field distortion appeared very low, and calculations based on available magnetometer data predict that the changes in apparent aspect sensitivity should be much smaller than those observed. This effort has been most marked when comparing aspect response plots generated in one case with data selected parallel to the L-shells contours and in the other case, perpendicular to these contours.

One very interesting observation is that in every observed case, the peak reflectivity occurs at almost precisely the same altitude. This phenomena would seem most unexpected in nature.

It has been noted in most applicable test cases that the slope of the aspect response function appears to flatten out at large off-perpendicular angles. This observation must be viewed with caution, for it may be simply an effect caused by the limitations of the radar. The radar beam consists not only of the main beam, but numerous sidelobes pointing in many directions. The energy measured in each echo is the superposition of echoes from the scatterers in the main beam as well as in the directions of all sidelobes. The radar associates all of this echo power with the main beam echo. The echo strength is thus increased somewhat by energy received in these unwanted echoes. Even when the main beam power is low, significant sidelobe power may still be detected and processed as an "apparent" main beam echo. The sidelobe blanking system cannot eliminate, reduce, or affect in any way sidelobe echoes when they are

**MEASURED ASPECT RESPONSE CURVES**

Test Case	Type of Aurora	Slope of Aspect Response Curve			
		Parallel to L-Shell		Perpendicular to L-Shell	
		dB/deg	Angle	Valid for Aspect Angles Centered About	Angle
270/1058	Edge of diffuse or discrete	7.34	3°	16.3	3°
70/666	Discrete	20.	2°		
70/666	Discrete	6.	4°	10.	3°
78/12	Discrete	5.	4°	16.63	3°
86/576	Discrete	5.83	4°	11.4	3°
86/632	Discrete	7.9	4°	11.75	3°
86/5557	Diffuse	5.5	4°	4.84	4°
86/5557	Diffuse	3.28	4°	0.85	15°
86/5571	Diffuse	12.	4°	6.7	2°
86/5571	Diffuse			2.84	8°
86/5571	Diffuse			1.0	15°
86/5622	Diffuse			6.7	4°
86/5622	Diffuse			3.5	9°
86/5622	Diffuse			1.9	15°
92/681	Diffuse	0.	3.5°	3.9	4°
92/681	Diffuse	11.9	6.5°	5.8	9°
92/681	Diffuse	6.68	4°	0.	15°
92/723	Diffuse			2.25	10°

**Table 5-1**

superimposed on detectable main beam echoes. This problem is especially severe in large-scale diffuse aurora because there is reflecting aurora in all directions, therefore, many sidelobes will be receiving and contributing unwanted power to the main beam echoes.

These sidelobe echoes affect the measurement of the aspect response function in a predictable fashion. Where the main beam makes small off-perpendicular angles, the total superimposed sidelobe power is small in relation to the main beam power; thus, the associated distortion to the aspect curve is small. As the main beam moves to greater off-perpendicular angles, where it is attenuated by aspect sensitivity, a number of sidelobes will always be pointed in the direction of small aspect angles. The echo power in this sidelobe is thus enhanced and the ratio of sidelobe-to-main beam power increases. The primary effect is that the aspect response slope flattens out, and at large aspect angles, where most of the signal power is actually contributed from the sidelobes, the scatter plot approaches a constant mean value. In one test case, 92/723, the aspect response had still not completely flattened even at 17° off-perpendicular. This may have happened because the main beam auroral reflectivity was so high at the large aspect angles that there was still enough power from the main beam to offset the unwanted sidelobe power.

Returning to the analysis of the aspect response, it should be explained that no attempt has been made to generate an average or composite aspect response curve for these cases because of the widely varying results already noted. Much has already been done to assure that the individual aspect curves represent the most accurate results possible using the existing quiescent magnetic field model. It is apparent that some changes are taking place in either the magnetic field or the auroral reflection mechanism which is causing these aspect curves to vary. Averaging of these curves would only mask the actual phenomena. It would appear that much more could be gained by utilizing the difference in these curves to help determine more accurately the mechanism and dynamics of this wave action which makes auroral backscatter possible. Other authors [3, 6] have noted that aspect sensitivity varies according to the magnetic index, as was shown in Figure 2-3. It has been observed that the auroral forms and, of course, the level of magnetic distortion also varies with the magnetic indices. For this reason, it cannot be assumed that the true aspect sensitivity relation varies. It may be simply that the quiescent magnetic field model may no longer be representative. These indices may then merely provide an indicator of the validity of the field model used.

Another of the differences between diffuse and discrete aurora can be seen by comparing the differences in apparent aspect sensitivity when sampling the two generally orthogonal regions where the sample region was elongated parallel to the L-shells and as in the other case, perpendicular to them. It can

be readily ascertained from the data which has been given that, for these examples, the apparent aspect sensitivity was always greater for discrete aurora when the data was sampled from a region elongated perpendicular to the L-shell. For diffuse aurora, aspect sensitivity was normally greater when the data was sampled from a region generally parallel to the L-shells. The effect was, however, less marked than for discrete aurora. The phenomena just described is not too surprising when one considers the differences in the magnetic field components which are induced by the current system associated with the two types of auroral forms. A further discussion of these induced fields is included in Section 6.

## 6. PERTURBATION OF THE GEOMAGNETIC FIELD BY IONOSPHERIC CURRENTS

It has been observed that there is considerable variation in the apparent aspect sensitivity of the different test cases, particularly between diffuse and discrete forms. Also, aspect sensitivity measured parallel to the L-shell differs from aspect sensitivity measured perpendicular to the L-shells. These observations suggest that the quiet geomagnetic field model used to determine aspect sensitivity is significantly perturbed by the presence of ionospheric currents. If the resulting aurora is an image of the bounds of the auroral electrojet as suggested by [11, 12], then the top-down maps provide a picture of the basic large-scale structure of the current system.

Our theory is that there may be a basic difference in the magnetic field distortion induced by the narrow discrete arcs as compared to that induced by the large-scale diffuse aurora. This is simply that the narrow discrete arcs act like line currents, and that the region where the field lines close around the arc is localized within the region of observation. If the arc is aligned with the L-shell, induced field distortion would occur primarily to the field components which are transverse to the direction of current flow; i.e., the L-shell contours. This theory also assumes that the current system associated with the diffuse aurora resembles a large current sheet.

The field induced by this sheet is significant in several ways. First, the effects are no longer localized but cover a large area, and the field lines do not encircle the aurora in the same fashion as with the discrete arc. Thus, within the reflecting mass, where the edge effects are not observed, the sheet current associated with large diffuse auroral forms causes little perturbation of the magnetic Z-component. The field lines from the sheet will be generally aligned perpendicular to the L-shell. The field strength will not decrease with altitude above and below the sheet as in the case of the line current in which varies inversely with range. This means that the diffuse aurora creates a type of field distortion which is fairly uniform, both geographically and with altitude, over the entire viewing region of the radar. This type of field distortion will tend to shift all of the off-perpendicular contours of the radar together with no significant change in shape or separation of the contours. There will hence be little change to the slope of the aspect sensitivity curve generated using a quiescent magnetic field model.

The more complex and localized current systems of the discrete arcs can result in extreme distortion to the off-perpendicular contours with an accompanying change in apparent aspect sensitivity when the quiescent field model is used.

To determine the feasibility of this explanation, a simplistic model was used to determine the gross quantitative effects which might be anticipated. The

model allows several line currents constrained to constant latitude and altitude to be superimposed onto the quiet geomagnetic field. It was determined that a single line current of  $10^5$  to  $10^6$  amperes at an altitude near the center of the arc would produce variations in the geomagnetic field similar to those observed on the Fort Churchill magnetometer data. Figure 6-1 shows a set of off-perpendicular contours at 105 km for the quiet geomagnetic field. An eastward flowing current of  $10^6$  amps at 110 km altitude and  $53.5^\circ$  latitude creates a region of high aspect gradient in the immediate vicinity, with minor perturbation north of the current and approximately  $1.5^\circ$  of increased aspect angle immediately south of the current merging with the original field further south. This is shown in Figure 6-2.

If a quiescent field model were used to determine the apparent aspect sensitivity when the distortion was similar to that shown in Figure 6-2, the slope of the apparent aspect response would be steeper than if the actual field model were used. This effect could account for the apparent increase in aspect sensitivity observed in discrete arcs. The edges of diffuse aurora will also be affected in this way because, at these edges, the current no longer acts like a sheet, and the field lines above and below the arc connect along the edge. The resultant field distortion acts much like that for discrete aurora.

## QUIESCENT GEOMAGNETIC ASPECT CONTOURS AT 105 KM FOR PAR

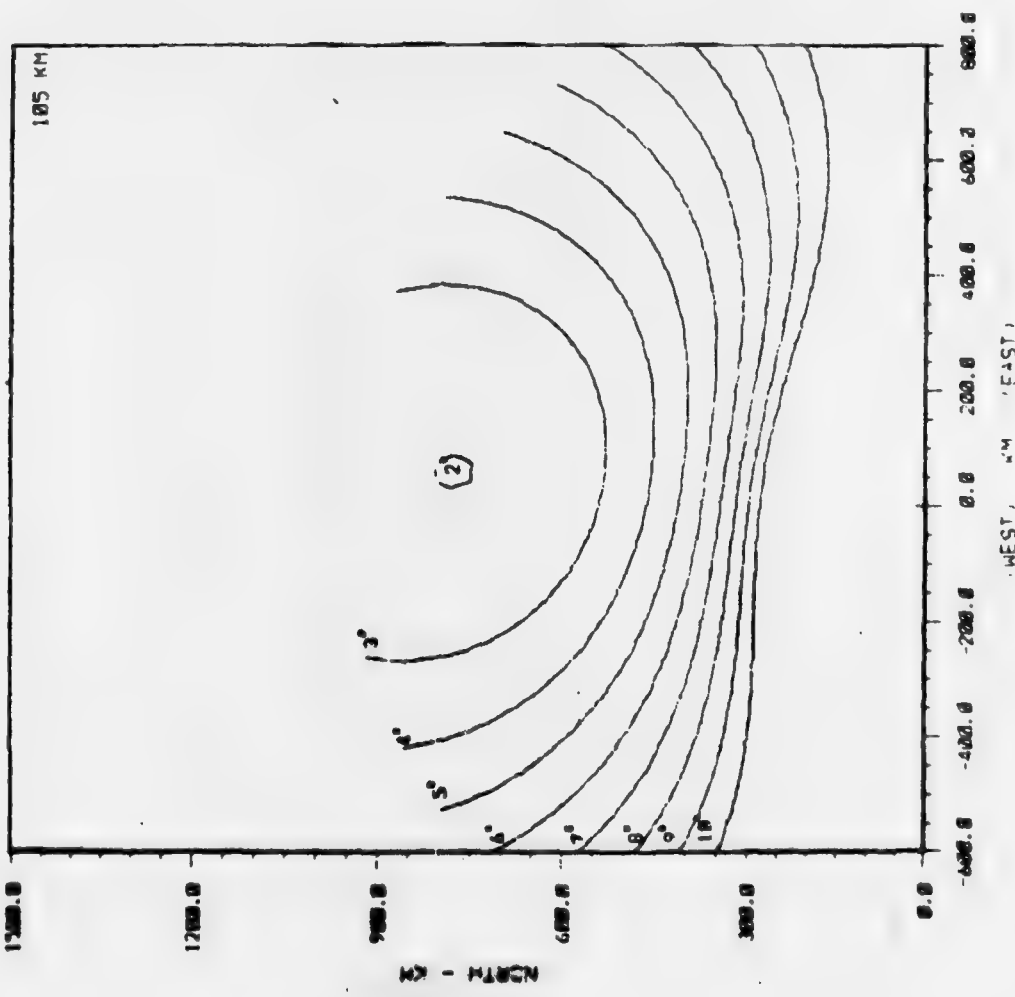


**Figure 6-1**

PERTURBED ASPECT CONTOURS AT 105 KM FOR PAR

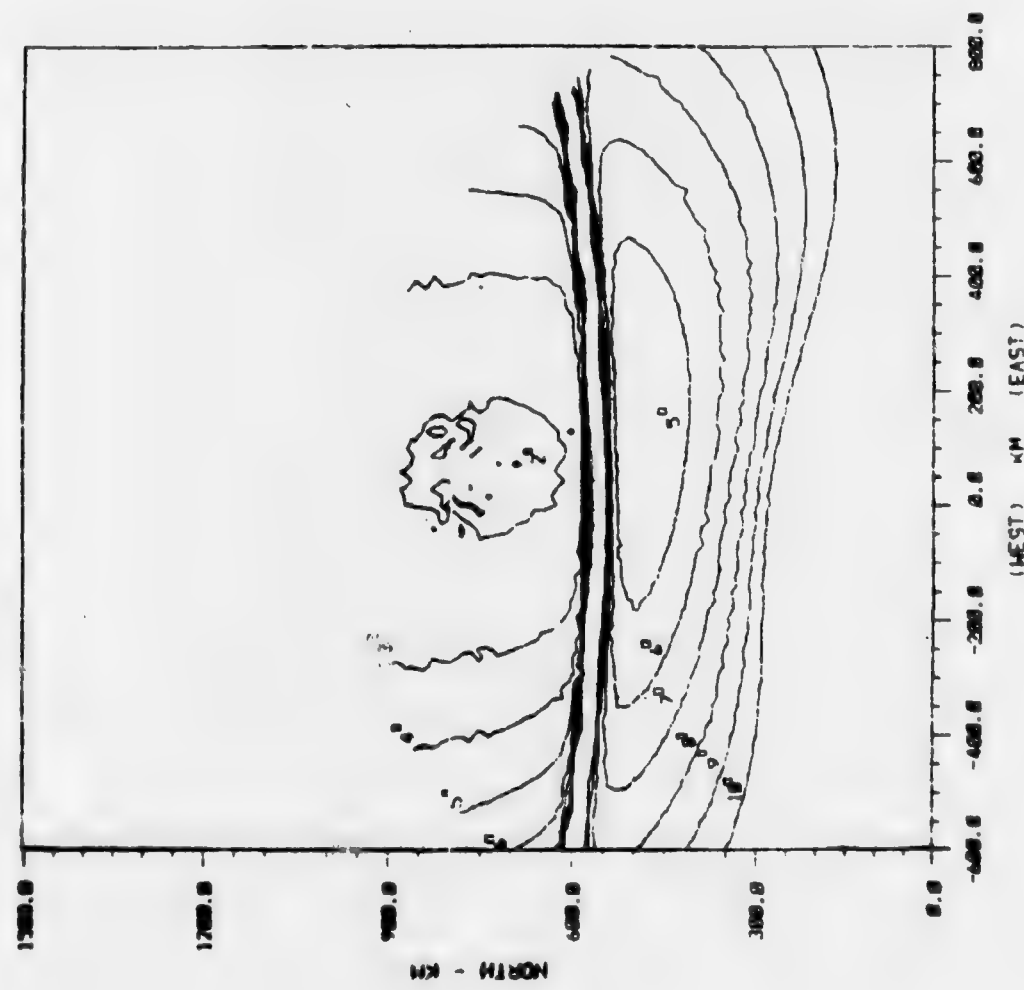


Figure 6-2

## 7. CONCLUSIONS

A number of potential problems have been identified which could seriously affect the determination of the aspect sensitivity response function. Techniques have been described for elimination or minimization of many of the detrimental effects of these problems. High resolution measurements made with one of the most powerful radars in the world have been used to generate auroral reflectivity maps and scatter plots which show the magnetic aspect response relationship. A technique was described which allowed the center of the reflecting arc to be accurately estimated so that only the most accurate data would be selected for processing.

By performing pulse-by-pulse averaging and by selecting echoes from homogeneous regions, the resulting points on most of the scatter plots have a tightly distributed relationship from which the "apparent" aspect response can be determined with high confidence. Despite attempts to minimize the effects of magnetic field distortion, a wide variation was found in the slopes of the scatter plots from different scans and even from different regions in the same scan. This phenomena is apparently related to the spatial characteristics of the sample region, with a clear cut and consistent difference between discrete and diffuse forms. In the case of discrete arcs, it appears that when the echo samples are selected from a region elongated perpendicular to the L-shells that the computed slope of the aspect response is much steeper than when the region is elongated along the L-shells. This contrast has not been observed for diffuse forms. A theory was presented which relates the phenomena to the magnetic field induced by the ionospheric current system. The results of this study support previous observations [6, 10] that the apparent aspect sensitivity seems to decrease at greater off-perpendicular angles. It has been shown, however, that the phenomena may result, at least in part, from the superposition of sidelobes and main beam echo power causing the apparent aspect slope flattening to be "illusory."

The findings noted here clearly indicated that radar observations of discrete arcs "appear" much more aspect-sensitive than for diffuse aurora. It was also shown that when the electrojet current is confined, as with the discrete arc, the magnetic field distortion can increase the "apparent" aspect sensitivity. The apparent variation in the magnetic aspect response may be merely a manifestation of our inability to simultaneously measure and correlate all of the spatial, magnetic, and temporal conditions which are critical to the determination of true aspect response function(s). The very fact that aurora exists means that the magnetic field is distorted by the resulting currents.

If the relationships suggested here are valid, and unique and consistent aspect response relationships were developed, then techniques may be developed to use the differences between the actual and apparent magnetic aspect angles

to determine quantitatively the structure of the auroral current systems. This technique would be fast and relatively inexpensive and might eliminate the need for certain, more expensive methods employing direct measurement.

## REFERENCES

- [1] Mitchell, M. J., PAR Auroral Study, Volume I, M&S Computing, Inc. Report No. 76-0013, March 15, 1976.
- [2] Mitchell, M. J., PAR Auroral Study, Volume II, M&S Computing, Inc. Report No. 76-0016, May 12, 1976
- [3] Mitchell, M. J., Alley, P. L., Brown, J. L., Cochran, M., PAR Auroral Study, Volume III, M&S Computing, Inc. Report No. 76-0027, August 6, 1976.
- [4] Chestnut, W. G., Hodges, J. C., and Leadabrand, R. L., Report No. RADC-TR-68-286, Stanford Research Institute, 1968.
- [5] Egeland, A., Holter, O., Omholt, A., Cosmical Geophysics, Scandinavian University Books, 1973.
- [6] Jaye, W. E., Chestnut, W. G., Craig, G., Analysis of Auroral Data From the Prince Albert Radar Laboratory, Stanford Research Institute, 1969.
- [7] Unger, H. H. W., Harding, R. H., Horan, R. J., Auroral Clutter in UHF Radar, Bell Laboratories and Lincoln Laboratory - Joint Study, 1973.
- [8] Battan, Louis J., Radar Meteorology, University of Chicago Press, 1959.
- [9] IAGA Commission Number 2, Working Group 4, "Analysis of the Geomagnetic Field," Journal of Geophysical Research, Volume 74, Number 17, August 15, 1976.
- [10] Unwin, R. S., "Studies of the Upper Atmosphere from Invercargill, New Zealand, Characteristics of Auroral Radar Echoes at 55 Mc/Sec.," Ann. Geophysics, Volume 15, Number 377, 1959.
- [11] McDiarmid, D. R., "On Errors in the Measurement of the Aspect Sensitivity of Radar Aurora," Journal of Geophysical Research, Volume 81, Number 22, August 1, 1976.
- [12] Tsunoda, R. T., Presnell, R. I., "The Spatial Relationship Between the Evening Radar Aurora and Field-Aligned Currents, Journal of Geophysical Research, Volume 81, Number 22, August 1, 1976.
- [13] Kamide, Y., Akasofu, S. I., "The Location of the Field-Aligned Currents with Respect to Discrete Auroral Arcs," Journal of Geophysical Research, Volume 81, Number 22, August 1, 1976.

**M&S COMPUTING, INC.**

P. O. Box 5183  
HUNTSVILLE, ALABAMA 35805  
(205) 772-3411